Doctoral Dissertation (Censored)

博士論文（要約）

A study on clarification of reaction processes and sources of sulfate aerosol based on chemical speciation

（化学種解析に基づく硫酸エアロゾルの反応過程や起源の解明）

A Dissertation Submitted for the Degree of Doctor of Philosophy
December 2019

令和元年１２月博士（理学）申請

Department of Earth and Planetary Science, Graduate School of Science,
The University of Tokyo

東京大学大学院理学系研究科

地球惑星科学専攻

Chihiro Miyamoto

宮本 千尋

Abstract

Aerosols, one of important atmospheric components, are particulate matters suspended in the atmosphere giving significant impacts on various environmental issues. These issues include air quality related to their health effects and influences on ecosystem and their important roles in the Earth's climate. However, these impacts by various compounds in aerosols depend on the chemical species of each element in aerosols, which is a main viewpoint of this thesis. In **Chapter 1**, I provide introduction and aims of this study, which focuses on the effect of aerosols on the Earth's climate, types of aerosols related to chemical reactions examined in this study, and the method for the chemical speciation.

The effects of aerosols on the Earth's climate can be divided into direct and indirect effects. The latter, which is better written as indirect radiative forcing, is caused by aerosols acting as cloud condensation nuclei (CCN); aerosols alter cloud's properties such as reflection efficiency and lifetime, which enhances its negative radiative forcing (Albrecht, 1989; Lohmann and Feichter, 2010; Twomey, 1959). Such indirect radiative forcing by aerosols to cool the earth climate is considered to play a significant role to offset warming effects by greenhouse gases, but its estimation still has the largest uncertainty to predict the future climate (IPCC, 2013). CCN activity of aerosols depends largely on the species and their physicochemical properties of the particles such as particle size and hygroscopicity. Sulfate is a major component of aerosols which is mostly formed secondarily in the atmosphere through gas-to-particle conversion from anthropogenic sulfur dioxide (SO_2) as precursor gases (e.g., Seinfeld and Pandis, 2006) Ammonium sulfate ($(NH_4)_2SO_4$) is considered as a dominate sulfate species in aerosols, because concentration of ammonia in aerosols is approximately equal to that of sulfate (e.g., Adams et al., 1999). $(NH_4)_2SO_4$ has high hygroscopicity with fine particle sizes. Consequently, sulfate aerosols can act as CCN and contribute largely to the indirect cooling effect (Bouche and Randall, 2013).

However, the chemical forms of aerosols are variable by undergoing chemical reactions in the atmosphere referred to as "aging process."

Mineral particles mainly emitted from natural sources account for about 30% of total aerosol mass globally (Satheesh and Moorthy, 2005), which can react with acids including SO_2 gases and sulfate in the atmosphere (e.g., Usher et al., 2003). Several mineral species in the particles are altered by aging process, which affects hygroscopicity of the particles. As a result, CCN activity of the mineral particles can either increase or decrease. Calcite ($CaCO_3$) is a highly reactive species in mineral particles with acids because of its high alkaline property (Al-Hosney and Grassian, 2005, 2004; Rubasinghege and Grassian, 2013; Usher et al., 2003). For example, reactions of $CaCO_3$ with nitric acid (HNO_3) or hydrochloric acid (HCl) form calcium nitrate ($Ca(NO_3)_2$) and calcium chloride ($CaCl_2$) in mineral particles, respectively, which increases CCN activity, because the reaction products have much higher hygroscopicity than that of $CaCO_3$ (Al-Hosney and Grassian, 2005; Goodman et al., 2000; Ma et al., 2012a; Sullivan et al., 2009; Usher et al., 2003). In contrast, $CaCO_3$ reacts with SO_2 and/or sulfate to form gypsum ($CaSO_4{\cdot}2H_2O$) with similar hygroscopicity to original $CaCO_3$ and increase of the CCN activity is subtle (Gu et al., 2017; Ma et al., 2013; Tang et al., 2015; Usher et al., 2003). Instead, presence of $CaSO_4{\cdot}2H_2O$ in the particles formed by the reaction processes may overestimate the CCN activity of sulfate aerosol, since $CaSO_4{\cdot}2H_2O$ is less hygroscopic species (e.g., $(NH_4)_2SO_4$). Therefore, formation of $CaSO_4{\cdot}2H_2O$ can decrease of hygroscopic sulfate aerosols such as $(NH_4)_2SO_4$ due to decrease of SO_2 and/or sulfate concentrations in the atmosphere, and alters size distribution of sulfate aerosols because mineral particles and hygroscopic sulfate particles are generally distributed in large and fine size fractions, respectively. Thus, $CaSO_4{\cdot}2H_2O$ formation can affect various physicochemical properties of sulfate aerosols and hence their contribution to the earth climate. Therefore, it is necessary to identify sulfate species in aerosol and their size distribution with related processes

in detail. However, there are few observation studies to observe the reduction of $(NH_4)_2SO_4$ by the formation of $CaSO_4 \cdot 2H_2O$ quantitatively in the field, though these processes are recognized in numerous studies in laboratory and in modelling (e.g., Dentener et al., 1996; Ma et al., 2013; Manktelow et al., 2010; Usher et al., 2003). In East Asia, emissions of anthropogenic materials including sulfate and mineral particles are significant relative to other regions (Crippa et al., 2016; Tegen and Schepanski, 2009). In addition, Asian dust contains much higher $CaCO_3$ than that of other regions (Krueger et al., 2004). Thus, it is important to investigate sulfate species in aerosols especially as well as their reaction and transportation processes in East Asia.

This thesis aimed to investigate the following three topics:

(i) Speciation of sulfate in aerosols with various degrees of hygroscopicity and their concentrations in the atmosphere

(ii) Effect of $CaSO_4 \cdot 2H_2O$ formation on the size distribution of sulfate aerosols and their CCN activity

(iii) Emission sources, reactions in the atmosphere, and aging processes during transportation of sulfate aerosols

To achieve these goals, aerosol samples with finely−size fractionation collected at four sites in East Asia and ice core drilled at Greenland were analyzed using X-ray absorption near-edge structure (XANES) spectroscopy as a main analytical method which is a direct speciation method suitable to this study. This thesis consists of four studies (Chapters 2, 3, 4, and 5) with general discussion and conclusions (Chapter 6). Their contents were briefly given below:

Chapter 2. Sulfate species in aerosol collected in Higashi-Hiroshima

In this chapter, seasonal variation of sulfate species in aerosol was analyzed and their formation process was discussed. Total suspended particle (TSP) samples without size-fractionation were collected at Higashi–Hiroshima, Japan from September 2012 to August 2013.

As a result of sulfur speciation by XANES, major sulfate species are those with high hygroscopicity except for $CaSO_4 \cdot 2H_2O$. The $CaSO_4 \cdot 2H_2O$ fraction to total sulfate increased especially during a period of high concentration of Ca^{2+} of non-sea salt (nss) origin such as Asian mineral dust event in spring. Inversely, the amount of hygroscopic sulfate was decreased presumably by the reaction to form $CaSO_4 \cdot 2H_2O$ by the reaction with $CaCO_3$ in the mineral dust. Subsequently, size-fractionated aerosol samples were collected at the same sampling site during winter (January 21 to 30, 2013), spring (March 4 to 9, 2013), summer (July 22 to August 5, 2013), and fall (November 11 to 25, 2013). As a result of Ca speciation analysis of the samples by XAFS, it was suggested that $CaSO_4 \cdot 2H_2O$ was formed secondarily at the surface of the particles by the reaction of sulfate and/or SO_2 with $CaCO_3$ in the atmosphere.

Chapter 3. Analysis of Ca species of whole and at surface of individual aerosol particles between 2 sampling sites

To confirm whether $CaSO_4 \cdot 2H_2O$ was formed by the reaction of $CaCO_3$, calcium (Ca) species of aerosols collected in Aksu (near source area of the mineral dust) and Qingdao (urban area in eastern China) during a large dust event recorded from 20 to 22 March 2002 were compared. Here, the depth-dependent Ca speciation using μ-XANES was for the first time applied to individual aerosol particles to investigate Ca species both in the whole particle and at surface of the particles to confirm the presence of $CaSO_4 \cdot 2H_2O$ at the surface. The results directly showed that $CaCO_3$ was subject to reaction with sulfate in the atmosphere and formed $CaSO_4 \cdot 2H_2O$ at the surface of the particle.

Chapter 4. Analysis of particles transported and trapped in Greenland ice core sample related to secular change of SO_2 emission

Calcium species in particles trapped mainly in spring in an ice core at southeast Greenland were analyzed by Ca K-edge XANES using micro X-ray beam. The ice core has a

record of aerosols from 1957 to 2014, and the samples corresponding to 1971, 1978, 1987, 1995, and 2004 were analyzed. As a result, $CaSO_4 \cdot 2H_2O$ fraction to total calcium in the ice core was larger in the recent layers (1995 and 2004) than those in the old layers (1971, 1978, and 1987), whereas $CaCO_3$ fraction indicated the opposite trend. The increase in $CaSO_4 \cdot 2H_2O$ was consistent with the increase of SO_2 annual emission in China. Since it was reported by several geochemical studies using Sr, Nd, and Hf isotopes that mineral dust from China containing a larger amount of $CaCO_3$ compared with other areas is transported to Greenland in spring (Bory et al., 2003, 2002), the present data suggested that $CaCO_3$ included in Chinese mineral dusts reacted with sulfur components emitted in China and formed $CaSO_4 \cdot 2H_2O$, which was recorded in the ice core.

Chapter 5. Sulfate aerosols collected in Noto peninsula: estimation of their species, sources, reaction process, and roles for CCN

Size-fractionated aerosol samples were collected at the head of Noto peninsula from July in 2017 to May in 2018. This sampling site faces to the Sea of Japan, therefore it is good for observation of aerosols transported form Asian continent. In this chapter, seasonal variation of sulfate species and their transportation process with emission sources and aging process were investigated about the size-fractionated aerosol samples. Sulfur K-edge XANES spectroscopy for the samples revealed size and seasonal variation of sulfate species in the aerosols. As a result, it was suggested that $CaSO_4 \cdot 2H_2O$ formation in the coarse particles caused large reduction of hygroscopic sulfate in the finer particles. Besides, emission source of sulfate aerosol was discussed using $[NO_3^-]/[nss{-}SO_4^{2-}]$ ratio, trace metal concentrations, and sulfur isotope compositions. Source of sulfate in coarse particles were mainly mineral particles and sea salts, and a part of them was considered to undergo reactions with anthropogenic sulfate components emitted from coal combustion in South China or domestic emission by oil combustion in Japan. On the other hand, sulfate sources of fine particles were considered to be biogenic emission and

oil combustion in Japan during summer. In winter and spring, effects of oil combustion in Japan and coal combustion in south China were independently observed. Additionally, in the light of particle diameter and sulfate species, it was possible to discuss not only sulfate sources but also aging effects during transportation in the atmosphere by the combination of size distribution of sulfate, its source analysis, and speciation of sulfate in aerosols.

Chapter 6. General discussion and conclusion

In this thesis, the maximum reduction fraction of hygroscopic sulfate by the formation of $CaSO_4 \cdot 2H_2O$ was estimated as 33% of total sulfate during spring, which in turn suggested that the number concentration of cloud droplet number concentration (CDNC) decreased by 15.1% according to the relationship of mass concentration of sulfate to CDNC reported in Seinfeld and Pandis (2016). The reduction of CDNC can change the radiative forcing by +0.35 W/m^2 at maximum which is comparable to absolute value of the radiative forcing due to the indirect cooling effect of aerosols reported by IPCC (2013). It is suggested that the effect of the formation of $CaSO_4 \cdot 2H_2O$ on the indirect radiative forcing by sulfate aerosol should not be ignored. In addition, the reaction of the sulfate with $CaCO_3$ provided from East Asia is suggested to increase the low hygroscopic fraction in the global sulfate budget. The interaction of cloud-aerosol related to the indirect radiative forcing has still large uncertainties. For accurate estimation of indirect radiative forcing and prospect of future climate, the observational studies such as this thesis is important to determine and to justify parameters needed for more accurate estimation and prospect.

Contents

Chapter 1.

Introduction of this thesis

1.1 Properties of atmospheric aerosols

Aerosols are particulate matters suspended in the atmosphere, and is one of important atmospheric components. Aerosols originate from (i) natural sources, such as eolian dust, sea spray, volcanic eruption, and vegetation, and (ii) anthropogenic activities such as fossil fuel combustion (e.g., Andreae and Rosenfeld, 2008; Calvo et al., 2012). Their physicochemical properties such as their particle size, morphology, and chemical composition are changeable depending on their emission sources and subsequent chemical processes. The emission and formation process of aerosols is categorized into 2 broad types; one is emitted directly as particles (primary particles) and other is formed in the atmosphere through gas-to-particle conversion processes (secondary particles) of vapor precursors (Whitby and Cantrell, 1976). Generally, the diameter of aerosols ranges from a few nanometers to below 100 μm and the particle size differs mainly depending on their emission and formation processes, which can be generally divided into (i) coarse particles (generally greater than 2.5 μm) consisting of primary particles that include natural particles (mineral particles, sea salt, volcanic ash, etc.) and anthropogenic particles emitted directory to the atmosphere (e.g., debris of paint materials on roads, brake pad etc.), and (ii) fine particles (generally less than 2.5 μm) which are mostly secondary particles mainly emitted from anthropogenic sources (Calvo et al., 2012; Seinfeld and Pandis, 2006). The particle diameter alters after emission to the atmosphere by various processes such as chemical reactions, condensation of vapor materials, evaporation of associated water, and coagulation with other particles. The aerosol size is an important factor to affect particle's lifetime in the atmosphere and their chemical and physical properties (Seinfeld and Pandis, 2006).

Aerosols contain various components both inorganic and organic materials (Calvo et al., 2012). Size distributions of elements and various compounds in aerosols differ depending on their sources and process of formation, transformation, and removal in/from the atmosphere. In

addition to the particle size, physicochemical properties such as concentration of elements and compounds, mixing state, chemical species, and isotope composition are important information to know emission and formation process, and to estimate their effects on the earth's environment and climate, human health, and atmospheric chemistry.

1.2 Aerosol's effect on the climate of the Earth

Aerosols have a direct and indirect radiative forcing to climate of the earth (e.g., Penner et al., 2011). The former is an effect that aerosols scatter and absorb solar and infrared radiation, which finally cools and warms the earth, respectively (Haywood and Boucher, 2000; Penner et al., 2011). In the latter case, aerosols act as cloud condensation nuclei (CCN) and ice nuclei (IN), which modifies cloud properties such as radiative properties and amount and lifetime of clouds (Albrecht, 1989; Forster et al., 2007; Lohmann and Feichter, 2010; Twomey, 1959). Ambient concentration of aerosols has been increased because of anthropogenic activities since the Industrial Revolution in 18^{th} century, which influenced the climate system by alteration of aerosol's radiation forcing. Indeed, the drastic increase of concentration of aerosol is one of strong factors to change earth's climate globally and locally during recent decades which has been presented by previous studies of ice core records (e.g., Fischer et al., 1998; Lavanchy et al., 1999).

The significant physicochemical properties of aerosols to determine the direct and indirect radiative forcing are the particle number concentration, particle size distribution, chemical composition, and mixing state (the extent of distribution of components among the particles) of aerosols. It is confidently considered that both direct and indirect radiative forcing of aerosols have large influence on the climate which totally offset global mean radiative forcing by greenhouse gases (IPCC, 2013). Storelvmo et al. (2016) estimated that the cooling effect by aerosols corresponds to about one third of the warming effects associated with greenhouse gases

emitted from 1964 to 2010, suggesting the significant impact of aerosols on the climate of the earth. However, the estimation of radiative forcing by aerosols in the latest IPCC report (2013) still has a large uncertainty especially in the indirect effect, though there was great improvement for the estimation methods after the last IPCC report (AR4; IPCC, 2007) according to the aerosol properties. The quantitative estimation of radiative forcing by aerosol is very difficult because (i) physicochemical properties of aerosols such as particle size and chemical compositions which greatly affect aerosol's lifetime and radiative effects have wide range, (ii) the conversion mechanism of precursors of aerosols into particles is not well understood, (iii) mass and number concentrations of aerosols in ambient air are greatly variable in space and time because of their short atmospheric lifetime (Penner et al., 2011). Therefore, quantitative understanding of aerosol's physicochemical properties and hence estimation of their radiative forcing is more difficult than that of greenhouse gases. Consequently, there is large variation in estimation results on the radiative forcing among different models and also between models and observations.

The indirect effect of aerosols is caused by acting as CCN to affect the cloud properties (Lohmann and Feichter, 2010; McFiggans et al., 2006; Penner et al., 2011). Increase of number concentration of CCN caused increase of number concentration of cloud droplets, which leads to enhancement of reflection of solar radiation by clouds when cloud thickness and liquid water content in cloud remain constant (Twomey, 1959). In addition, increase of number concentration of CCN reduces the precipitation efficiency, thus cloud lifetime and hence reflection of solar radiation of cloud are enhanced (Albrecht, 1989). However, the aerosol-cloud interaction or the indirect forcing still has the largest uncertainties in the estimate as noted above (IPCC, 2013). CCN behavior of aerosols is determined by the water saturation ratio in ambient and ability of aerosols to absorb enough water. The particle's ability of the latter largely depends on particle size and content of hygroscopic components (McFiggans et al., 2006). Köhler theory (Köhler, 1936)

described the CCN activity based on the relationship between critical supersaturation and diameter of droplet determined by physicochemical property of particles such as mass and density of solute and water, diameter of a dry particle, molecular weight, and activity coefficient. Petters and Kreidenweis (2007) introduced hygroscopic parameter, κ, to Köhler theory (κ-Köhler theory). The value of κ is described by parameters only depending on chemical components, and κ of each particle is given by simple mixing of volume ratio of several species, their κ value, and dissolved faction in a particle, but not depends on the particle size (Petters and Kreidenweis, 2008, 2007). Therefore, κ-Köhler theory is widely used to discuss CCN activity of aerosols focusing on their chemical components. The value of κ or degree of hygroscopicity varies greatly among chemical species. Interaction between aerosol particles and cloud droplets is one of most poorly understood issue to estimate the indirect effects of aerosols (Boucher and Lohmann, 1995). Therefore, understanding of chemical compositions and their mixing state is necessary to estimate CCN activity of aerosols in the atmosphere and hence describe cloud droplets formation process accurately.

1.3 Sulfate aerosols

Sulfate is a major component in tropospheric aerosols which accounts for about 10 to 30% by mass of main components of aerosols at various sites (Boucher and Randall, 2013), which is mainly formed secondarily in the atmosphere through either aqueous or gaseous phase reactions from precursor gases such as sulfur dioxide (SO_2) (e.g., Seinfeld and Pandis, 2006). At present, SO_2 is dominantly emitted by anthropogenic activities as fossil fuel combustions which accounts for about 72% of total SO_2 global emission and partly from biomass burning (about 2%). Besides, natural sources of SO_2 are dimethyl sulfate (DMS) emitted by marine phytoplankton (about 19%) and volcanic emission (about 7%). These emission estimates are summarized in Haywood and

Boucher (2000), and Forster et al. (2007). Since the Industrial Revolution, anthropogenic emission of SO_2 has rapidly increased globally. In recent decades, the emission of SO_2 in Europe and USA decreased after 1980s and the global emissions are suggested to decrease in recent years. However, the amounts from Asia and other developing countries have increased during the same period (e.g., Crippa et al., 2016; Smith et al., 2011; Streets et al., 2003). Because of its relatively short lifetime in the atmosphere due to the removal by deposition (24 to 56% of emitted SO_2 is removed from the atmosphere), the proportion varies dependent on the type of models used for estimation. The rest of SO_2 remaining in the atmosphere is mostly oxidized to sulfate aerosol (Penner et al., 2011).

In the atmosphere, the amount of sulfuric acid in the gas phase is negligibly small, , ammonium sulfate ($(NH_4)_2SO_4$) in the solid and aqueous phases is preferentially formed as sulfate species (Seinfeld and Pandis, 2013). Emission amount of ammonia from Asia and other developing countries have increased during the same period in recent years in common with SO_2 (Crippa et al., 2016). It is widely considered that sulfate in aerosols are mostly neutralized by ammonia because the global mean ammonium to sulfate equivalent ratio (NH_4^+/SO_4^{2-}) in the atmosphere is approximately one (Adams et al., 1999). Therefore, the sulfate is mainly present as $(NH_4)_2SO_4$, sulfuric acid (H_2SO_4), and intermediate compounds such as NH_4HSO_4 depending on the availability of ammonium to react with sulfate. Besides, sulfate is found mostly in fine particles, because sulfate is formed by gas-to-particles reaction in the atmosphere (Seinfeld and Pandis, 2006). Sulfate is expected to contribute largely to direct cooling effect of aerosol by light scattering (Boucher and Lohmann, 1995), while sulfate is also considered to act well as CCN, because $(NH_4)_2SO_4$ has a high hygroscopicity. Effective radiative forcing of aerosols estimated either from all anthropogenic aerosols or from sulfate aerosol only was estimated using various models in IPCC (2013), but the difference between the two estimation results is generally small

(Boucher and Randall, 2013). Consequently, Storelvmo et al. (2016) suggested that warming by 0.5℃ in Arctic region since 1980 was related to decrease of emission of sulfate in Europe. These results indicate a significant role of sulfate in radiation forcing by aerosols.

1.4 Mineral dusts and its influence on sulfate aerosols

As referred above, content of hygroscopic sulfate species such as $(NH_4)_2SO_4$ in aerosols is an important factor to determine CCN activity. Therefore, sulfate aerosols generally have large contribution to indirect cooling effect acting as CCN in terms of their large emission amounts, size distribution in the atmosphere, and chemical species in aerosols. However, chemical reactions in the atmosphere have a possibility to change the species and size distribution of sulfate aerosols, which enhances or suppresses CCN activity of the particles.

One of important reactants with acids (e.g., SO_2, H_2SO_4, HNO_3) in the atmosphere is mineral particles. Mineral particles are one of main components in aerosols, which account for about 30% of total aerosol emission amount by mass globally (Satheesh and Moorthy, 2005) and have impacts on direct and indirect radiative forcing (Usher et al., 2003). Mineral dusts contain various mineral components. The surface of mineral particles is considered as an important reaction site with gases and droplets in the atmosphere, and various reaction processes have been investigated by numerous studies mainly by laboratory experiments (e.g., Goodman et al., 2000; Usher et al., 2003; Ma et al., 2013, 2012; Ma and He, 2012; Sullivan et al., 2009; Tang et al., 2015). Observational studies suggested that the reaction forms secondary materials at particle surfaces (Li and Shao, 2008; Matsuki et al., 2009; Ooki and Uematsu, 2005; Takahashi et al., 2008a). Thus, the chemical reactions can change mineral components and hence converts their physiochemical properties such as hygroscopicity, or CCN activity of the particles. Calcite ($CaCO_3$) is a reactive component of mineral particles with acids because of its high alkaline

property (Al-Hosney and Grassian, 2005; Rubasinghege and Grassian, 2013; Usher et al., 2003). For example, reaction of $CaCO_3$ with HNO_3 or HCl forms calcium nitrate and calcium chloride, respectively, which in turn increases CCN activity due to the high hygroscopicity of the reaction products whose hygroscopic parameters (κ) are more than 100 times higher than that of $CaCO_3$ (Sullivan et al., 2009; Tang et al., 2015). By contrast, the reaction of $CaCO_3$ with SO_2 and/or sulfate forms gypsum ($CaSO_4 \cdot 2H_2O$), which has a low hygroscopic nature equivalent to $CaCO_3$ (Gu et al., 2017; Ma et al., 2013). Therefore, $CaSO_4 \cdot 2H_2O$ formation does not induce enhancement of CCN activity of mineral particles. Instead, it is considered that if sulfate is present as $CaSO_4 \cdot 2H_2O$ in aerosol instead of $(NH_4)_2SO_4$, the formation of $CaSO_4 \cdot 2H_2O$ should decrease CCN activity of sulfate aerosols due to the lower hygroscopicity of $CaSO_4 \cdot 2H_2O$ than $(NH_4)_2SO_4$. More importantly, $CaSO_4 \cdot 2H_2O$ formation should decrease number concentration of hygroscopic sulfate such as $(NH_4)_2SO_4$ in the atmosphere due to uptake of SO_2 (a precursor of sulfate) and/or sulfate by $CaCO_3$ in mineral particles; this causes (i) decrease of hygroscopic sulfate due to uptake by $CaCO_3$ and (ii) suppression of formation and growth of hygroscopic sulfate due to decrease of the amount of SO_2 and/or H_2SO_4. In addition, $CaCO_3$ in mineral particles originally have a lager particle diameter, whereas the hygroscopic sulfate is mainly present in fine particles. Therefore, $CaSO_4 \cdot 2H_2O$ formation would decrease fine sulfate aerosols, altering their size distribution. These effects lead to reduction of CCN concentration in the atmosphere, and hence influence evaluation of indirect cooling effects of aerosols. Therefore, quantitative understanding of chemical species mainly focusing on hygroscopicity, their mixing fraction in ambient particles, and size distribution of the particles is strongly needed. Several state-of-the art models have been constructed to explain mineral-sulfate interactions, but still there is lack of knowledge on chemical species and their size distributions (Manktelow et al., 2010).

1.5 East Asia: its significance as a research field

Indirect radiative forcing of aerosols differs substantially, depending on regions (Lohmann and Feichter, 2010). East Asia is the highest emission source of anthropogenic SO_2 by fossil fuel combustion in global scale during the last few decades (IPCC, 2013; Crippa et al., 2016; Qu et al., 2016). Besides, East Asia is the second largest emission source of mineral particles next to the Sahara Desert (Kellogg and Griffin, 2006; Usher et al., 2003). Major mineral compositions of Asian mineral dust are clay minerals, mica, feldspar, quartz, and calcite (Nishikawa et al., 2000). A unique characteristic of mineral dust composition in East Asia is its $CaCO_3$ content much higher than those in other regions (Krueger et al., 2004). As mentioned above, reaction of $CaCO_3$ in mineral particles with SO_2 and/or sulfate can change physicochemical properties of sulfate aerosol, which affects CCN activity of sulfate aerosol and indirect radiative forcing. Therefore, it is necessary to investigate sulfate species in aerosols in the atmosphere including their reaction and transportation processes in East Asia which has the highest concentrations of anthropogenic sulfate and mineral particles. These components also have large impacts on the indirect effects regionally and globally. However, direct and quantitative researches of sulfate aerosol species and interaction between sulfate and mineral particles are not enough, while the interaction has been suggested in numerous laboratory experiments and modeling studies. Therefore, this thesis focused on speciation of several elements including sulfur in aerosols.

1.6 Chemical speciation analysis of various elements in aerosols

In this thesis, X-ray absorption fine structure (XAFS) spectroscopy was applied as a main analytical method of identification of chemical species in the samples, which is a direct speciation method to clarify chemical state of a target element in the sample such as valence,

electronic state, elements of the ligands, and interatomic distances.

1.6.1 General information of XAFS

Each element has an inherent binding energy of the specific electron to the nucleus. When incident X-ray energy corresponds to the binding energy of a core electron, the core electron is excited, and absorption probability of X-ray rapidly increases. The energy is called as absorption edge. XAFS is a fine structure in the X-ray absorption spectrum (XAS) appeared in the higher energy region from the absorption edge.

XAFS is divided into X-ray absorption near edge structure (XANES) and extended X-ray absorption fine structure (EXAFS) by their energy ranges from the absorption edge of the electron of the target elements. XANES is the fine structure at the vicinity of absorption edge energy range (~ around 50 eV), which reflects valence and electronic state of the target element. Features of the structure depends on resonance electron transition and also on multiple-scattering of photoelectrons ejected at low kinetic energy level. EXAFS is the structure found in the energy range above 1000 eV from the absorption edge, which reflects interatomic distances and coordination numbers of surrounding atoms. In this thesis, XAENS was applied to aerosol samples to identify the counter ion of target elements in the samples. There are several methods to obtain the spectra described bellows.

1.6.2 Transmission mode

XAFS spectrum is variation of absorption depending on energy of incident X-ray. Absorbance of X-ray is expressed as follows:

$$\mu t(E) = \ln\left(\frac{I_0(E)}{I(E)}\right)$$

$$I(E) = I_0(E)\exp(-\mu t)$$

where $I_0(E)$ is an intensity of incident X-ray at certain energy (= E), $I(E)$ is an intensity of transmitted X-ray, μ is a linear absorption coefficient (cm^{-1}), and t is thickness of the sample (cm).

Transmission mode is a method strictly following the fundamental X-ray absorption phenomenon. However, samples need to be prepared to have appropriate thickness and concentrations of the target element, which is subject to limitation in the detection ability, or sensitivity. In addition, it is difficult to measure sulfur XAFS spectra, focused in this thesis, by the transmission mode, because the binding energy of 1s electron of sulfur is at lower energy region (soft X-ray region). In the soft X-ray region, the incident and transmitted X-ray is absorbed readily by air and the sample itself, which makes it difficult to be measured by X-ray detectors (e.g., ion chambers).

1.6.3 Fluorescence yield (FY) mode

X-ray fluorescence arises secondarily when the target elements is excited by incident X-ray. There is a relationship between intensity of X-ray fluorescence and absorption coefficient (μ) as below:

$$I_f = I_0 \alpha \left(\frac{\mu_x(E)}{\mu_T(E) + \mu_T(E_f)} \right) \left[1 - \exp\left\{ -\left(\mu_T(E) + \mu_T(E_f) \right) t \right\} \right]$$

where I_f is an intensity of fluorescence X-ray, I_0 is an intensity of incident X-ray, α is fluorescence quantum yield, μ_T is a full linear absorption coefficient of a sample (cm^{-1}), μ_x is a linear absorption coefficient of a target element (cm^{-1}), E is energy of incident X-ray, E_f is energy of fluorescence X-ray, t is thickness of a sample (cm). When (i) $\mu_T(E) + \mu_T(E_f) << 1$ (= infinitely thin limit), or (ii) $(\mu_T(E) + \mu_T(E_f))t >> 4.6$ (= infinitely thick limit) are accepted, I_f is proportional to μ_x ($I_f = \mu_x t I_0$), which can be treated as the degree of absorption when normalized by incident X-ray (= $\mu t(E)$). FY mode has high sensitivity, which enables us to measure samples with low concentration of target elements. In this study, fluorescence X-ray is detected by Lytle detector, or the fluorescent ion chamber detector which measures fluorescent x-ray emission.

1.6.4 Conversion electron yield (CEY) mode

When the sample is exposed to incident X-ray, Auger electrons which is defined as electrons with energy below 40 eV (Schroeder, 1996) and subsequent secondary electrons are

emitted from the target element, which are measured in the CEY mode. Auger electrons are released due to transition of excess energy caused by inner shell transition. Therefore, variation of the intensity of the Auger and secondary electrons depending on the energy of incident X-ray becomes similar to XAFS spectrum detected by the transmission mode. The escape depth of auger electrons is very shallow by up to sub-micron. Therefore, the information of the XAFS spectra measured in CEY mode are sensitive to the surface of the samples. In the CEY mode, we detect current between the sample and an electrode close (about 2-3 cm) to the sample in a chamber purged with helium (He) which can contribute to amplification of the signal. The voltage bias loaded between the electrode and the sample is usually 100 V in this study.

1.7 Purpose of this thesis

The following three issues are the main purposes of this thesis:

1. To reveal sulfate species in aerosols and their concentrations in the atmosphere, which unravels content ratio of each species with various hygroscopicity.
2. To estimate effects of $CaSO_4 \cdot 2H_2O$ formation in the particles on the properties of sulfate aerosols including (i) variation of CCN activity of sulfate aerosol in total, (ii) number concentration and production amount of hygroscopic sulfate species, and (iii) size distribution of sulfate aerosols.
3. To examine sulfate emission sources and reaction and aging processes during transportation.

To accomplish the purposes above, two approaches were mainly employed in this thesis:

1. To collect and use various samples for certain purposes; filter-base aerosol samples with 7 size fractionated collection at four sites in East Asia and ice core drilled at

Greenland.

2. To apply direct speciation method, X-ray absorption fine structure (XAFS) spectroscopy was employed as a main analytical method for the speciation of sulfate and other elements in the samples.

Chapter 2.

Sulfate species in aerosols and their formation process

This chapter has been published in the following paper: C. Miyamoto, K. Sakata, Y. Yamakawa, and Y. Takahashi, Determination of calcium and sulfate species in aerosols associated with the conversion of its species through reaction processes in the atmosphere and its influence on cloud condensation nuclei activation, Atmospheric Environment, published, https://doi.org/10.1016/j.atmosenv.2019.117193

2.1 Chapter Introduction

Aerosols affect the global climate due to their influence on radiative forcing, causing global warming and cooling effects (Penner et al., 2011). One of the cooling effects is caused indirectly by hygroscopic aerosols acting as cloud condensation nuclei (CCN), but the quantitative evaluation of such effect has not yet been achieved (Lohmann and Feichter, 2010; Seinfeld and Pandis, 2006; Sun and Ariya, 2006). Chemical species is an important parameter in determining the physicochemical properties of aerosols, such as its hygroscopicity. Therefore, species and their concentrations in aerosols must be clarified to estimate the degree of the indirect cooling effect. Sulfate aerosol, one of the major components of aerosols formed by the oxidization of sulfur dioxide (SO_2) in the atmosphere, is considered an important component of CCN because it primarily consists of hygroscopic species, such as ammonium sulfate ($(NH_4)_2SO_4$) in the atmosphere (Pilinis et al., 1987; Wang et al., 2008).

Mineral particles are major components of aerosols. Some mineral particles can also act as CCN and ice nuclei. The surface of mineral particles is an important reaction site with gases and droplets in the atmosphere (Dentener et al., 1996; Tang et al., 2017a; Usher et al., 2003). The reaction forms secondary species and converts their physicochemical properties from low to high hygroscopicity, increasing the CCN activity of aerosols. Calcite ($CaCO_3$) is one of the major components of mineral aerosols (Jeong, 2008; Usher et al., 2003). $CaCO_3$ is reactive with acids in the atmosphere due to its alkaline property (Al-Hosney and Grassian, 2004; Rubasinghege and Grassian, 2013). The reaction of $CaCO_3$ with SO_2 and/or sulfate forms gypsum ($CaSO_4{\cdot}2H_2O$), which has low hygroscopic nature (Gu et al., 2017; Ma et al., 2013). $CaSO_4{\cdot}2H_2O$ is also formed after the drying of a droplet that contains Ca^{2+} and SO_4^{2-}. SO_2 is mostly converted to sulfate in the atmosphere in gas or droplet phase, which mostly consists of $(NH_4)_2SO_4$. Therefore, the formation of $CaSO_4{\cdot}2H_2O$ reduces the atmospheric concentration of hygroscopic species acting

as CCN in the atmosphere. Thus, sulfate species in aerosols must be elucidated to estimate the contributions of aerosols to the indirect cooling effect because their CCN activity differs substantially depending on their chemical species. These species can be altered through heterogeneous reactions in the atmosphere.

Asian dust is originated from arid areas and deserts in China and Mongolia such as Gobi and Taklimakan Deserts (Seinfeld and Pandis, 2006). One of the characters of the mineral composition of Gobi and Taklimakan Deserts is high content of $CaCO_3$ (Krueger et al., 2004). The Asian mineral particles are extensively transported by winds through urban regions in East Asia, for example, large cities in China, Korea, and Japan. On the other hand, East Asia is one of the significant regions of high SO_2 emission since 1950s because of fossil fuel combustion (e.g., Smith et al., 2011). $CaCO_3$ fraction in mineral dust is considered to change by reaction with anthropogenic SO_2 and/or sulfate and form $CaSO_4 \cdot 2H_2O$ during transportation, which will change sulfate species in aerosol and hygroscopicity.

In this section, total suspended particles (TSP) in the atmosphere were collected for 1 year in Higashi–Hiroshima in southwestern Japan. Besides, size-fractionated aerosol samples (seven fractions) were obtained during each season. The sampling site was affected by materials transported from China, which largely contributed to the global emission of SO_2 (Crippa et al., 2016; Ohara et al., 2007; Smith et al., 2011; Streets et al., 2003). Sulfate and Ca species in aerosols were determined by X-ray absorption near-edge structure (XANES) analysis based on previous studies (Takahashi et al., 2006, 2009). Subsequently, the contribution of these components to CCN activity was estimated based on speciation results and hygroscopicity parameters. This chapter is important to understand the formation process of secondary components in particles which can increase or decrease CCN activities of mineral particles suggested in laboratory experiments and modeling studies (Dentener et al., 1996; Goodman et al., 2000; Ma et al., 2013)

through the analysis of actual aerosol samples in the atmosphere on the basis of the speciation of both sulfur (S) and Ca in aerosols. Such processes will be eventually linked to the degree of cooling effect altered by the reactions between sulfate and $CaCO_3$ in mineral dusts.

2.2 Materials and Methods

2.2.1 Aerosol samples collected in Higashi−Hiroshima

Total suspended particle (TSP) samples without size-fractionation were collected at Hiroshima University, Higashi–Hiroshima (34°40′ N, 132°71′ E; Fig. 2.1) from September 2012 to August 2013 using a high-volume air sampler (HV-500, Shibata, Tokyo, Japan) loaded with polyflon filters (PF050, Advantec, Tokyo, Japan). Each sampling period for the TSP samples was typically 1 week. The details of the 33 TSP samples analyzed in this thesis are described in Table 2.1.

Size-fractionated aerosol samples were also collected at the same sampling site during winter (January 21 to 30, 2013), spring (March 4 to 9, 2013), summer (July 22 to August 5, 2013), and fall (November 11 to 25, 2013). The sampling period for the four samples was 2 weeks. The samples were collected using a high-volume air sampler (MODEL-123SL, Kimoto, Japan) with a 7-stages cascade impactor (TE-236, Tisch Environmental Inc., USA). The classification of particle diameter was as follows: >10.2 μm (sampling stage 1; average diameter is 15 μm), 4.2–10.2 μm (stage 2; 7.2 μm), 2.1–4.2 μm (stage 3; 3.2 μm), 1.3–2.1 μm (stage 4; 1.7 μm), 0.69–1.3 μm (stage 5; 1.0 μm), 0.39–0.69 μm (stage 6; 0.54 μm), and < 0.39 μm (backup filter; 0.24 μm). The filters used for the samplings were cellulose (stages 1–6: TE-230WH, Tisch Environmental, Inc., USA; backup filter: 8 inches ×10 inch, Whatman, USA). In this chapter, the four upper stages (stages 1–4) were identified as coarse particles (average diameter: ≥1.0 μm), and the three lower

stages were identified as fine particles (average diameter: <1.0 μm). The details of the sampling information are described in Table 2.2.

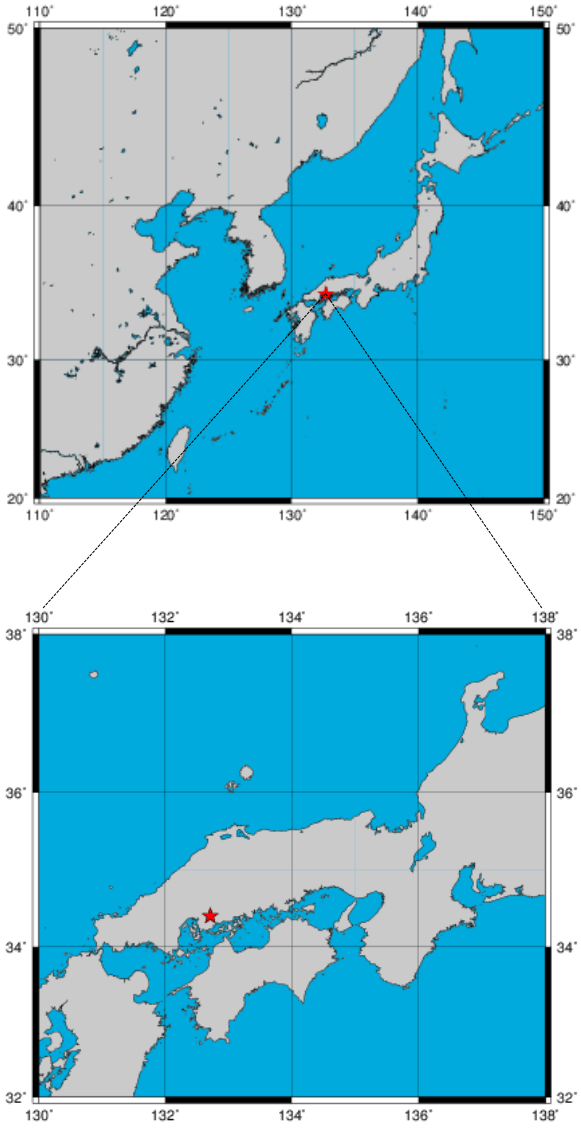

Fig. 2.1. Sampling site: Hiroshima University located at 34˚40’N, 132˚71’E).

Table 2.1. Sampling information of TSP samples.

Sample No.	Time	Period	Total volume (m^3)
Fall-1	3 days	2012. 9.5-9.8	3309.0
Fall-2	3 days	2012.9.8-9.11	3175.0
Fall-3	7 days	2012.9.11-9.18	5718.0
Fall-4	4 days	2012.9.18-9.22	2863.6
Fall-5	7 days	2012.9.22-9.29	5628.5
Fall-6	7 days	2012.9.29-10.6	6479.7
Fall-7	6 days	2012.10.6-1.6	3787.3
Fall-8	7 days	2012.10.23-10.29	4553.2
Fall-9	5 days	2012.10.29-11.3	4023.3
Fall-10	5 days	2012.11.12-11.17	4055.4
Fall-11	5 days	2012.11.26-12.1	3650.8
Winter-1	5 days	2012.12.10-12.15	4025.3
Winter-2	5 days	2012.12.24-12.29	3934.4
Winter-3	5 days	2013.1.7-1.12	3806.3
Winter-4	5 days	2013.1.21-1.26	3826.5
Winter-5	2 days	2013.1.30-2.1	1752.3
Winter-6	5 days	2013.2.4-2.9	4045.4
Winter-7	5 days	2013.2.18-2.23	4075.2
Spring-1	5 days	2013.3.4-3.9	2908.9
Spring-2	5 days	2013.3.9-3.14	4075.2
Spring-3	4 days	2013.3.18-3.22	3013.1
Spring-4	5 days	2013.3.25-3.30	4036.8
Spring-5	5 days	2013.4.1-4.5	3446.6
Spring-6	5 days	2013.4.8-4.13	3773.7
Spring-7	5 days	2013.4.22-4.27	3888.5
Spring-8	5 days	2013.4.27-5.2	4038.4
Spring-9	5 days	2013.5.13-5.18	4075.2
Spring-10	5 days	2013.5.27-6.1	3988.7
Summer-1	5 days	2013.6.10-6.15	3628.1
Summer-2	5 days	2013.6.24-6.29	4059.6
Summer-3	5 days	2013.7.8-7.13	3914.9
Summer-4	5 days	2013.7.22-7.27	4072.9
Summer-5	5 days	2013.8.5-8.10	4075.3
Summer-6	4 days	2013.8.19-8.23	2969.6

Table 2.2. Sampling information of size-fractionated samples (only RH is data measured at Hiroshima city).

Sample	Period	Time	Total volume (m^3)	Average temperature (ºC)	Total precipitation (mm)	Average RH (%)
Winter	2013.1.21-1.30	9 days	7624.5	1.6	16.5	66.6
Spring	2013.3.4-3.9	5 days	4840.2	8.6	0.00	61.0
Summer	2013.7.22-8.5	14 days	11429.0	26.7	17.5	70.7
Fall	2013.11.11-11.25	14 days	11698.3	7.5	38.5	66.4

2.2.2 Major ions in the aerosol samples measured by ion chromatography

Water-soluble major ions (Na^+, K^+, NH_4^+, Mg^{2+}, Ca^{2+}, F^-, Cl^-, NO_3^-, and SO_4^{2-}) in the aerosol samples were measured by ion chromatography (ICS-1100, Dionex, Japan). The twentieth part of one filter (approximately 0.1 g) of the size-fractionated aerosol samples was soaked in a polypropylene (PP) beaker with 5 mL of ultrapure pure water (MQ; >18.2 MΩ, Merck Millipore, MA, USA). An equivalent section of the filter (approximately 0.1 g) was used for the same procedure for the TSP samples. The major ions were leached out by ultrasonic treatment for 30 minutes. Polypropylene beakers used in this process were washed with MQ in advance, and the background of the filters was negligibly lower than those measured for the samples. This analytical method followed previous studies (Sakata et al., 2014). Sources of K^+, Ca^{2+}, Mg^{2+}, and SO_4^{2-} are generally derived from sea salt (ss) and other sources, thus concentrations of these ions of non-sea salt (nss) origins were calculated as follows:

$$[\text{nss-}X]_{\text{aerosol}} = [\text{Total-}X]_{\text{aerosol}} - ([X]/[\text{Na}])_{\text{seawater}} \times [\text{Na}]_{\text{aerosol}}, \quad (1)$$

where X is either K^+, Ca^{2+}, Mg^{2+}, or SO_4^{2-}.

2.2.3 Analysis of sulfate and calcium species in aerosols by X-ray absorption fine structure (XAFS) spectroscopy

2.2.3.1 Sulfur K-edge XANES

Sulfur chemical species in the aerosol were analyzed by XANES spectroscopy according to Takahashi et al. (2006). The measurements were conducted at BL-9A in the Photon Factory, a synchrotron radiation facility of High Energy Accelerator Research Organization (KEK), in Tsukuba, Japan. Energy calibration for S K-edge was conducted at the peak of the XANES spectrum of native sulfur at 2472.0 eV. X-ray beam was applied directory to particles collected on the sampling filter or separated particles dispersed on carbon tape (Cat. No.731, Nisshin EM Co.,Ltd., Japan) from the sampling filter.

To estimate fractions of each sulfate species in particles, XANES spectrum of each sample was fitted by a model spectrum obtained by a linear combination of reference materials which are expected to exist in aerosols such as sodium sulfate ($Na_2SO_4 \cdot 10H_2O$), ammonium sulfate ($(NH_4)_2SO_4$), ammonium hydrogen sulfate (NH_4HSO_4), and sulfate solution as a hydrated state of sulfate (hydrated-SO_4^{2-}). The sulfate compounds other than the solution were purchased from Wako Pure Chemicals of analytical grade (Japan). Hydrated-SO_4^{2-} was prepared by dissolving $Na_2SO_4 \cdot 10H_2O$ in ultrapure water and measured as a solution. The others were prepared in powdered state and measured. The fitting analysis were conducted by minimizing the sum of squares between the spectra of sample and model using an analysis software for XAFS, REX2000 (Rigaku Co., Japan). The goodness of fit was evaluated using the *R* value related to the residual between the measured and model spectra as follows:

$$R = \frac{\left(\sum_{E=E_1}^{E_2}\left(I_M(E) - I_S(E)\right)^2\right)^{1/2}}{\left(\sum_{E=E_1}^{E_2} I_M(E)^2\right)^{1/2}}, \quad (2)$$

where I_S and I_M is the absorption of the fitted and measured spectra, respectively; and E_1 and E_2 are the start and end values of the fitting energy range, respectively.

The fitting energy region was 2482–2500 eV based on Takahashi et al. (2006). Generally, spectral fitting analysis of XANES was focused on an energy range before and after the absorption edge where differences of structure among various species are significant. Sulfur components in aerosols are mainly present as sulfate (S(VI)) and the absorption structures around absorption peak of various sulfate species are very similar. In contrast, sulfates spectra have clear differences among various species particularly in the energy region after the main XANES peak depending on its counter cation. Therefore, 2482–2500 eV was employed as a fitting energy region in this thesis to determine sulfate species. These experimental conditions are listed in Table 2.3. Sulfur XANES spectra of reference materials as candidates for sulfate in aerosols are shown in Fig. 2.2a.

Table 2.3. Experimental conditions for sulfur and calcium speciation by XAFS.

	Sulfur	Calcium
Absorption edge	K edge	K edge
Electron binding energy	2472.0 eV	4028.5 eV
Calibration material	Native sulfur (peak top)	$CaCl_2 \cdot 2H_2O$ (peak top)
Calibration energy	2472.0 eV	4038.1 eV
Fitting energy range	2482–2500 eV	4027–2080eV
Experiment station	PF BL-9A	PF BL-9A
Reference materials	$CaSO_4 \cdot 2H_2O$ $Na_2SO_4 \cdot 10H_2O$ $(NH_4)_2SO_4$) NH_4HSO_4 hydrated-SO_4^{2-}	$CaCO_3$ $CaC_2O_4 \cdot 2H_2O$ $CaCl_2 \cdot 2H_2O$ $Ca(NO_3)_2 \cdot 4H_2O$ $CaSO_4 \cdot 2H_2O$

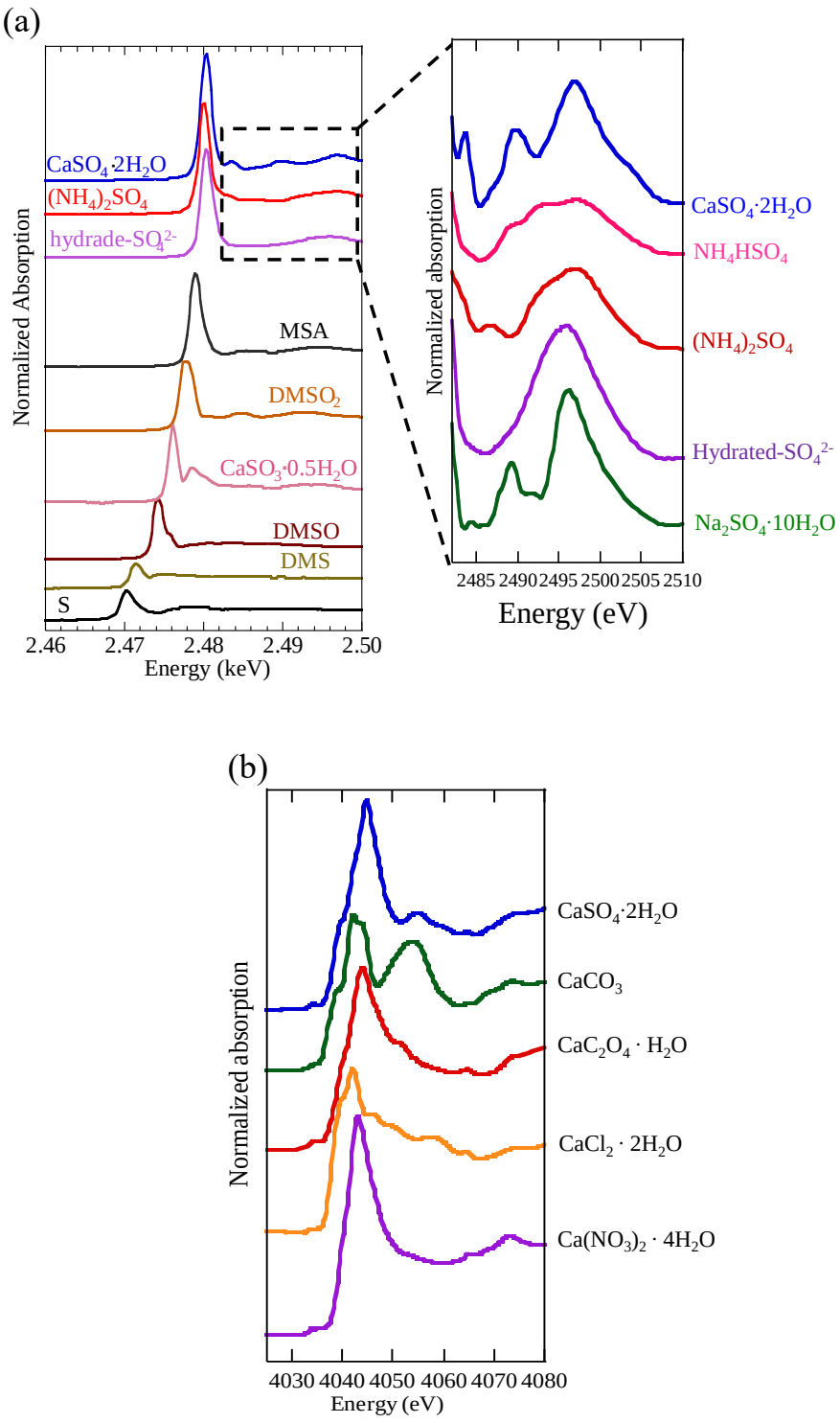

Fig. 2.2. XANES spectra of reference materials of sulfur (a) and calcium (b).

2.2.3.2 Calcium K-edge XANES

Calcium chemical species in the aerosol samples were analyzed by Ca K-edge XANES spectroscopy using a similar method as sulfur K-edge XANES. Energy calibration for Ca K-edge was conducted at the peak of the XANES spectrum of $CaCl_2 \cdot 2H_2O$ as 4038.1 eV. Reference materials obtained from Wako pure Chemicals used for the fitting analysis were as follows: calcite ($CaCO_3$), calcium oxalate dihydrate ($CaC_2O_4 \cdot 2H_2O$), calcium chloride dihydrate ($CaCl_2 \cdot 2H_2O$), calcium nitrate tetrahydrate ($Ca(NO_3)_2 \cdot 4H_2O$), and $CaSO_4 \cdot 2H_2O$. All of them were measured in the powdered state. Fitting energy region was 4027–2080eV based on previous studies (Takahashi et al., 2009, 2008b). These experimental conditions are also listed in Table 2.3. Additionally, to confirm the reaction on the surface of the particles, we simultaneously measured the XANES spectra of the samples both in fluorescence yield (FY) mode and conversion electron yield (CEY) modes. FY–XANES can be regarded as a bulk method, because its probing depth is greater than 6.5 μm. By contrast, CEY–XANES is surface sensitive with a probing depth of less than 0.25 μm (Schroeder, 1996). Calcium XANES spectra of reference materials as candidates for Ca species in aerosols are shown in Fig. 2.2b.

2.2.4 Calculation of the hygroscopicity parameter (κ)

The CCN activity of aerosol can be estimated based on κ-Köhler theory, which explains the saturation ratio of water vapor as a function of the diameter of the droplet (particles containing water) (Petters and Kreidenweis, 2007). The saturation ratio (S) of an aqueous solution droplet can be calculated using Köhler theory and expressed by the following equation:

$$S = a_w exp\left(\frac{4\sigma_{s/a}M_w}{RT\rho_w d_{wet}}\right), \quad (3)$$

where a_w is the activity of water, $\sigma_{s/a}$ the surface tension of the solution/air interface, M_w the molar weight of water, R the universal gas constant, T the temperature, ρ_w the density of water, and d_{wet}

the diameter of the droplet. Petters and Kreidenweis (2007) proposed the hygroscopicity parameter κ with the relationship between a_w and κ as described by the following equations:

$$\frac{1}{a_w} = 1 + \kappa \frac{V_{dry}}{V_{water}}, \quad (4)$$

$$a_w = \frac{d_{wet}^3 - d_{dry}^3}{d_{wet}^3 - d_{dry}^3(1-\kappa)}, \quad (5)$$

where V_{dry} and V_{water} are the volumes of dry particulate matter and water, respectively. The κ value depends on the chemical composition of the particle, which varies from 0 to a maximum of ~1.4; for example, the value for sodium chloride (NaCl) is 1.28. A low κ value indicates low hygroscopicity or low activation as CCN. When a particle consists of several components, κ is described as follows:

$$\kappa = \sum_i \varepsilon_i \kappa_i, \quad (6)$$

Where ε_i is the volume ratio of component i in the dry particle. The κ value of each component was determined in previous studies (Petters and Kreidenweis, 2007; Sullivan et al., 2009) which are shown in Table 2.4. In the current chapter, the κ value of the size-fractionated samples was calculated using Eq. (6) from the κ_i reported in previous studies and the ε_i of each species calculated using its molar weight, density, and mole ratio determined by the XANES analysis.

Table 2.4. Hygroscopicity parameters of each species (κ_i)

Species	κ_i
$Ca(NO_3)_2 \cdot 4H_2O$	0.43 [a]
$CaCl_2 \cdot 2H_2O$	0.68 [a]
$CaCO_3$	6.8×10^{-3} [a]
$CaC_2O_4 \cdot H_2O$	6.0×10^{-3} [a]
$CaSO_4 \cdot 2H_2O$	7.8×10^{-3} [a]
$(NH_4)_2SO_4$	0.61[b]
NH_4HSO_4	0.93
$Na_2SO_4 \cdot 10H_2O$	0.80
$C_2O_4H_2 \cdot H_2O$	0.71 [a]
NH_4NO_3	0.67[b]
NaCl	1.28[a,b]

[a] Sullivan et al. (2009), [b] Petters and Kreidenweis (2007)

2.2.5 Back trajectory analysis

Back trajectory analysis was conducted using the hybrid single-particle Lagrangian integrated trajectory model (HYSPLIT) (Stein et al., 2015) to identify the pathway of the air mass arriving at an altitude of 1000 m above ground level (AGL) at the sampling site during each sampling period. Each trajectory was traced back for 72 h.

2.3 Results and Discussion

2.3.1 TSP samples

2.3.1.1 Transport pathway of air mass reaching to Higashi-Hiroshima

Back trajectory analysis was conducted to know seasonal variation of transport pathways of air mass that reached Higashi-Hiroshima during each sampling period (Fig. 2.3). During the periods from winter to spring, air mass came from the Asian continent, which was mainly transported from the west or northwest China and Mongolia, then passed through industrial areas in coastal China and Korean Peninsula. Besides, transportation distance for 72 hours from winter to spring was generally longer than that during fall and summer. In contrast, during summer, air mass hardly came through the Asian continent. Air mass was transported from various directions in the fall. In early fall, the tendency of its transportation pathway was similar to that in summer and gradually changed the pathway to that from the Asian continent toward winter.

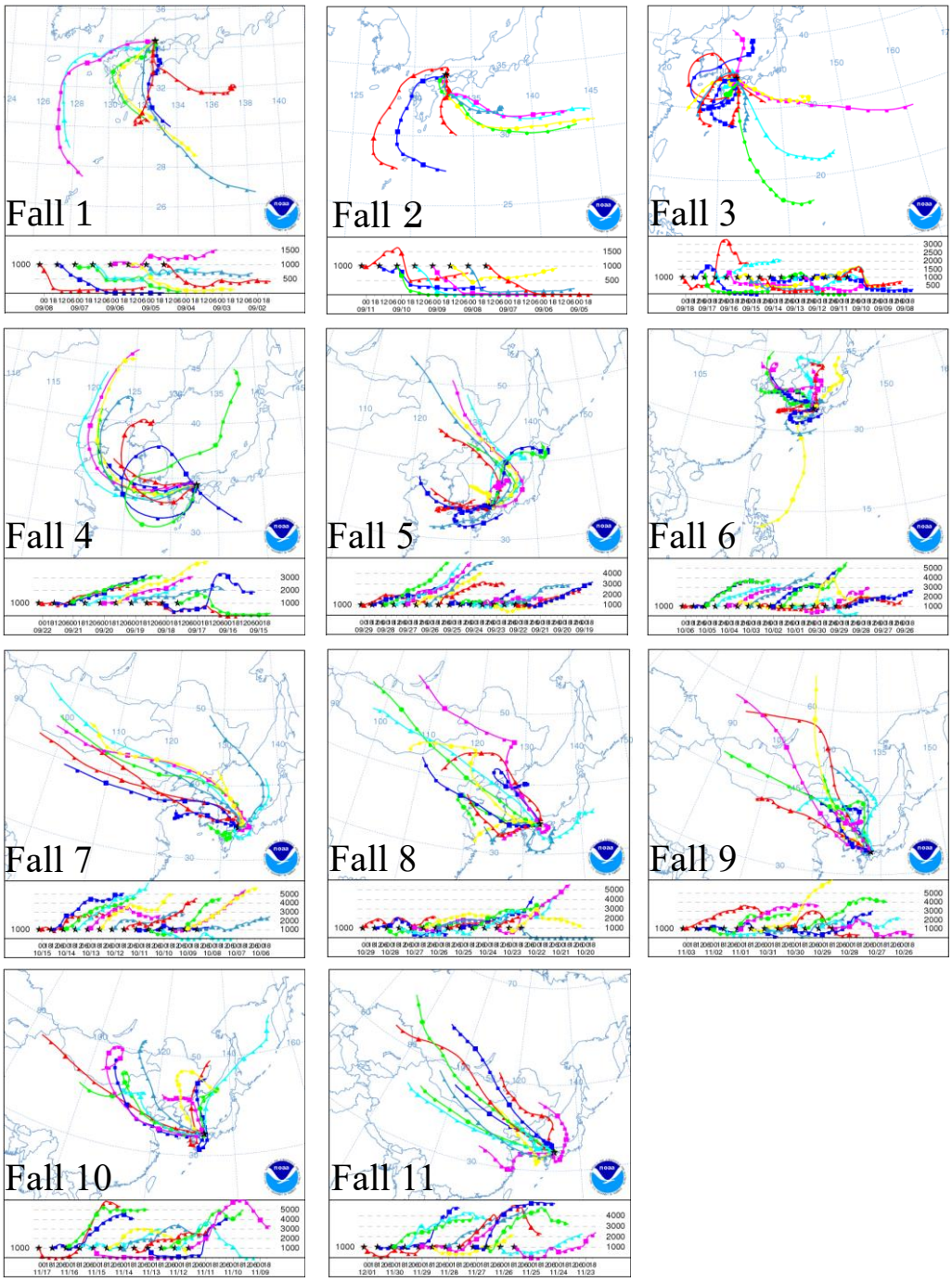

Fig. 2.3. Back trajectory analysis during individual sampling periods of TSP samples. The pathways reached at 1000m high above sampling site were analyzed back for 72 hours. The trajectories were calculated every 12 hours expressed by lines with different colors.

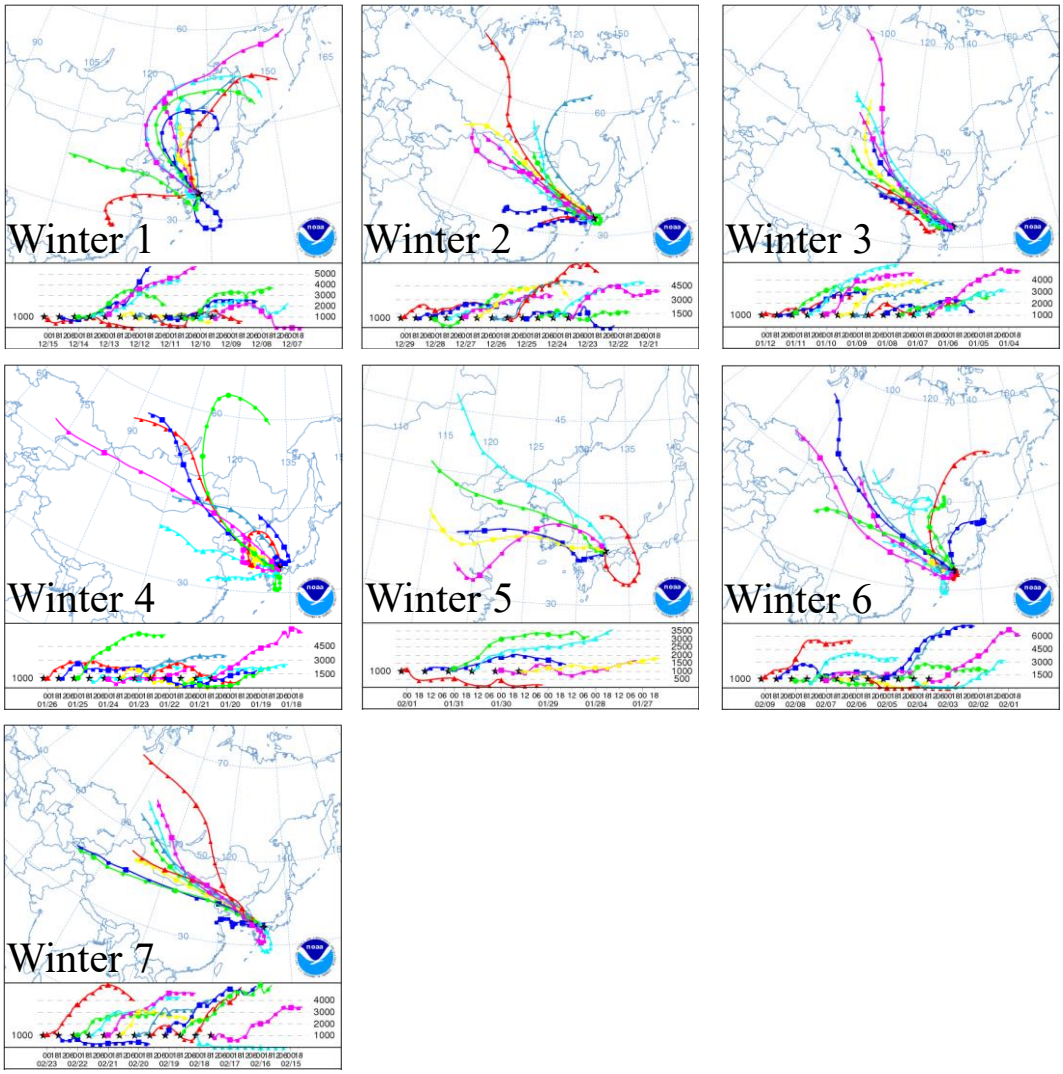

Fig. 2.3. Back trajectory analysis during individual sampling periods of TSP samples. The pathways reached at 1000m high above sampling site were analyzed back for 72 hours. The trajectories were calculated every 12 hours expressed by lines with different colors.

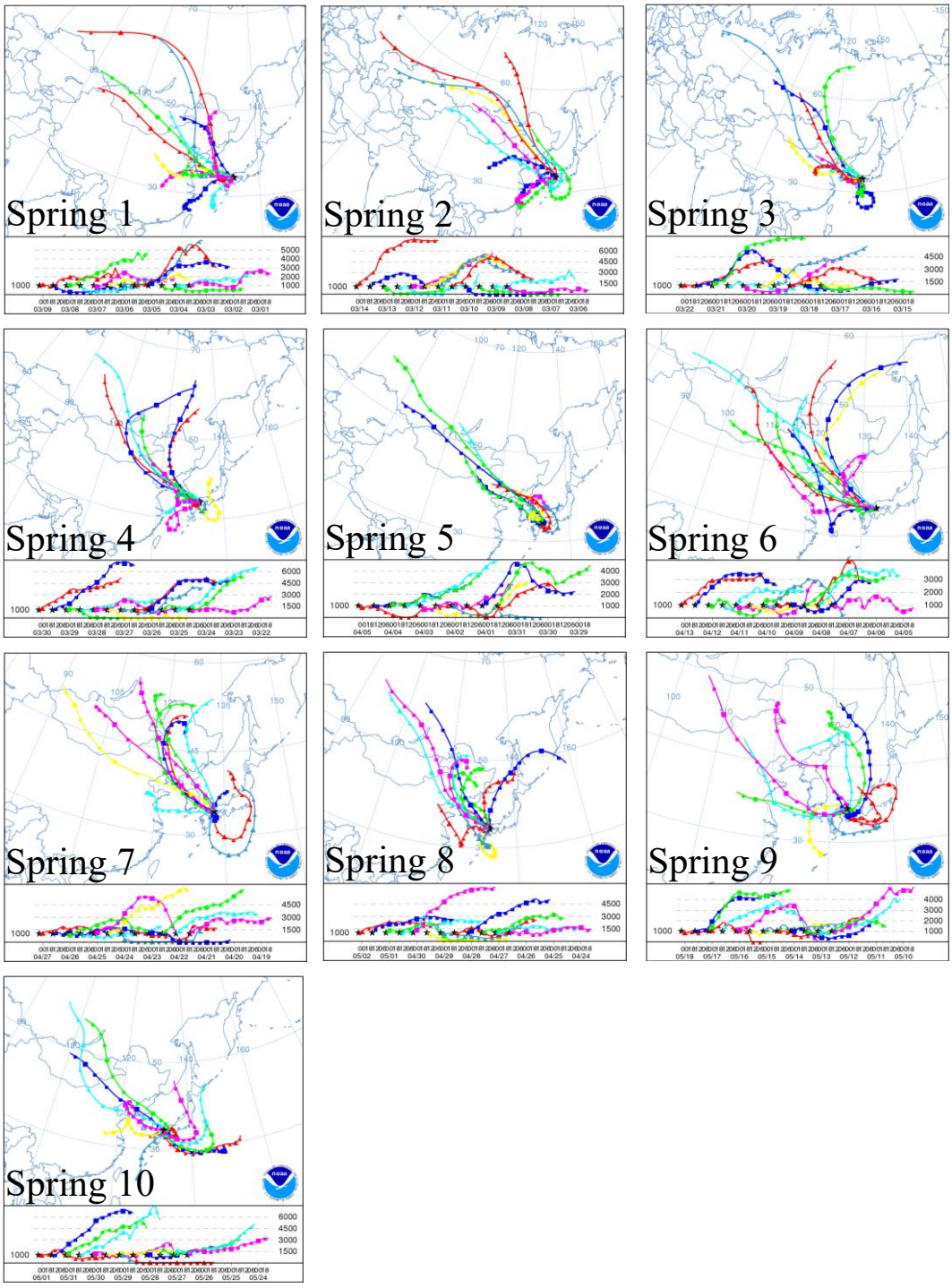

Fig. 2.3. Back trajectory analysis during individual sampling periods of TSP samples. The pathways reached at 1000m high above sampling site were analyzed back for 72 hours. The trajectories were calculated every 12 hours expressed by lines with different colors.

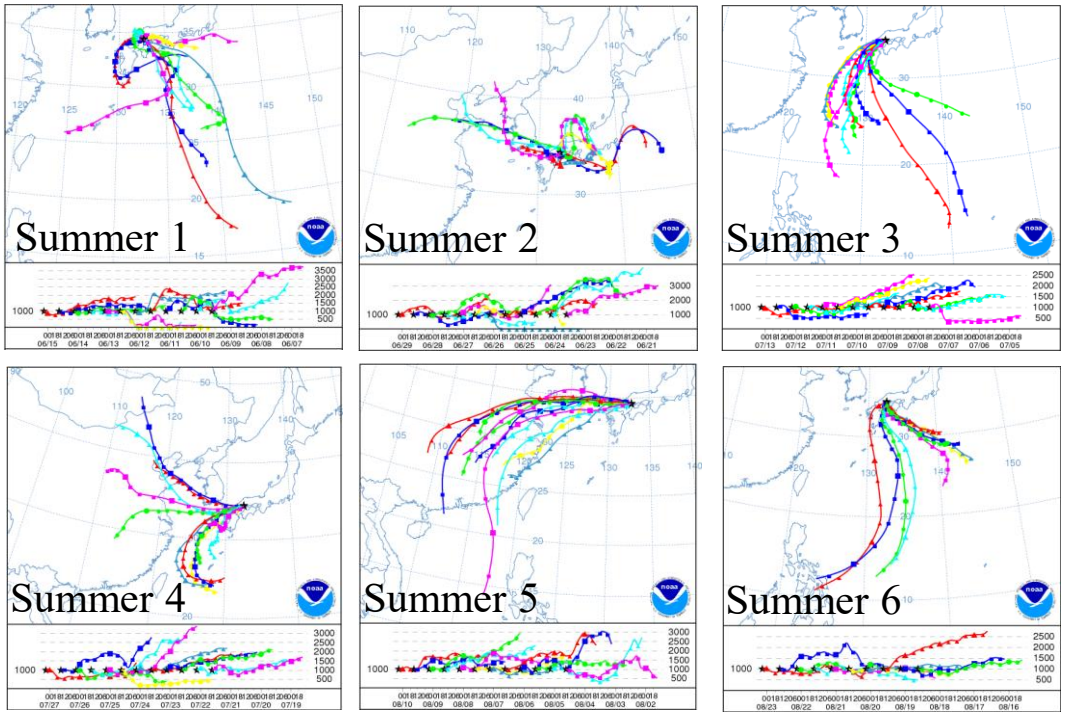

Fig. 2.3. Back trajectory analysis during individual sampling periods of TSP samples. The pathways reached at 1000m high above sampling site were analyzed back for 72 hours. The trajectories were calculated every 12 hours expressed by lines with different colors.

2.3.1.2 Seasonal variation of major ion concentrations

Fractions of nss ([nss-X]/[total-X]) are shown in Fig. 2.4. This result showed that contribution of sea salt was low for SO_4^{2-}, K^+, and Ca^{2+}, since their [nss-SO_4^{2-}]/[SO_4^{2-}] ratios were more than 0.8 through the year. Fig. 2.5 shows seasonal variations of atmospheric concentrations of NH_4^+, nss-Ca^{2+}, NO_3^-, and nss-SO_4^{2-}. The annual average concentration of nss-SO_4^{2-} was 59 nmol/m^3, and there were some periods when we observed a large amount of nss-SO_4^{2-} around 140 nmol/m^3. The atmospheric concentration of nss-SO_4^{2-} was high especially from winter to spring. The variation of nss-SO_4^{2-} concentration was similar to that of NH_4^+. There is a good correlation between the concentrations of NH_4^+ and nss-SO_4^{2-} ($r = 0.92$) and the slope of linear regression is 0.98 which means that there has been approximately enough amount of NH_4^+ to balance nss-SO_4^{2-} (Fig. 2.6). Several data are plotted above a line with slope 1 (Fig. 2.6), which means that these data have excess nss-SO_4^{2-} to NH_4^+ in the sample. The interpretation of these samples is provided in the next section.

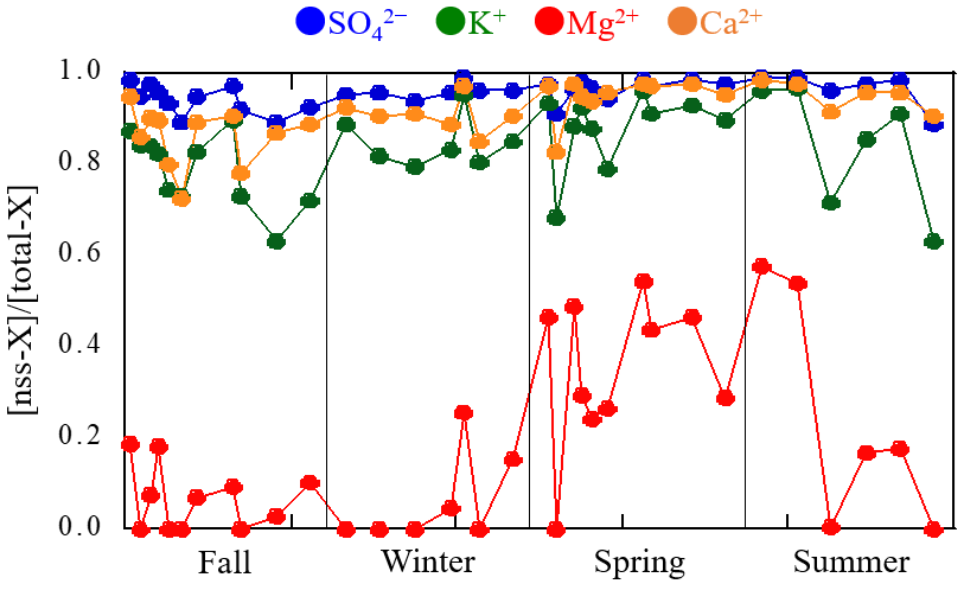

Fig. 2.4. Fractionation of non-sea-salt *X* ion (nss-*X*) to total *X* ion in TSP samples (*X* is SO_4^{2-}, K^+, Mg^{2+}, or Ca^{2+}).

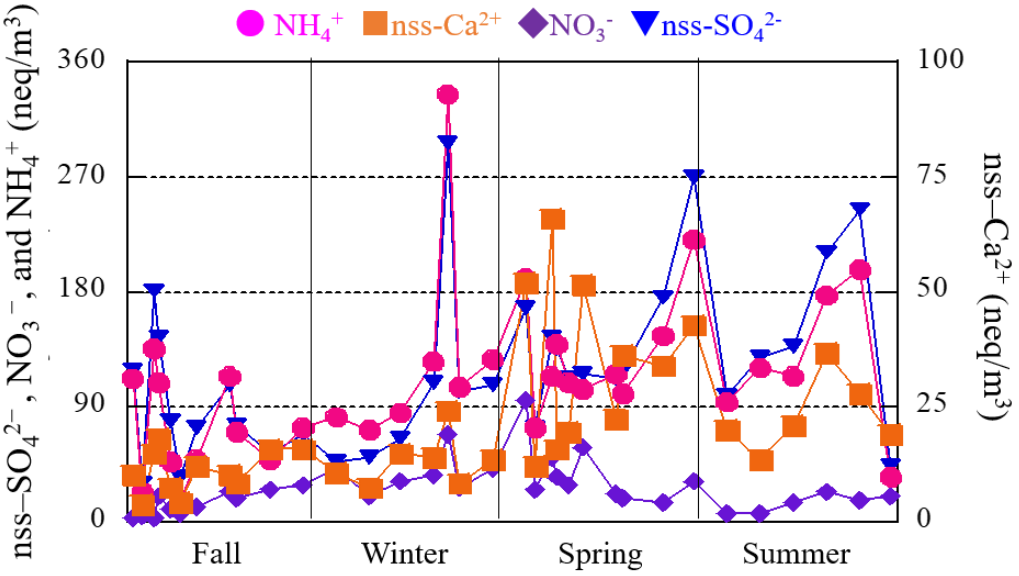

Fig. 2.5. Seasonal variation of atmospheric concentrations of nss–SO_4^{2-}, NO_3^-, NH_4^+, and nss–Ca^{2+}.

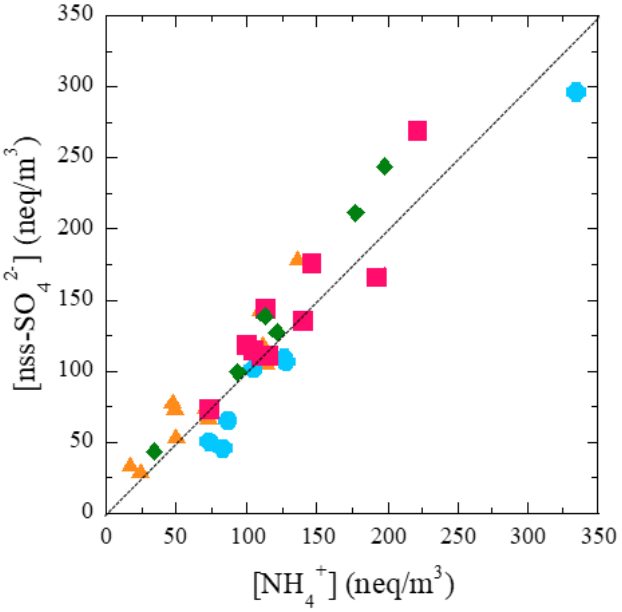

Fig. 2.6. Correlation of NH_4^+ and nss-SO_4^{2-}. The slope of linear regression was 0.98, and correlation coefficient ratio is 0.92. Black dashed line is slope 1.

2.3.1.3 Seasonal variation of sulfate species in aerosol

Sulfur XANES spectra of the TSP samples are shown in Fig. 2.7. These spectra were well fitted by the linear combination of those of $CaSO_4 \cdot 2H_2O$, $(NH_4)_2SO_4$, NH_4HSO_4, and hydrated SO_4^{2-}, suggesting that they were major components of sulfate aerosols, and other species were minor. The fitting results are shown in Fig. 2.8 and Table 2.5. The error of the fitting analysis was up to approximately 30 % with largest *R* value of a sample (Summer-4). Seasonal variation of the ratio of atmospheric concentration of high hygroscopic sulfates, i.e., $(NH_4)_2SO_4$, NH_4HSO_4, and hydrated SO_4^{2-} ions, to that of total sulfate (= [high hygroscopic sulfates]/[Total sulfate]) is shown in Fig. 2.9. A low value of the ratio means that the sample contains a large fraction of $CaSO_4 \cdot 2H_2O$ with low hygroscopicity. It appeared that the fractions of high hygroscopic sulfates were dramatically decreased in some of the fall and spring samples. In other words, during this period, $CaSO_4 \cdot 2H_2O$ with low hygroscopicity was dominant in sulfate species in aerosol and fractions of that were higher than that of other samples. Previous studies (Adams et al., 1999; Fowler et al., 2013; Wang et al., 2008) have suggested that $(NH_4)_2SO_4$ is the dominant sulfate species in aerosols. However, our results showed that $CaSO_4 \cdot 2H_2O$ is also an important sulfate species, which cannot be disregarded, even though a relatively large seasonal variation was found in Higashi–Hiroshima. At that time, nss-Ca^{2+} concentration increased (Fig. 2.5). The increase of Ca^{2+} concentration is a good indicator of a dust event in East Asia (Choi et al., 2001). Additionally, calcium original species in mineral particles in East Asia is mainly $CaCO_3$, but the abundance of $CaSO_4 \cdot 2H_2O$ in our samples was low (Miyamoto et al., 2016; Takahashi et al., 2009) as reported in previous study (Nishikawa et al., 2000). Thus, it is suggested that $CaSO_4 \cdot 2H_2O$ was secondarily formed during transportation in the atmosphere.

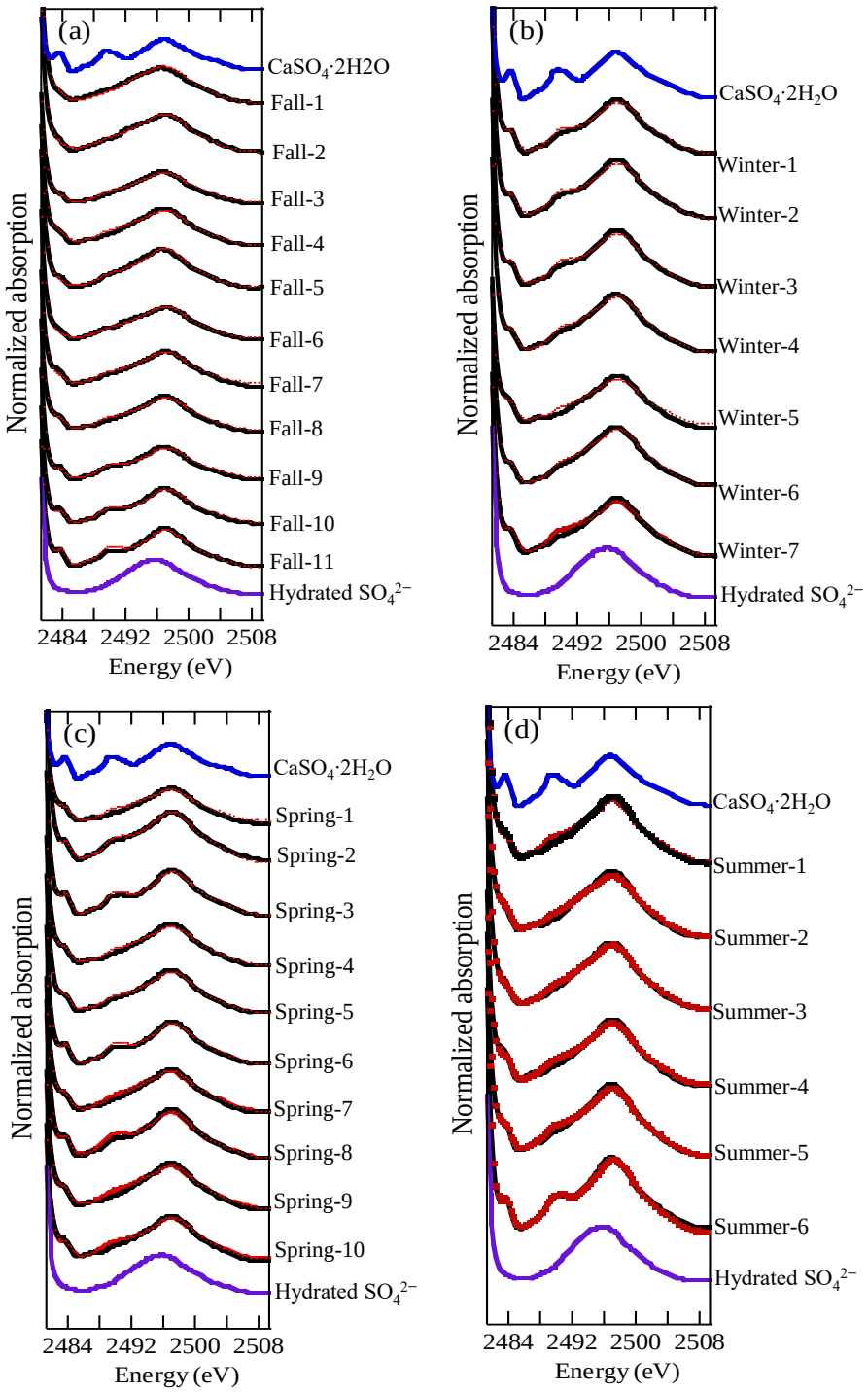

Fig. 2.7. Sulfur K-edge XANES spectra of TSP samples collected in fall (a), winter (b), sprig (c), and summer (d) with spectra of reference materials ($CaSO_4 \cdot 2H_2O$ and hydrated SO_4^{2-}).

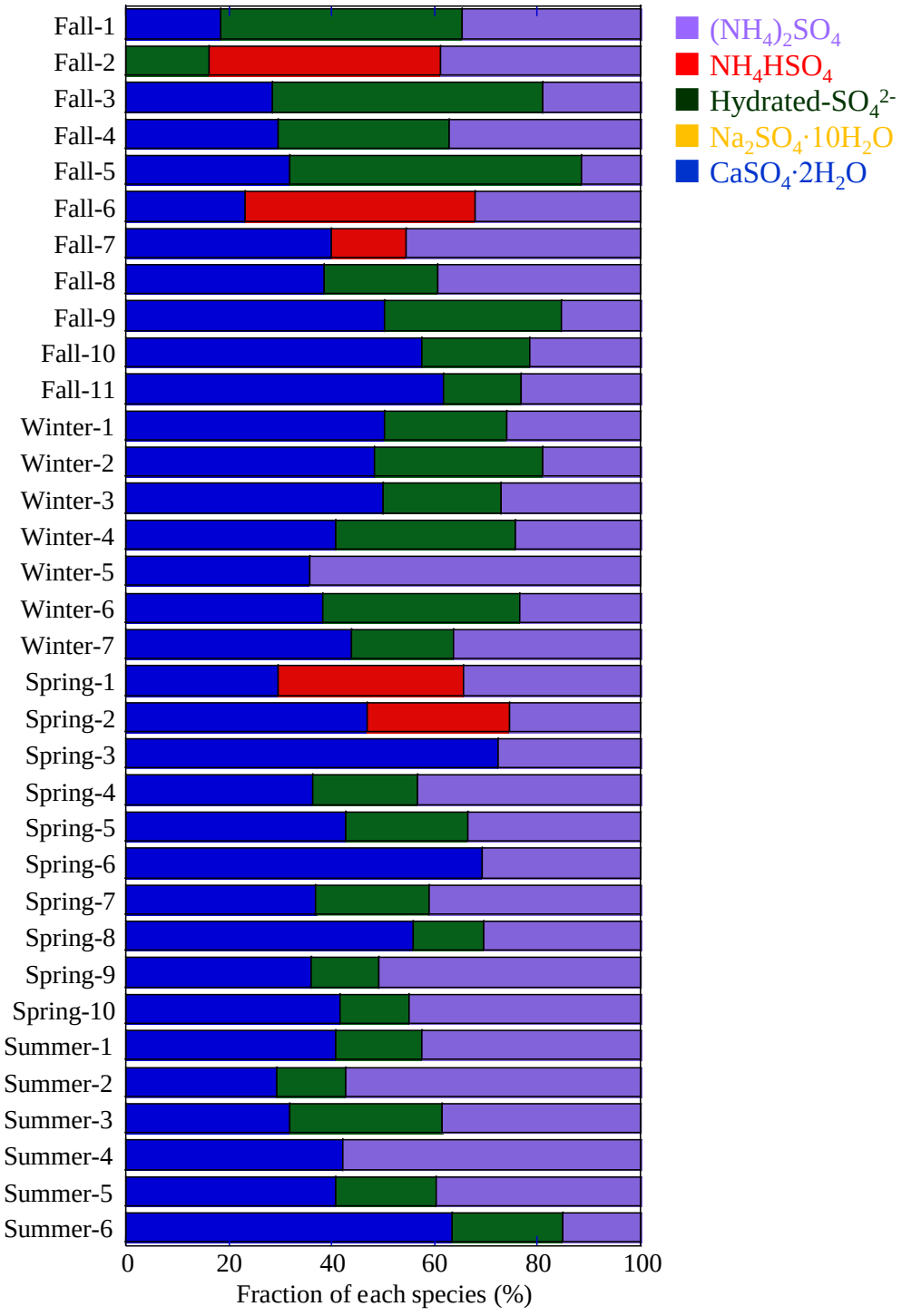

Fig. 2.8. Fraction of sulfate species (%) in TSP samples.

Table 2.5. Fraction of each sulfate species in the TSP samples determined

Sample No.	$(NH_4)_2SO_4$	NH_4HSO_4	Hydrate SO_4^{2-}	$CaSO_4 \cdot 2H_2O$	R value
Fall-1	34.7		46.9	18.4	0.036
Fall-2	38.7	45.0	16.3		0.038
Fall-3	18.9		52.7	28.4	0.037
Fall-4	36.9		33.3	29.7	0.054
Fall-5	11.5		56.5	32.0	0.034
Fall-6	32.2	44.6		23.2	0.038
Fall-7	45.6	14.4		40.0	0.059
Fall-8	39.3		22.2	38.5	0.047
Fall-9	15.4		34.4	50.2	0.038
Fall-10	21.6		20.7	57.7	0.042
Fall-11	23.2		15.1	61.7	0.047
Winter-1	25.9		23.9	50.2	0.041
Winter-2	19.0		32.6	48.4	0.043
Winter-3	27.0		23.1	49.9	0.046
Winter-4	24.4		34.8	40.8	0.038
Winter-5	64.1			35.9	0.065
Winter-6	23.6		38.1	38.4	0.036
Winter-7	36.3		19.7	44.0	0.051
Spring-1	34.2	36.1		29.7	0.066
Spring-2	25.5	27.6		47.0	0.040
Spring-3	27.6			72.4	0.047
Spring-4	43.3		20.2	36.4	0.053
Spring-5	33.5		23.7	42.8	0.034
Spring-6	30.7			69.3	0.047
Spring-7	41.1		22.1	36.8	0.044
Spring-8	30.4		13.7	55.9	0.058
Spring-9	50.8		13.1	36.1	0.062
Spring-10	44.9		13.4	41.7	0.061
Summer-1	42.4		16.8	40.8	0.050
Summer-2	57.1		13.6	29.3	0.065
Summer-3	38.5		29.7	31.8	0.053
Summer-4	57.8			42.2	0.075
Summer-5	39.6		19.6	40.7	0.059
Summer-6	15.1		21.6	63.3	0.035

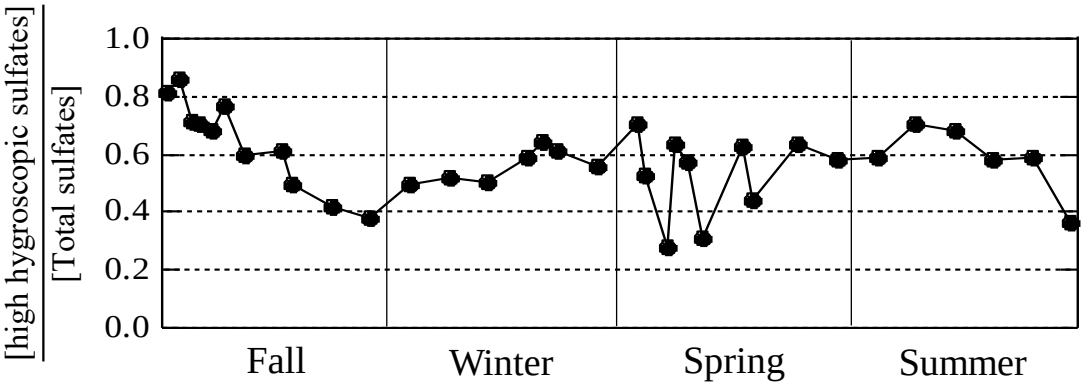

Fig. 2.9. Seasonal variation of the ratio of atmospheric concentration of high hygroscopic sulfates, i.e., $(NH_4)_2SO_4$ and hydrated SO_4^{2-} ions, to that of total sulfate, indicating the fraction of high hygroscopic species in TSP, i.e., [high hygroscopic sulfates]/[Total sulfate].

As described above, the correlation between charge concentration of NH_4^+ and that of nss-SO_4^{2-} had good correlation and the slope of linear regression was 0.98 (Fig. 2.6). Therefore, if ammonium sulfate preferentially formed in the particles compared with other sulfate species, almost all sulfate can be present as $(NH_4)_2SO_4$. However, $CaSO_4 \cdot 2H_2O$ accounted for more than 20% of sulfate in the aerosol samples. Figure 2.10a shows that the $CaSO_4 \cdot 2H_2O$ fraction in particles is not dependent on total sulfate concentration, because $CaSO_4 \cdot 2H_2O$ is controlled by Ca^{2+} concentration in aerosols. Ca^{2+} can react with sulfuric acid in the atmosphere. By contrast, the $(NH_4)_2SO_4$ fraction was approximately correlated with total sulfate concentration (R^2=0.352, Fig. 2.10b), since the amount of available sulfate was large when (i) total sulfate concentration was large, and (ii) $CaSO_4 \cdot 2H_2O$ contribution to total sulfate was low. Thus, the correlation of the $(NH_4)_2SO_4$ fraction was improved when the horizontal axis of Fig. 2.10c is changed from total sulfate concentration to [Total-SO_4^{2-}] – [$CaSO_4 \cdot 2H_2O$] (R^2=0.391, Fig. 2.10c). The results based on the speciation of sulfate by XANES suggest that the reaction for forming $CaSO_4 \cdot 2H_2O$ preferentially occurs rather than $(NH_4)_2SO_4$, but the remaining sulfate forms ammonium salt in aerosols. The results also indicated that $CaSO_4 \cdot 2H_2O$ formed in the particle was stable and not converted to $(NH_4)_2SO_4$ once $CaSO_4 \cdot 2H_2O$ was formed. When there was excess nss-SO_4^{2-} to NH_4^+ in the sample, i.e., the data are plotted above the line of slope 1 in Fig. 2.6, [high hygroscopic sulfates]/[Total sulfate] ratio did not always decrease (Fig. 2.9). Consequently, the formation of $CaSO_4 \cdot 2H_2O$ in the atmosphere probably consumes sulfate ion or the oxidation products of SO_2 and finally suppresses the formation of high hygroscopic sulfate. A similar role of $CaCO_3$ conversion has been discussed largely through modeling and laboratory studies (Dentener et al., 1996; Sullivan et al., 2009; Tang et al., 2016), and the analysis in this chapter obtained similar conclusions based on natural observation coupled with XANES spectroscopy.

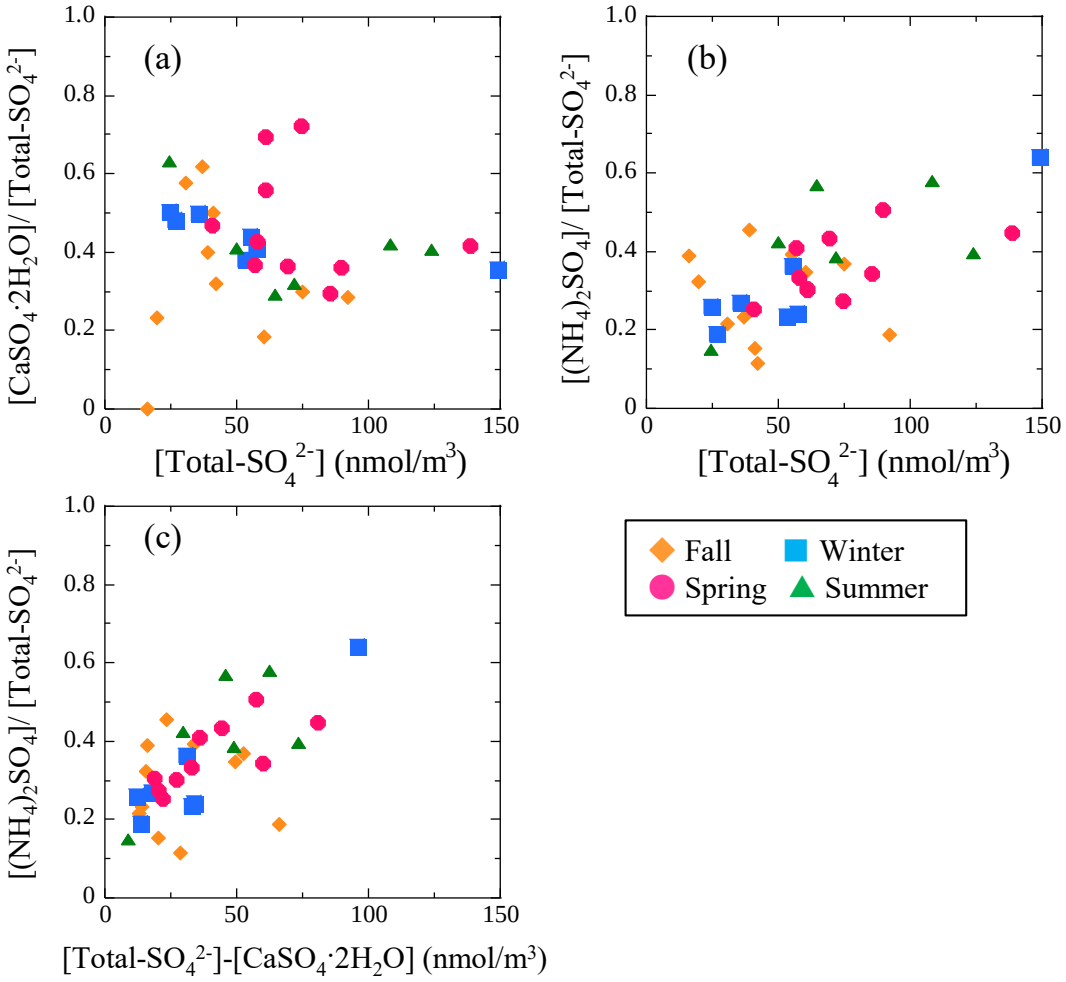

Fig. 2.10. Correlation between total sulfate concentration and $CaSO_4 \cdot 2H_2O$ fraction to total sulfate (a) and $(NH_4)_2SO_4$ (b). The correlation between [Total−SO_4^{2-}]–[$CaSO_4 \cdot 2H_2O$] concentration and $(NH_4)_2SO_4$ fraction to total sulfate is shown in (c).

2.3.2 Size-fractionated samples

2.3.2.1 Characteristic of samples in each season

To understand chemical species in aerosols and their properties depending on particle size, size-fractionated samples collected in each season were analyzed. Figure 2.11 shows the mass concentration of sulfate and mineral dust around East Asia simulated with a numerical model (SPRINTARS; Takemura et al., 2005, 2002, 2000). The concentration of mineral dust during spring was high and extended from arid areas and deserts in China and Mongolia (e.g., Gobi and Taklimakan Deserts), which are the sources of Asian dust to western Japan, including our sampling site. Dust storms are observed frequently during spring in the arid and desert areas caused by winds and the dry surface condition in the source region (Lee and Sohn, 2009). Consequently, a large amount of mineral dust is transported to Japan and the Pacific, as suggested by the back-trajectory analysis (Fig. 2.12). In addition, Choi et al. (2001) described that a remarkable increase in Ca^{2+} concentration is caused by the dust event in Asia. Because of the influence of Asian dust, the nss-Ca^{2+} fraction in the coarse particles was large, particularly during spring as described later in Fig. 2.13. By contrast, sulfate mass concentration around the sampling site was high in any season. During each season, air mass passed through the high sulfate concentration region (large cities) and coastal urban areas in China, which can be sources of anthropogenic components, including sulfate transported to the sampling area (Figs. 2.11 and 2.12).

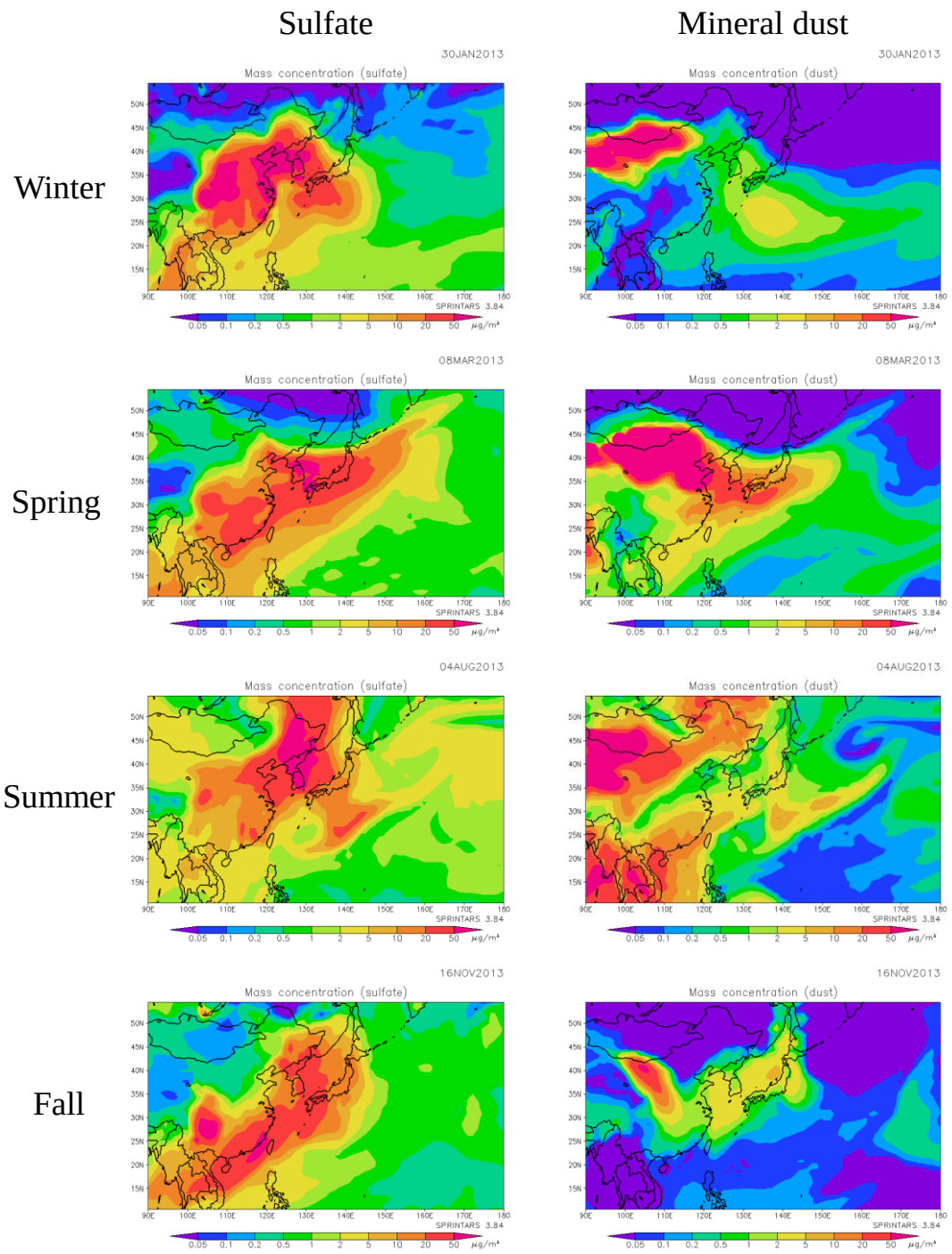

Fig. 2.11. Distribution of the mass concentration of sulfate (upper) and mineral dust (lower) around East Asia during each sampling period simulated using SPRINTARS (Takemura et al., 2000, 2002, 2005). The results for one day during each sampling period are shown.

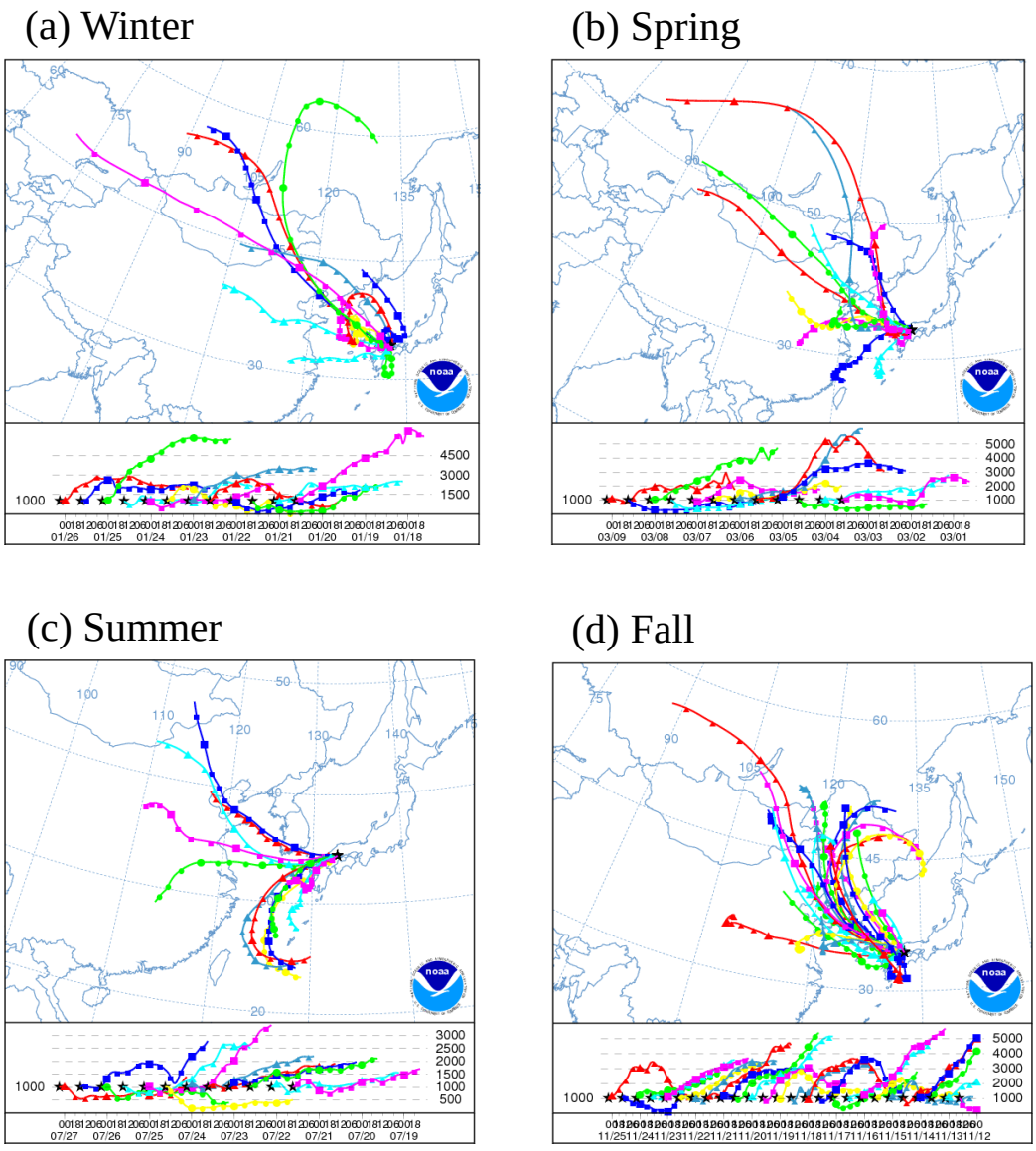

Fig. 2.12. Back trajectory analysis during individual sampling periods of size-fractionated samples. The pathways reached at 1000m high above sampling site were analyzed back for 72 hours.

Figure 2.13 shows size distributions of NH_4^+, nss-Ca^{2+}, NO_3^-, nss-SO_4^{2-}, and oxalate ion concentration in the unit of equivalent concentrations (neq/m^3) in each sample. The size distribution of NH_4^+ and nss-SO_4^{2-} ions for all samples showed that their concentration was higher in fine particles then that in coarse particles. These concentrations in fine particles were high in winter and spring. In addition, there was high correlation between the size distributions of concentration of NH_4^+ and nss-SO_4^{2-}, especially in the fine particles. On the other hand, the size distribution of concentration of nss-Ca^{2+} had a maximum in course particle range whose diameter is 2.1−4.2 μm, and its concentration was the highest in spring. NO_3^- concentration was the highest in the fine particles in winter, whereas in the coarse particles in summer. In the fall or spring sample, there were bimodal size distribution of NO_3^- in the coarse and fine particles, respectively. The bimodal distribution is caused by the reaction of primary particles such as sea salts and mineral particles with nitric aids in coarse particles, while nitric acid/ammonia reaction to form ammonium nitrate (NH_4NO_3) in fine particles (Seinfeld and Pandis, 2006). Fractions of nss components ([nss−*X*]/[total−*X*]) are shown in Fig. 2.14. In course particles, contributions of sea-salt were quantified. The ss-Ca^{2+} and ss-SO_4^{2-} accounted for about 10−20 and 10−60 % in coarse particles, respectively. The fraction became small when the particle diameter was small except for the summer samples. However, only in spring, the contribution of ss−Ca^{2+} was small at any particle diameters.

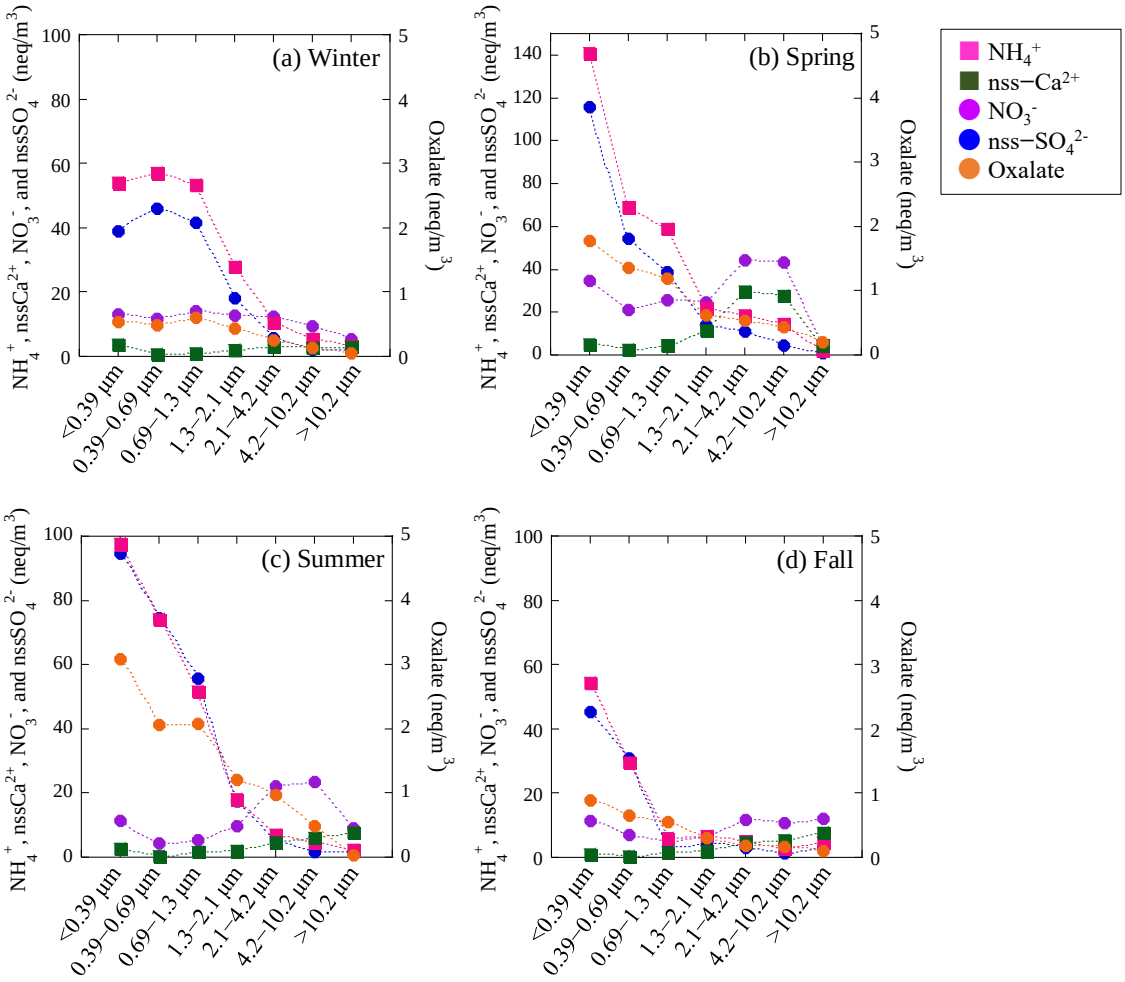

Fig. 2.13. Size distribution of NH_4^+, nss-Ca^{2+}, NO_3^-, nss-SO_4^{2-} and oxalate ion equivalent concentrations (neq/m^3) of winter (a), spring (b) summer (c), and fall (d). Horizontal axis is particle size (μm), and vertical axis is atmospheric concentration (neq/m^3). It is noted that maximum value of left vertical axis is 100 neq/m^3 for (a), (c) and (d), 150 neq/m^3 for (b).

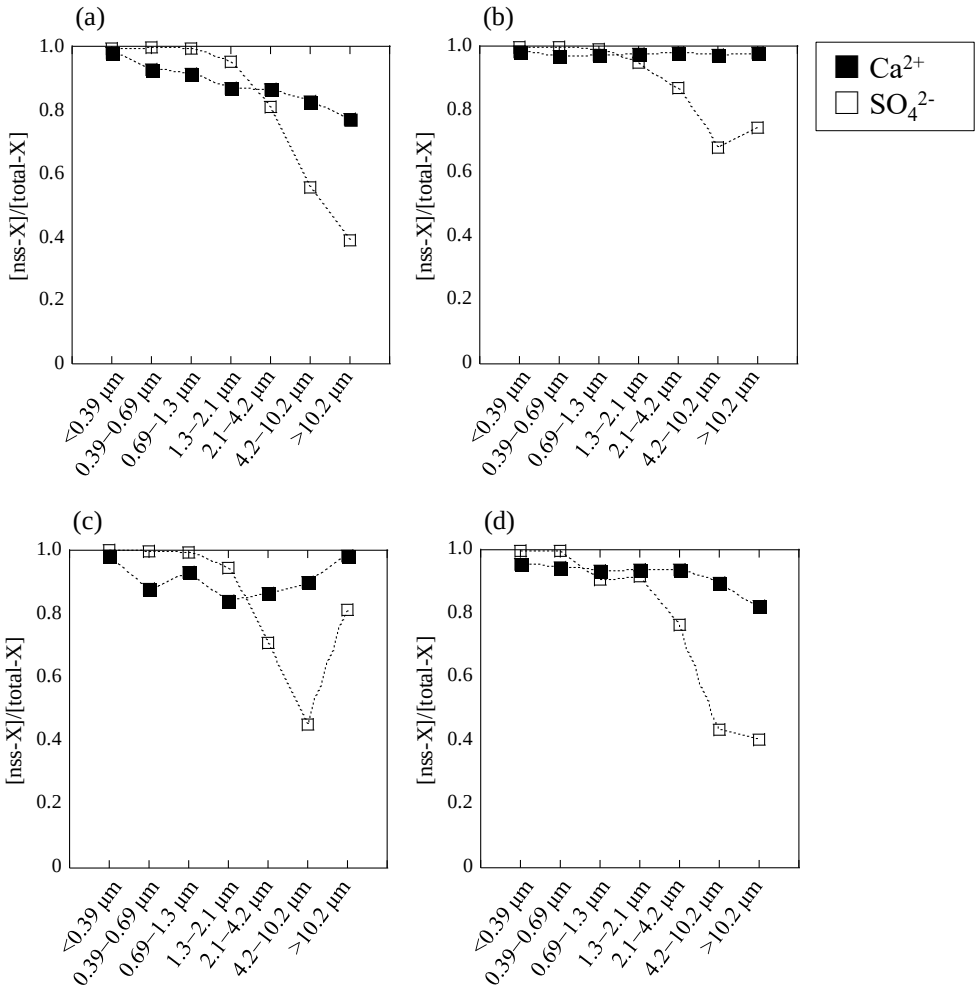

Fig. 2.14. Fraction of non-sea-salt ([nss-X]/[total-X], X is Ca^{2+} or SO_4^{2-}) of winter (a), spring (b) summer (c), and fall (d).

NO_3^- and nss-SO_4^{2-} generally originate from anthropogenic emissions as acid gases, which form secondary particles through gas-to-particle conversions, such as NH_4NO_3 and $(NH_4)_2SO_4$ in fine particles (Fowler et al., 2013). However, NO_3^- exhibited an evident peak of size distribution in coarse particles with particle size ranging from 2.1 μm to 10.2 μm in spring and summer samples (Fig. 2.13). Within the same size range, nss-SO_4^{2-} concentration was also higher during spring compared with those during other seasons (Fig. 2.13). These variations in the size distribution of NO_3^- and nss-SO_4^{2-} were caused by the heterogeneous reaction with sea salts and mineral particles, which are important reactants with acids (Rossi, 2003; Rubasinghege and Grassian, 2013; Usher et al., 2003).

NaCl in sea salts reacts with acids in the atmosphere as follows (Rossi, 2003):

$$NaCl + HNO_3 \rightarrow NaNO_3 + HCl\ (g), \quad (7)$$

$$2NaCl + H_2SO_4 \rightarrow Na_2SO_4 + 2HCl\ (g). \quad (8)$$

Reaction generally occurs preferentially with HNO_3 (Sander et al., 2011). The amount of emitted HCl (Cl^- loss) is calculated as follows:

$$[Cl^-\ \text{loss}] = [Na^+] \times ([Cl^-]/[Na^+])_{seawater} - [Cl^-]$$
$$([Cl^-]/[Na^+])_{seawater} = 1.17. \quad (9)$$

Most of the samples indicated that the amount of NO_3^- was equivalent to that of a sum of Na^+ unbound with Cl and NH_4^+ ($\{[Cl^-\ \text{loss}] + [NH_4^+]\} \fallingdotseq [NO_3^-]$). That is, NO_3^- is present either as $NaNO_3$ or NH_4NO_3. Several spring and summer samples indicated that excess NO_3^- was present relative to their sum ($\{[Cl^-\ \text{loss}] + [NH_4^+]\} < [NO_3^-]$). These fractions were likely to react with mineral particles.

The reaction of nitric acid with $CaCO_3$ in mineral particles to form $Ca(NO_3)_2$ is an important process (Goodman et al., 2000; Usher et al., 2003). Previous studies observed particles using electron microscopies, such as transmission electron microscopy (TEM) and energy-

dispersive X-ray spectroscopy (EDX) (e.g., Li et al., 2016; Li and Shao, 2008; Matsuki et al., 2009). They reported that $Ca(NO_3)_2$ was detected in the coating of mineral particles, which was considered to be formed in the atmosphere. The hygroscopicity of $Ca(NO_3)_2$ is considerably higher than that of $CaCO_3$. Therefore, this reaction is expected to enhance the CCN activities of mineral particles, particularly in coarse particles. Our results for the speciation of Ca in particles using X-ray absorption fine structure (XAFS) analysis are provided in the Section 2.3.2.3.

2.3.2.2 Size distribution of sulfate species in aerosol particles

Sulfur K-edge XANES spectra of the aerosol samples are shown in Fig. 2.15. The characteristic structure of the $CaSO_4 \cdot 2H_2O$ spectrum with three small peaks at 2484, 2490, and 2497 eV was observed in the coarse particles (>10.2 μm, 4.2−10.2 μm, 2.1−4.2 μm, and 1.3−2.1 μm), indicating that $CaSO_4 \cdot 2H_2O$ was found as a major species of sulfate in the coarse particles. By contrast, the features of the spectrum of $CaSO_4 \cdot 2H_2O$ were not appreciable in the fine particles (0.69−1.3 μm, 0.39−0.69 μm, and <0.39 μm), but they consist of high hygroscopic species such as $(NH_4)_2SO_4$, NH_4HSO_4, and hydrated SO_4^{2-} ion. These results suggested that the estimation of sulfur species based on the correlation written above is reasonable for fine particles (Fig. 2.16). In marine areas, sodium sulfate, which is an important component of CCN, can be a major species. However, the aerosol samples measured in this thesis were collected on land, and sodium sulfate was not detected. As a result of the speciation, sulfate species in the aerosol samples were hygroscopic except for $CaSO_4 \cdot 2H_2O$.

The results of fitting analysis are shown in Fig.2.17 and Table 2.6. Especially in spring, $CaSO_4 \cdot 2H_2O$ fractions in coarse particles were high even in relatively small particles. Similar size distribution was shown in aerosol samples collected in Tsukuba City in Japan, during a large dust event in 2002 (Takahashi et al., 2006).

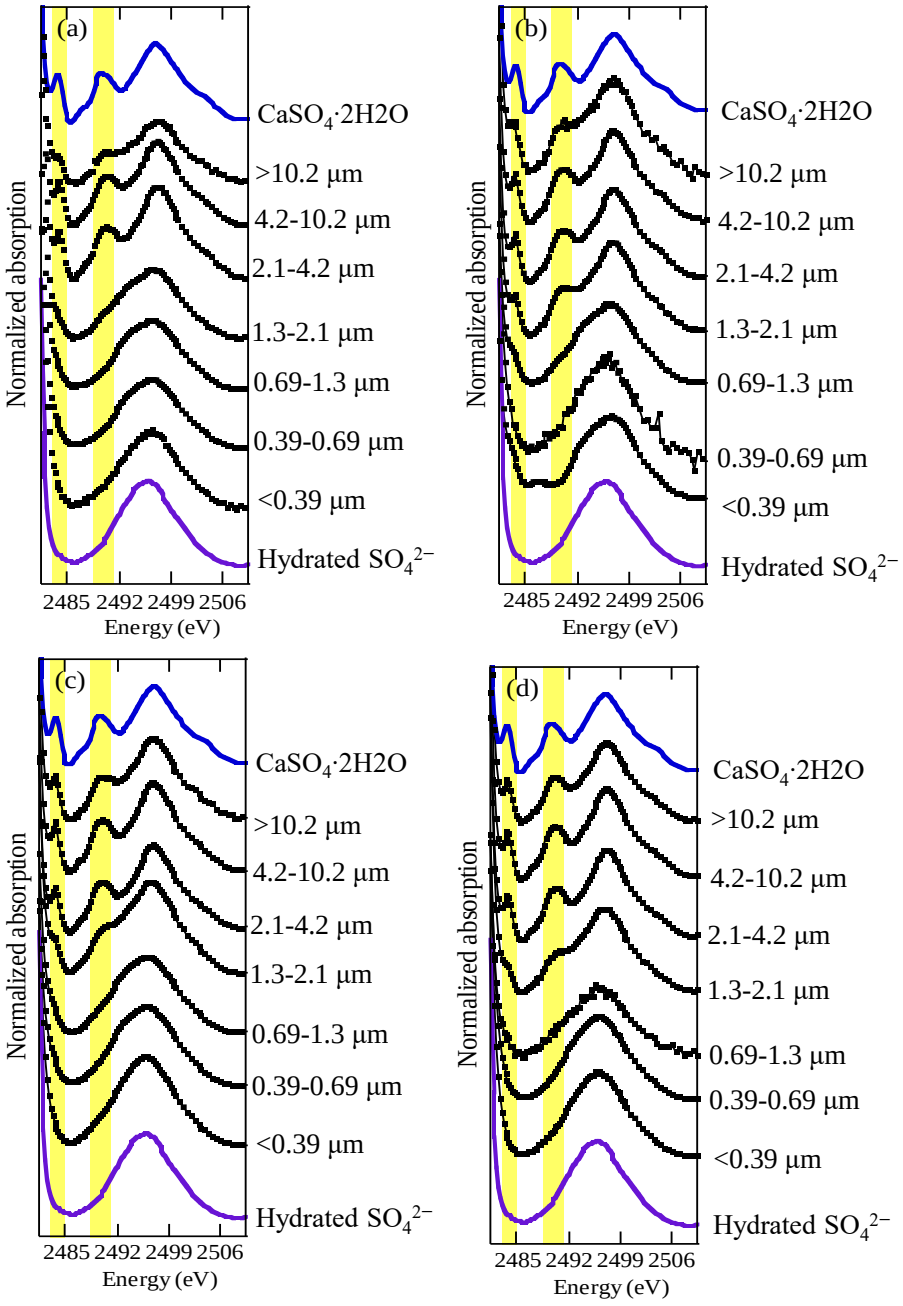

Fig. 2.15. Sulfur K-edge spectra of the size-fractionated samples collected during winter (a), spring (b) summer (c), and fall (d) with the spectra of the reference materials, i.e., $CaSO_4 \cdot 2H_2O$ and hydrated SO_4^{2-}.

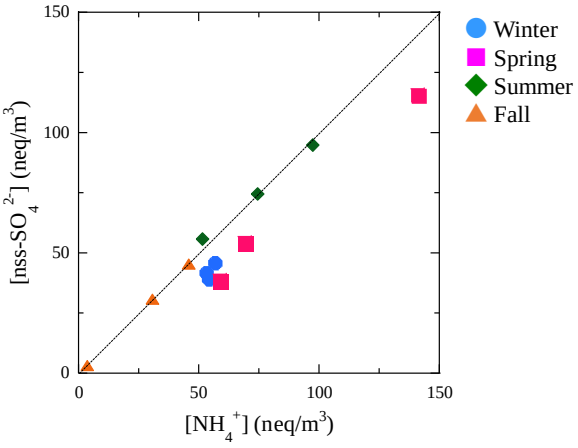

Fig. 2.16. Correlation between NH_4^+ (horizontal axis) and nss-SO_4^{2-} (vertical axis) in fine particles (< 1.0 μm, average diameter) about size-fractionated sample. Black dashed line is slope 1.

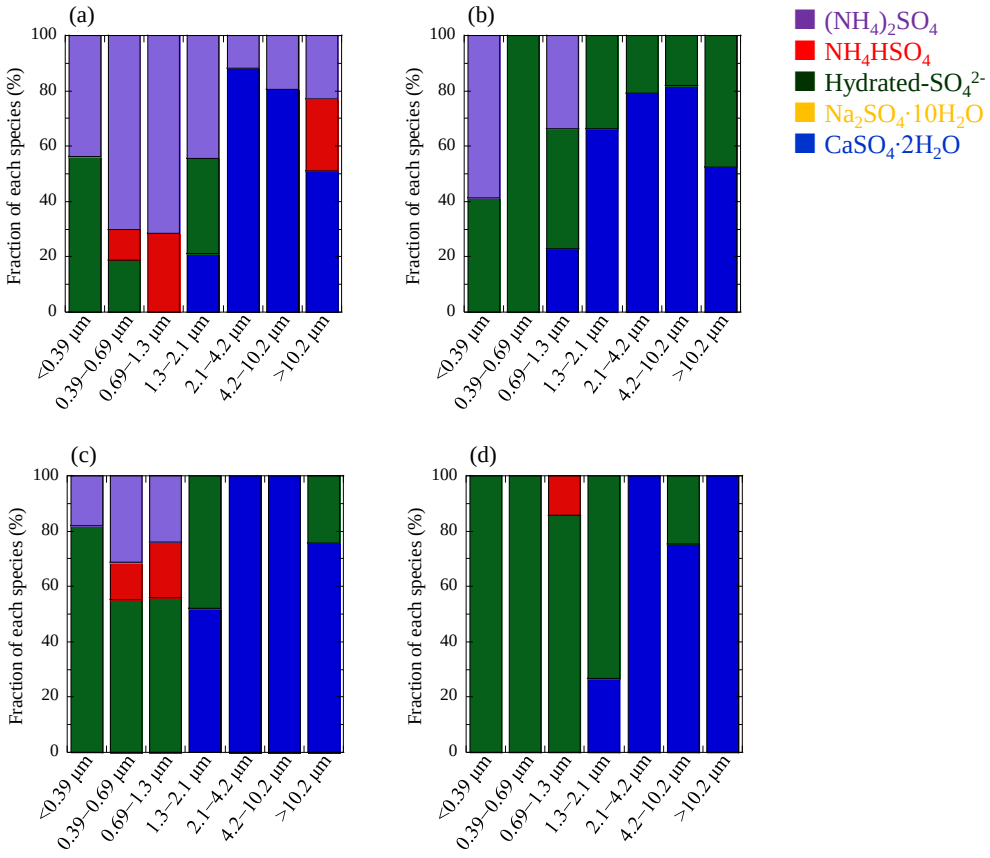

Fig. 2.17. Fraction of sulfate species (%) in the size-fractionated samples collected during winter (a), spring (b), summer (c), and fall (d). The horizontal axis denotes particle size (μm), and the vertical axis indicates fraction (%).

Table 2.6. Size distribution of fraction (%) of each sulfate species about each season determined by XAFS.

	Particle size (μm)	<0.39	0.39-0.69	0.69-1.3	1.3-2.1	2.1-4.2	4.2-10.2	>10.2
Winter	$(NH_4)_2SO_4$	43.9	70.1	71.5	44.4	11.7	19.5	23.0
	NH_4HSO_4		11.2	28.5				25.8
	$Na_2SO_4 \cdot 10H_2O$							
	Hydrate SO_4^{2-}	56.1	18.7		34.3			
	$CaSO_4 \cdot 2H_2O$				21.3	88.3	80.5	51.2
	R value	0.040	0.055	0.063	0.045	0.025	0.034	0.019
Spring	$(NH_4)_2SO_4$	58.6		33.6				
	NH_4HSO_4							
	$Na_2SO_4 \cdot 10H_2O$							
	Hydrate SO_4^{2-}	41.4	100	43.6	33.5	20.8	18.1	47.4
	$CaSO_4 \cdot 2H_2O$			22.8	66.5	79.2	81.9	52.6
	R value	0.048	0.081	0.053	0.047	0.046	0.041	0.056
Summer	$(NH_4)_2SO_4$	17.9	31.1	24.0				
	NH_4HSO_4		13.8	20.1				
	$Na_2SO_4 \cdot 10H_2O$							
	Hydrate SO_4^{2-}	82.1	55.1	55.9	48.0			24.3
	$CaSO_4 \cdot 2H_2O$				52.0	100	100	75.7
	R value	0.035	0.039	0.038	0.025	0.044	0.045	0.030
Fall	$(NH_4)_2SO_4$							
	NH_4HSO_4			14.1				
	$Na_2SO_4 \cdot 10H_2O$							
	Hydrate SO_4^{2-}	100	100	85.9	73.2		24.7	
	$CaSO_4 \cdot 2H_2O$				26.8	100	75.3	100
	R value	0.079	0.062	0.049	0.075	0.097	0.051	0.069

2.3.2.3 Size distribution of calcium species in aerosol particles

Calcium species in the size-fractionated aerosol samples were also investigated. The normalized Ca K-edge XANES spectra of aerosol samples (Fig. 2.18) with fitting by the endmembers (Fig. 2.2b) provided the size distribution of Ca species in each season (Fig. 2.19 and Table 2.7). $CaSO_4 \cdot 2H_2O$ was also found by Ca speciation in common with sulfate speciation, which showed that $CaSO_4 \cdot 2H_2O$ constituted the majority of the Ca species for nearly all particle sizes. $CaC_2O_4 \cdot 2H_2O$ and $CaCO_3$ were also major species in all seasons, while $CaC_2O_4 \cdot 2H_2O$ accounted for a large fraction of Ca species in spring. Such a result was also found by Furukawa and Takahashi (2011). Notably, $Ca(NO_3)_2 \cdot 4H_2O$ and $CaCl_2 \cdot 2H_2O$ were minor Ca species in any seasons. $Ca(NO_3)_2 \cdot 4H_2O$ was not found by XAFS analysis in spring and summer samples. This is, excess NO_3^- relative to the sum of Na^+ unbound with Cl^- and NH_4^+ did not combine with Ca^{2+} and considered to form nitrate species with other cations. Although identification of nitrate counteraction is difficult, the charge balance of cations and anions was confirmed in the sample, suggesting that the nitrate in the coarse particles form potassium and/or magnesium salts during spring and summer. A previous laboratory study indicated that the coexistence of $Ca(NO_3)_2$ and oxalic acid led to an aqueous reaction in particles to form $CaC_2O_4 \cdot 2H_2O$ and release HNO_3 (Ma and He, 2012). $Ca(NO_3)_2$ was probably once formed in the particles and converted to $CaC_2O_4 \cdot 2H_2O$, which was actually formed in our samples.

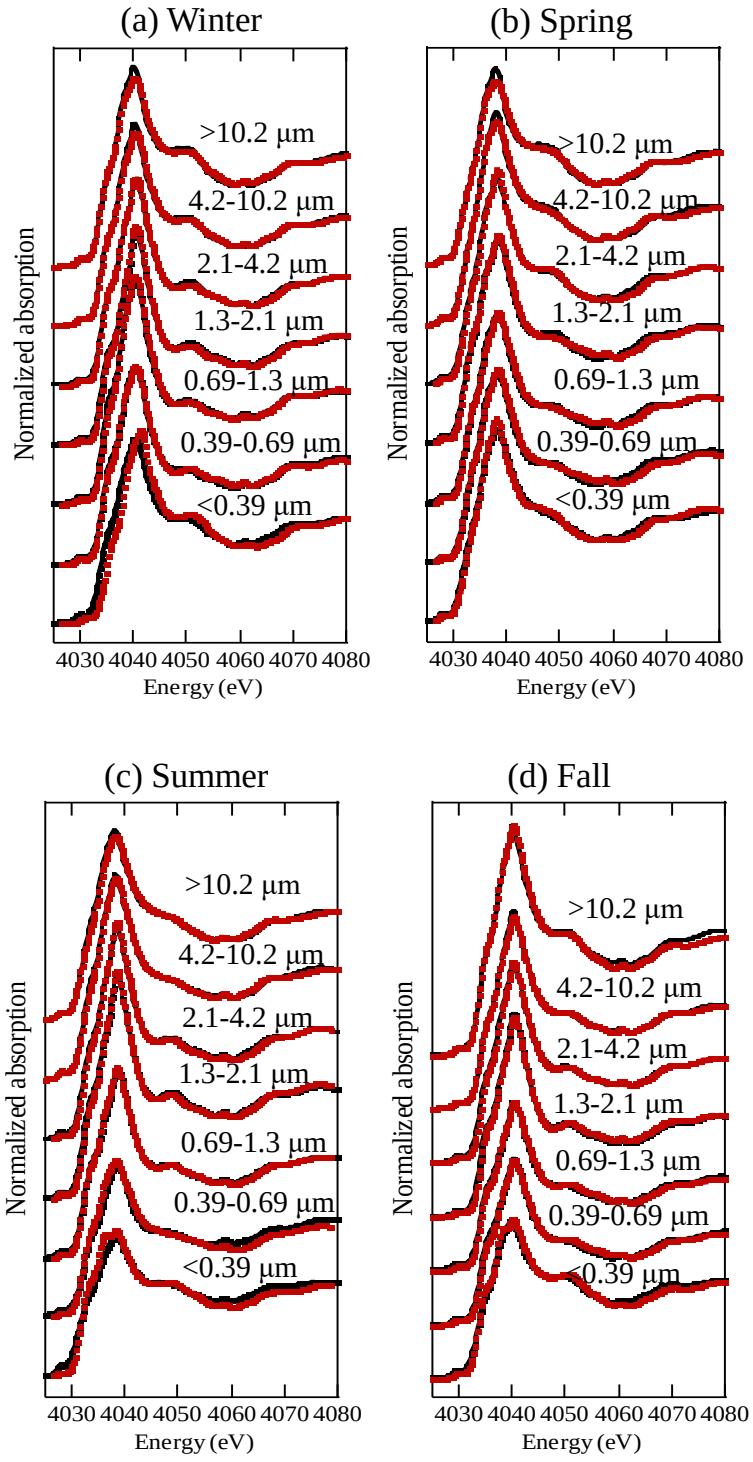

Fig. 2.18. Calcium K-edge XANES spectra of aerosol samples collected in winter (a), spring (b), summer (c), and fall (d). The red dashed line in normalized spectra and the black solid line is fitting line.

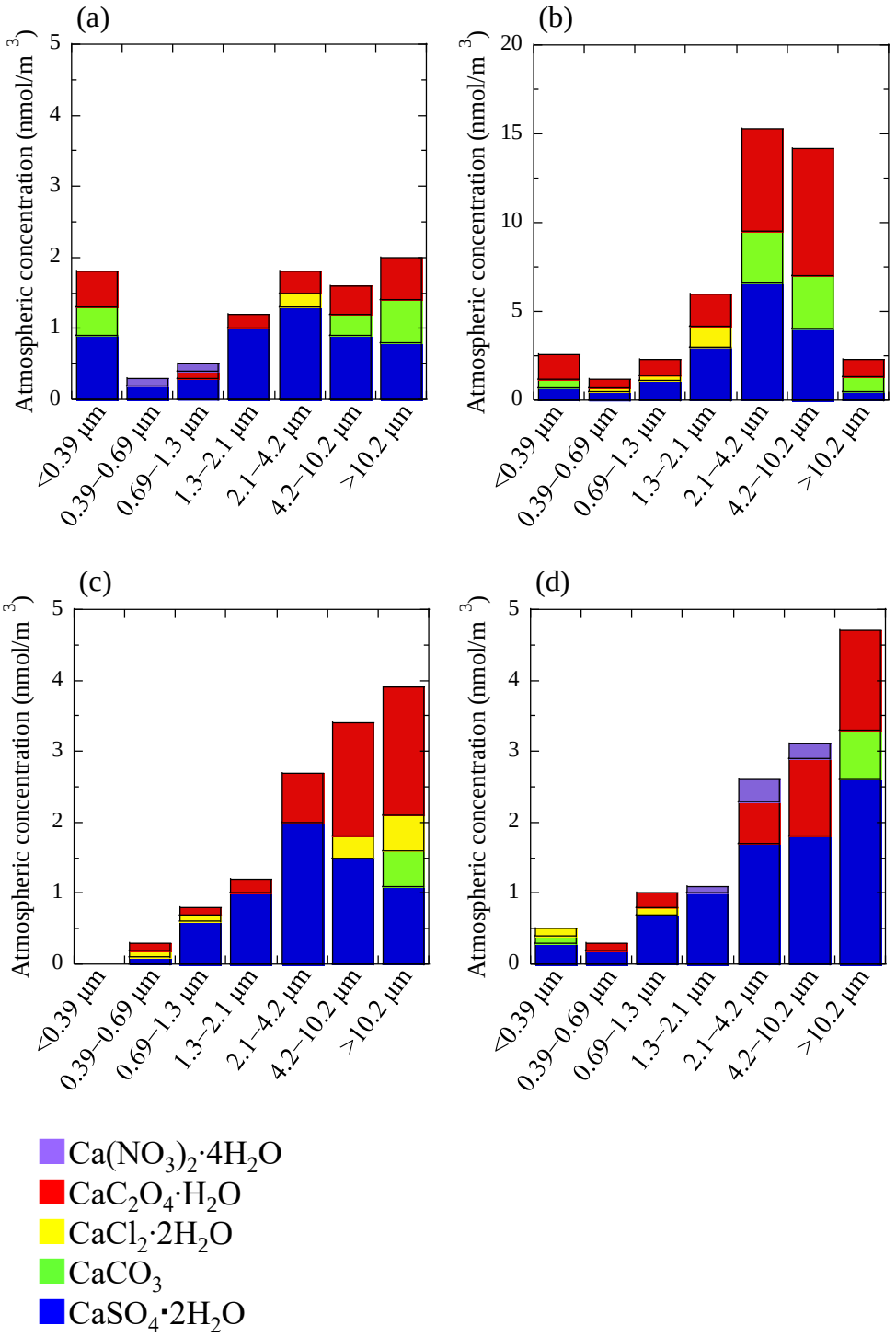

Fig. 2.19. Size distribution of each Ca species (nmol/m^3) in the aerosol samples collected during winter (a), spring (b), summer (c), and fall (d). The horizontal axis denotes particle size (μm), and the vertical axis indicates atmospheric concentration (nmol/m^3). Notably, the maximum value of the vertical axis is 20 nmol/m^3 for (b) and 5 nmol/m^3 for (a), (c), and (d).

Table 2.7. Size distribution of fraction of each Ca species about each season determined by XAFS. The species of whole particle were determined by FY-XANES, and surface species were determined by CEY-XAENS.

	Particle size	< 0.39 μm		0.39-0.69 μm		0.69-1.3 μm		1.3-2.1 μm		2.1-4.2 μm		4.2-10.2 μm		> 10.2 μm	
		Whole	Surface	Whole	Surface	Whole	Surface	Whole	Surface	Whole	Surface	Whole	Surface	Whole	Surface
Winter	$Ca(NO_3)_2 \cdot 4H_2O$			19.9		20.8	20.0								
	$CaC_2O_4 \cdot H_2O$	28.4				16.6	15.2	19.3		16.6	17.3	27.2	14.9	28.0	21.4
	$CaCl_2 \cdot 2H_2O$		No data	13.7	No data					11.4					
	$CaCO_3$	24.0										19.7	11.2	32.2	15.4
	$CaSO_4 \cdot 2H_2O$	47.6		66.5		62.6	64.8	80.7	100	72.0	82.7	53.0	73.8	39.8	63.2
	R factor	0.330		0.021		0.026	0.020	0.025	0.018	0.018	0.019	0.025	0.016	0.034	0.018
		Whole	Surface	Whole	Surface	Whole	Surface	Whole	Surface	Whole	Surface	Whole	Surface	Whole	Surface
Spring	$Ca(NO_3)_2 \cdot 4H_2O$						20.8								
	$CaC_2O_4 \cdot H_2O$	52.3		42.4		37.9	24.2	30.1	36.2	37.7	30.4	50.7	34.7	42.7	
	$CaCl_2 \cdot 2H_2O$		No data	15.4	No data	15.3		19.6	16.5						No data
	$CaCO_3$	19.7								19.1	12.9	21.3	16.1	34.7	
	$CaSO_4 \cdot 2H_2O$	28.0		42.2		46.8	54.2	50.2	47.3	43.2	56.7	28.0	49.2	22.6	
	R factor	0.029		0.031		0.022	0.035	0.026	0.041	0.026	0.027	0.029	0.023	0.031	
		Whole	Surface	Whole	Surface	Whole	Surface	Whole	Surface	Whole	Surface	Whole	Surface	Whole	Surface
Summer	$Ca(NO_3)_2 \cdot 4H_2O$														
	$CaC_2O_4 \cdot H_2O$			38.3		15.9	19.2	18.6	20.3	27.0	24.8	47.9	36.2	45.6	37.2
	$CaCl_2 \cdot 2H_2O$	No data	No data	24.9	No data	13.4						9.4		12.4	
	$CaCO_3$													12.5	
	$CaSO_4 \cdot 2H_2O$			36.8		70.7	80.8	81.4	79.7	73.0	75.2	42.7	63.8	29.5	62.8
	R factor			0.053		0.019	0.020	0.023	0.036	0.026	0.016	0.021	0.021	0.025	0.064
		Whole	Surface	Whole	Surface	Whole	Surface	Whole	Surface	Whole	Surface	Whole	Surface	Whole	Surface
Fall	$Ca(NO_3)_2 \cdot 4H_2O$						11.2	12.2	13.0	9.8	11.6	5.7	10.6		13.3
	$CaC_2O_4 \cdot H_2O$		19.2	23.6	23.6	15.9				23.4		34.3	5.4	30.5	12.4
	$CaCl_2 \cdot 2H_2O$	28.2		15.3		12.8									
	$CaCO_3$	23.0	30.4											15.2	
	$CaSO_4 \cdot 2H_2O$	48.8	50.4	61.1	76.4	71.2	88.8	87.8	87.0	66.9	88.4	60.0	84.0	54.3	74.3
	R factor	0.037	0.034	0.020	0.052	0.020	0.028	0.022	0.035	0.018	0.032	0.026	0.039	0.041	0.068

Previous studies on aerosols collected in Aksu, which is close to one of the source regions of Asian dust in western China, showed that $CaCO_3$ is the major Ca species in the particles (Miyamoto et al., 2016; Nishikawa et al., 2000; Takahashi et al., 2009). $CaCO_3$ has also been reported as an important component of Asian dust (Jeong, 2008; Krueger et al., 2004). By contrast, other species, such as $CaSO_4 \cdot 2H_2O$, comprise less than 20% of the total Ca in the aerosol collected near the source region (Miyamoto et al., 2016; Takahashi et al., 2009). The surface of mineral particles is an important reaction site in the atmosphere, and $CaCO_3$ is reactive with acids because of its highly alkaline property (Rubasinghege and Grassian, 2013). Therefore, the $CaSO_4 \cdot 2H_2O$ and $CaC_2O_4 \cdot 2H_2O$ detected in our samples were formed during transport in the atmosphere. Laboratory experiments indicated that $CaSO_4 \cdot 2H_2O$ and CaC_2O_4 were formed through the conversion of $CaCO_3$ when hygroscopic components (e.g., nitrate salts) promoted leaching of Ca^{2+} and acids contained in particles (Ma et al., 2019, 2013). Given that $CaSO_4 \cdot 2H_2O$ and $CaC_2O_4 \cdot 2H_2O$ are thermodynamically insoluble and stable in a solution, it is reasonable that they will eventually form in the particles.

Surface-sensitive CEY-XANES analysis confirmed the presence of $CaSO_4 \cdot 2H_2O$ on the surface. $CaSO_4 \cdot 2H_2O$ fraction on the particle surface was larger than that in the whole particle, and vice versa for $CaCO_3$ in coarse particles for all the samples (Fig. 2. 20 and Table 2.7). Therefore, it is suggested that each Ca species was not present as external mixing particles but formed by chemical reactions mostly on the particle surface and present as internal mixing particles. In addition, it is considered that the formation of insoluble species, such as $CaSO_4 \cdot 2H_2O$, on the surface inhibited further reaction of $CaCO_3$ (Takahashi et al., 2009), which was also indicated by laboratory experiments (Ma et al., 2019, 2013).

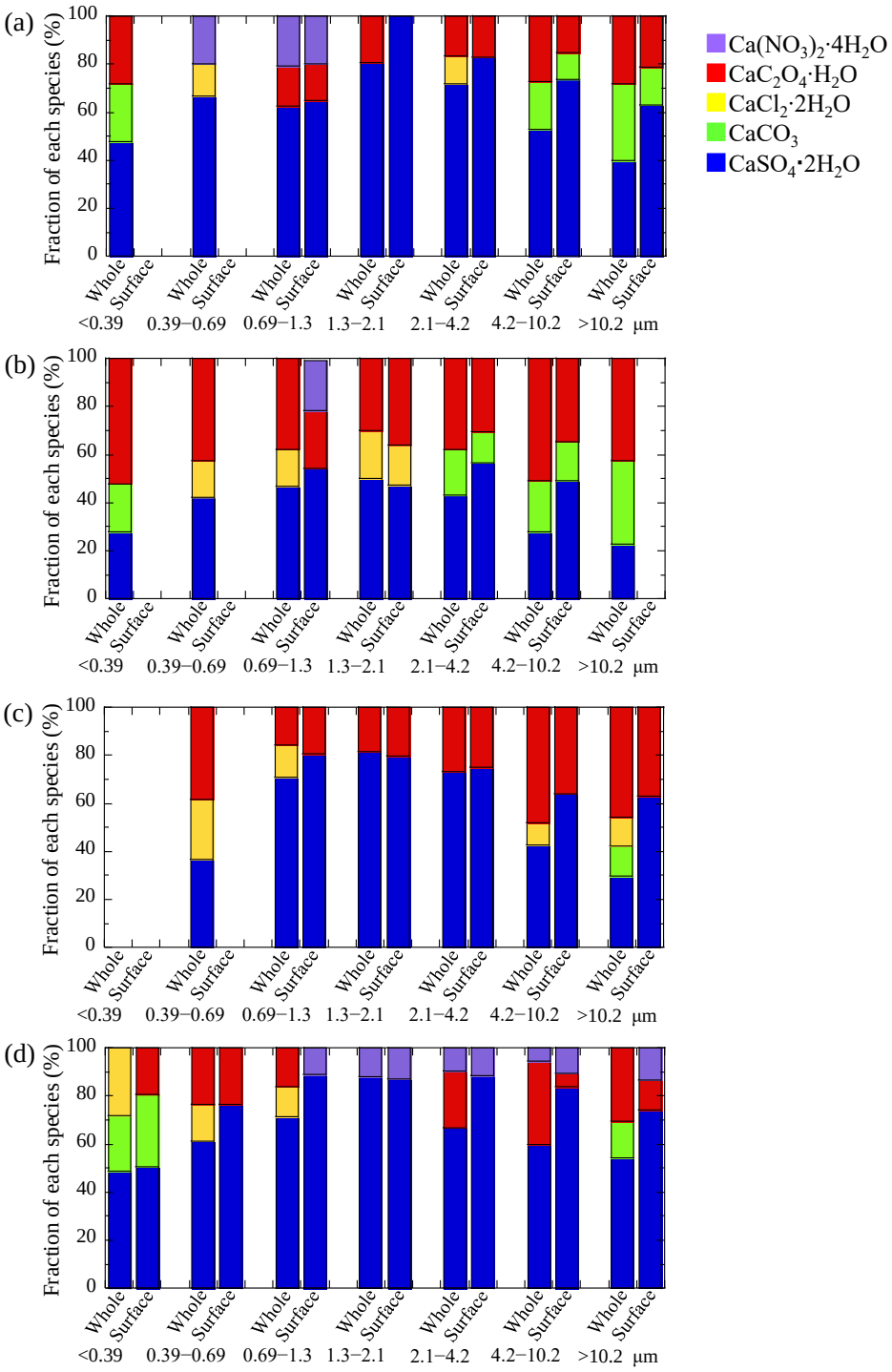

Fig. 2.20. Size distribution of fraction of each Ca species about each season determined by XANES. The species of whole particle were determined by FY-XANES, and species at particle surfaces were determined by CEY-XAENS.

2.3.2.4 Contribution of the reaction of $CaCO_3$ in mineral particles for aerosol CCN activity

Hygroscopicity parameters of endmembers κ_i are provided in Table 2.4. $CaCO_3$ originally does not exhibit a high CCN activity due to its low hygroscopicity of 6.8×10^{-3} (Sullivan et al., 2009; Tang et al., 2015). Previous studies have suggested that the CCN activity of particles that contain $CaCO_3$ will be higher than the original particles, since $CaCO_3$ changes into highly hygroscopic species, such as $Ca(NO_3)_2{\cdot}4H_2O$ and $CaCl_2{\cdot}2H_2O$, through reactions in the atmosphere. Their κ values are 0.43 and 0.68, respectively, which are higher than that of $CaCO_3$ by more than three orders of magnitude. However, our Ca speciation results from XANES spectroscopy analysis indicated that these hygroscopic species are minor Ca species. By contrast, $CaSO_4{\cdot}2H_2O$ and $CaC_2O_4{\cdot}H_2O$ were dominant in the aerosols throughout the year. Therefore, it is considered that CCN activity does not dramatically change compared with that of $CaCO_3$.

The κ value of each sample was calculated based on the Ca XANES speciation results and Eq. (6). For this calculation, we assumed that the volume fraction of the respective Ca species in each particle was the same among all the particles in each size fraction (i.e., each stage). The κ values of Ca species were determined using Eq. (6), as shown in Table 2.8. The estimated κ values of the aerosol samples ($\kappa_{aerosol}$) were nearly the same as the κ value of $CaCO_3$ (κ_{CaCO3}) when only $CaSO_4{\cdot}2H_2O$ and $CaC_2O_4{\cdot}H_2O$ were formed in the particles (e.g., aerosol samples larger than 2.1 μm during spring as shown in Figs. 2.19 and 2.20, and Table 2.7), confirming that the CCN activities of Ca aerosols did not change. However, when $Ca(NO_3)_2{\cdot}4H_2O$ and/or $CaCl_2{\cdot}2H_2O$ were included in the particles, $\kappa_{aerosol}$ became 34 times higher than κ_{CaCO3} at most. Even in the latter case, $\kappa_{aerosol}$ was approximately one-third of $\kappa_{(NH4)2SO4}$ and κ_{NH4NO3}, which are considered typical hygroscopic aerosols. Therefore, the effects of secondary Ca species in aerosols formed by the reaction on CCN activity are insufficiently large to influence the hygroscopicity of aerosols. In

addition, low hygroscopic Ca species, such as $CaSO_4 \cdot 2H_2O$ fraction on the particle surface, was larger than that in the whole particle, as indicated by the CEY-XANES analysis. This result emphasized that the enhancement of hygroscopicity by soluble materials formed on a particle surface is unlikely related to Ca species.

Table 2.8. Results of calculated $\kappa_{aerosol}$ value of Ca species in aerosol samples.

	Winter	Spring	Summer	Fall
>10.2 μm	7.03×10^{-3}	6.68×10^{-3}	0.104	7.15×10^{-3}
4.2−10.2 μm	7.17×10^{-3}	6.69×10^{-3}	7.67×10^{-2}	4.75×10^{-2}
2.1−4.2 μm	8.98×10^{-2}	6.97×10^{-3}	7.34×10^{-3}	7.46×10^{-2}
1.3−2.1 μm	7.47×10^{-3}	0.150	7.49×10^{-3}	8.87×10^{-2}
0.69−1.3 μm	0.140	0.119	0.104	0.100
0.39−0.69 μm	0.218	0.120	0.188	0.118
<0.39 μm	7.11×10^{-3}	6.67×10^{-3}	No data	0.232

Similarly, κ values of sulfate in each sample were calculated based on the sulfur XANES speciation results and Eq. (6) (Table 2.9). The κ values of endmembers have high values among 0.61 to 0.93, except for $CaSO_4 \cdot 2H_2O$ with 7.8×10^{-3} (Table 2.4). Because sulfate species in fine particles hardly contain $CaSO_4 \cdot 2H_2O$, the $\kappa_{aerosol}$ values of sulfate indicated relatively high values near that of $(NH_4)_2SO_4$ ($\kappa_{(NH4)2SO4}$= 0.61). In contrast, $\kappa_{aerosol}$ values of sulfate in coarse particles were totally lower than that in fine particles because of larger fraction of $CaSO_4 \cdot 2H_2O$.

As a result of calculation of κ values by considering both Ca and sulfate species in the aerosol samples, it was suggested that the reaction of $CaCO_3$ in mineral particles totally act to decrease CCN activity of aerosol.

Table 2.9. Results of calculated $\kappa_{aerosol}$ value of sulfate species in aerosol samples.

	Winter	Spring	Summer	Fall
>10.2 μm	0.366	0.295	0.156	7.80×10^{-3}
4.2−10.2 μm	0.126	0.118	7.80×10^{-3}	0.158
2.1−4.2 μm	0.079	0.135	7.80×10^{-3}	7.80×10^{-3}
1.3−2.1 μm	0.483	0.211	0.298	0.450
0.69−1.3 μm	0.692	0.474	0.667	0.650
0.39−0.69 μm	0.641	0.610	0.649	0.610
<0.39 μm	0.610	0.610	0.610	0.610

2.3.2.5 Reduction of the number of hygroscopic sulfate aerosols by the reaction of $CaCO_3$ in mineral particles

From the result of Ca speciation in Section 2.3.2.3, it is suggested that $CaSO_4{\cdot}2H_2O$ in the particles was not original but formed by the reaction in the atmosphere. SO_2, a precursor of sulfate, was mostly converted to sulfate in the atmosphere in gas or droplet phase. From the result of the sulfate speciation analysis by XANES in Section 2.3.2.2, sulfate species in the aerosol samples were hygroscopic except for $CaSO_4{\cdot}2H_2O$. If $CaSO_4{\cdot}2H_2O$ was not formed in aerosols, a considerable amount of SO_2 must have formed to $CaSO_4{\cdot}2H_2O$ should form hygroscopic sulfate aerosols, such as $(NH_4)_2SO_4$, which is an important species in CCN. Therefore, these results suggested that the formation of $CaSO_4{\cdot}2H_2O$ in aerosols may reduce the amount of SO_2, which is finally converted to hygroscopic sulfate aerosols acting as CCN. Thus, estimating the reduction amount of high hygroscopic sulfate, i.e., $(NH_4)_2SO_4$, in fine particles by forming low hygroscopic sulfate, i.e., $CaSO_4{\cdot}2H_2O$, in coarse particles is essential. If the formation of $CaSO_4{\cdot}2H_2O$ does not occur, then we can assume that 1 mole of $CaSO_4{\cdot}2H_2O$ in coarse particles will form 1 mole of hygroscopic sulfate in fine particles. Here, we assumed that the fraction of mole concentration

of $CaSO_4 \cdot 2H_2O$ determined by S XANES analysis in Section 2.3.2.2 to mole concentration of total sulfate in all size fraction indicates fraction of reduced hygroscopic sulfate in the atmosphere. As a result of the calculation, the fraction of reduced hygroscopic sulfate was calculated to be comparable to approximately ~20% of total amount of sulfate in fine aerosols (winter: 9.0%; spring: 14.3%; summer: 8.5%; fall: 17.7%). The degree of reduction of the hygroscopic sulfate is equivalent to that of $(NH_4)_2SO_4$ which should be present in fine particles. The reduction amount was highest in the spring and fall samples, which were strongly affected by mineral dust. Consequently, the formation of $CaSO_4 \cdot 2H_2O$ in the atmosphere likely consumes sulfate ion, or oxidation products of SO_2, and finally suppresses the formation of high-hygroscopic sulfate. A similar role of conversion of $CaCO_3$ has been discussed mainly by modeling and laboratory studies (Dentener et al., 1996; Sullivan et al., 2009; Tang et al., 2016). I here emphasize that the present chapter obtained similar conclusions based on the natural observation coupled with XANES spectroscopy for the speciation analysis of actual aerosol samples.

2.4 Conclusions

Here, seasonal variation of sulfate species in both TSP and size-fractionated aerosol samples and their characteristics were investigated based on XANES spectroscopy. As a result of speciation of sulfate in TSP samples, major sulfate species has high hygroscopicity except for $CaSO_4 \cdot 2H_2O$. The $CaSO_4 \cdot 2H_2O$ fraction to total sulfate increased especially during high nss-Ca^{2+} period such as mineral dust event. It was suggested that $CaSO_4 \cdot 2H_2O$ fraction in aerosols does not dependent on total sulfate concentration because $CaSO_4 \cdot 2H_2O$ is controlled by Ca^{2+} concentration. By contrast, the $(NH_4)_2SO_4$ fraction was better correlated with [Total-SO_4^{2-}] – [$CaSO_4 \cdot 2H_2O$] than total sulfate concentration. This result suggested that the reaction forming $CaSO_4 \cdot 2H_2O$ preferentially occurs rather than $(NH_4)_2SO_4$. Therefore, it is suggested that

$CaSO_4 \cdot 2H_2O$ formed was stable and not converted to $(NH_4)_2SO_4$ once $CaSO_4 \cdot 2H_2O$ was formed. In addition, analysis of size-fractionated aerosol clarified that $CaSO_4 \cdot 2H_2O$ was major in coarse particles but high hygroscopic sulfate such as $(NH_4)_2SO_4$, NH_4HSO_4, and hydrated SO_4^{2-} were major in fine particles. The formation of $CaSO_4 \cdot 2H_2O$ in the atmosphere likely consumes sulfate and consequently suppresses the formation of high hygroscopic sulfate such as $(NH_4)_2SO_4$. The hygroscopicity parameter of sulfate aerosol decreased depending on the increase of the $CaSO_4 \cdot 2H_2O$ fraction to total sulfate. Besides, the amount of hygroscopic sulfate in fine particles was decreased by the reaction that formed $CaSO_4 \cdot 2H_2O$ in coarse particles which is strongly affected by mineral dust. Although similar results have been suggested in other studies based on modeling and laboratory investigations, this chapter demonstrated similar conclusions based on natural observation coupled with XANES spectroscopy for the speciation of sulfate in actual aerosol samples.

As a result of Ca speciation analysis of the same samples using combination of FY and CEY−XANES analysis, $CaSO_4 \cdot 2H_2O$ fraction on the particle surface was larger than that in the whole particle, and vice versa for $CaCO_3$ in coarse particles. Therefore, it was suggested that $CaSO_4 \cdot 2H_2O$ was formed secondarily on the surface of the aerosol by reaction of $CaCO_3$ in the atmosphere. Besides, $CaSO_4 \cdot 2H_2O$ and $CaC_2O_4 \cdot H_2O$ were identified as major species formed by the reaction of $CaCO_3$, because a major Ca species in Asian dust is originally $CaCO_3$. The CCN activity of Ca aerosols was not considerably changed by the reaction from the original species because the low hygroscopic Ca species such as $CaSO_4 \cdot 2H_2O$ and $CaC_2O_4 \cdot H_2O$ were major in particles, meanwhile high hygroscopic such as $Ca(NO_3)_2 \cdot 4H_2O$ and $CaCl_2 \cdot 2H_2O$ were minor

Chapter 3.

$CaSO_4 \cdot 2H_2O$ formation by reaction of $CaCO_3$ in the atmosphere

This chapter has been published in the following paper: C. Miyamoto, M. A. Marcus, K. Sakata, M. Kurisu, and Y. Takahashi, Depth-dependent Calcium Speciation in Individual Aerosol Particles by Combination of Fluorescence Yield and Conversion Electron Yield XAFS Using X-ray Microbeam, Chem. Lett. 2016, 45, 934. doi:10.1246/cl.160392

3.1 Chapter introduction

Mineral particles are one of major component of aerosols emitted from arid and semiarid regions and its annual flux reaches 1000−3000 Tg yr-1 (e.g., Zender et al., 2004). They have large impacts on visibility, air quality, and direct and/or indirect radiative forcing (e.g., Mikami et al., 2006; Tang et al., 2004; Usher et al., 2003). In addition, various chemical reactions related to various important environmental phenomena can occur on the particle surfaces in the atmosphere (Tang et al., 2015; Usher et al., 2003). Among them, calcite ($CaCO_3$) is a reactive mineral component with acids because of their high alkaline property (Rubasinghege and Grassian, 2013). $CaCO_3$ is one of major components in mineral dusts originated form arid area or desert in western China and Mongolia (Krueger et al., 2004; Nishikawa et al., 2000). A huge amount of mineral particle including $CaCO_3$ is often emitted by Asian dust event in every spring and transported to North Pacific through urban area in East Asia (Kellogg and Griffin, 2006). In recent years, urban area in China is a significant emission source of anthropogenic SO_2 derived from fossil fuel combustion globally (Crippa et al., 2016; Qu et al., 2016; Streets et al., 2003). Therefore, it is considered that $CaCO_3$ can react with SO_2 and/or sulfuric acids in the atmosphere when mineral dust passes through the urban area, which can alter their species. Various previous studies have indicated reaction of mineral particles during transportation. For example, Takahashi et al. (2009) analyzed calcium (Ca) species in aerosol samples collected in Aksu (near the Taklimakan Desert), Qingdao (urban area in eastern China), and Tsukuba (eastern Japan) during a large dust event in March, 2002 using Ca K-edge X-ray absorption near-edge structure (XANES) spectroscopy, or the structure near absorption edge in X-ray absorption fine structure (XAFS). The main Ca species in the spectra were $CaCO_3$ and gypsum ($CaSO_4{\cdot}2H_2O$), and the mole ratio of $CaSO_4{\cdot}2H_2O$ converted from $CaCO_3$ by reaction in the atmosphere to total Ca (= measured by ion chromatography) were estimated. The $CaSO_4{\cdot}2H_2O$ fraction determined by the bulk analysis

increased in the order from Aksu, Qingdao to Tsukuba. Additionally, $CaSO_4 \cdot 2H_2O$ fraction was relatively larger near the surface of particles than that in entire particles which was confirmed by Ca K-edge XANES measured in (i) fluorescence yield (FY) and (ii) conversion electron yield (CEY) modes. FY-XANES and CEY-XANES analysis provide information of Ca species in the whole and at the surface of the particles, respectively. Coupling of the two modes enables us to compare fraction of Ca species in the whole and at the surface of the particles. Thus, these results suggested that $CaSO_4 \cdot 2H_2O$ was formed by reaction of $CaCO_3$ at the surface of particles during transport. However, this analysis using mm-size X-ray beam still has a problem, because the method shows average Ca species as bulk analysis of lots of particles recovered on the aerosol filters. This means that relatively larger ratio of $CaSO_4 \cdot 2H_2O$ at particles surfaces suggested by CEY mode does not indicate formation of $CaSO_4 \cdot 2H_2O$ at the $CaCO_3$ surface, but the secondary formation of $CaSO_4 \cdot 2H_2O$ can occur at surface of other particles.

In this chapter, X-ray fluorescence (XRF) mapping and Ca K-edge XANES measurement both in FY and CEY modes were conducted using a μm-size X-ray beam. This method, which can be referred to as depth-dependent μ-XAFS, allows Ca speciation of individual mineral aerosols both in the whole and at the surface of the particles, respectively.

3.2 Materials and Methods

3.2.1 Aerosol samples collected in Aksu and Qingdao

Particle size-fractionated samples were collected using a 9-stage Andersen-type air sampler (AN-200, Sibata, Japan) in Aksu and Qingdao (Fig. 3.1) during a large dust event recorded from 20 to 22 March 2002 in the Aeolian Dust Experiment on Climate Impact (ADEC) project (Mikami et al., 2006). Results of bulk chemical analysis of the major ions and Ca chemical species in the aerosol sample for all size stages were reported in Takahashi et al. (2009). Here, we

report analysis of aerosol samples with 3.3-4.7 μm particle diameter. Details of the sampling were shown in Table 3.1.

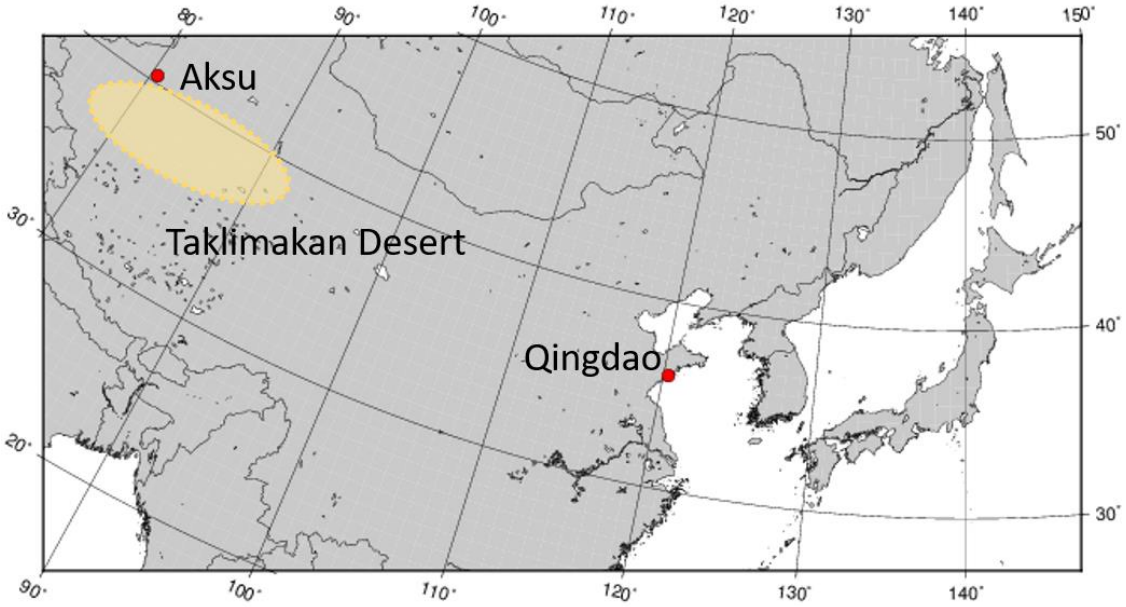

Fig. 3.1. Sampling site: Aksu and Qingdao are located at 40˚37', 80˚44 and 36˚07', 120˚33', respectively.

Table 3.1. Information about the sampling.

Sampling site	**Aksu**	**Qingdao**
Location	The Aksu Water Budget Experiment Station, Chinese Academy of Science	Ocean University of China
Lat/Long	40°37'N, 80°44'E	36°07'N, 120°33'E
Height	7.0 m (above sea level)	80 m (above sea level)
Sampling Period	15-21 March 2002	20-23 March 2002
Temperature	−2.7~ +17.9 °C	+1.9~+11.0 °C
Average Daily Precipitation	0.00 mm	0.67 mm
R.H.	14.5~59.7 %	39.4~82.1 %

3.2.2 Chemical speciation analysis in individual aerosol particles using X-ray microbeam

Micro-XRF-XAFS analysis was conducted at beamline 10.3.2 at the Advanced Light Source in Lawrence Berkeley National Laboratory, U.S.A (Marcus et al., 2004). Particles collected on the PTFE filter in the air sampler were dispersed on a carbon tape (Cat. No. 731, Nissin EM, Japan). To identify Ca-rich particles, μ-XRF analysis was conducted for the aerosol particles dispersed on the carbon tape. Mapping was performed with a beam size of 3×3 μm^2 or 5×5 μm^2 for identifying 3-5 μm particles collected in the sample. Subsequently, Ca K-edge μ-XANES spectra were measured for the Ca-rich particles using 6×6 μm^2 beam. The XRF and XANES spectra were measured in a cell with two electrodes purged with helium, which enables us to measure μ-XANES in CEY mode (Girardeau et al., 1992). In addition, fluorescence X-ray was detected by a Canberra 7-element Ge detector (Ultra LEGe, 50 mm^2 per element) through a thin film of aluminised Mylar used as a window of the CEY cell. The combination of FY-mode (probing depth: 6.5 μm) and CEY-mode (probing depth: about 0.25 μm) defined in Schroeder (1996) makes it possible to determine Ca species in the whole and at the surface of each particle (Takahashi et al., 2009, 2008a).

XANES spectra obtained were fitted by a linear combination of spectra of reference materials as reported in Takahashi et al. (2008) to estimate mole ratios of Ca species present in the individual particle. The least-squares fitting of the spectra was conducted using REX2000 (Rigaku Co., Tokyo, Japan). The range of uncertainty of fitting analysis was approximately ±15~30% with smallest and largest *R* value determined using Eq. (2) in Chapter 2, respectively.

3.3 Results and Discussion

The results obtained for the samples at Aksu are described first. Aksu located in western China close to the Taklimakan Desert, which is the main source of dust transported from the desert. It is expected that the degree of conversion of $CaCO_3$ is much lower than that in eastern China such as in Qingdao. Bulk FY- and CEY-XANES spectra using a mm-size beam for the Aksu sample showed that the Ca species in the bulk samples are mainly $CaCO_3$ and $CaSO_4 \cdot 2H_2O$ (Takahashi et al., 2009). The $CaSO_4 \cdot 2H_2O$ fractions of the bulk analysis determined by the FY- and CEY-modes were almost identical around 15 mole%. The fact that the $CaSO_4 \cdot 2H_2O$/ $CaCO_3$ ratios are identical between the two modes for the bulk sample suggested that $CaSO_4 \cdot 2H_2O$ is not formed secondarily at the surface of the particles in the Aksu samples. The particle size as a possible factor to cause the difference of the mole ratios can be ignored here, because the samples were collected as a fraction with specific particle size (3.3-4.7 μm) by the size-fractionated sampling. The content of 15 mole% $CaSO_4 \cdot 2H_2O$ suggested here is reasonable, considering that $CaSO_4 \cdot 2H_2O$ is also found in sands in the Taklimakan Desert as primary minerals, but its concentration is much lower than that of $CaCO_3$ (Chang et al., 2000; Honda and Shimizu, 1998).

Similar results were obtained by μ-XRF-XAFS for individual particles. The XRF mapping illustrated distribution of single particles containing Ca on the carbon tape for the same aerosol samples collected in Aksu (Fig. 3.2). Three particles were selected for the measurement of Ca K-edge XANES individually. Spectra of one particle measured by both FY- and CEY-modes were shown in Fig. 3.3 along with the reference spectra of $CaCO_3$, aragonite (a polymorph of calcite), and $CaSO_4 \cdot 2H_2O$. The shapes of XANES spectra measured in FY- and CEY-modes were almost identical to the spectrum of $CaCO_3$. The least-squares fitting considering various Ca species including $CaCO_3$, aragonite, $CaSO_4 \cdot 2H_2O$, anhydrite, anorthite, dolomite, and apatite showed that these spectra of the aerosol samples can be fitted by assuming the two components,

$CaCO_3$ and $CaSO_4 \cdot 2H_2O$.

Table 3.2 is mole fraction (f_{cal}, %) of $CaCO_3$ in the particles determined by least-squares fitting analysis. The f_{cal} of Particle 1 was f_{cal} = 86% vs. 81% in the FY- and CEY-modes, respectively. Similar measurements for the other two particles showed that f_{cal} = 73% vs. 78% in the FY- and CEY- modes, respectively, for Particle 2, and f_{cal} = 100% in both modes for Particle 3. The $CaSO_4 \cdot 2H_2O$ fraction is not large compared with those measured in Qingdao as described below. In addition, the $CaSO_4 \cdot 2H_2O$ mole fractions (100- f_{cal} %) were almost the same between FY- and CEY-modes, showing that $CaSO_4 \cdot 2H_2O$ is not formed at the particle surface of $CaCO_3$, but the two species are homogeneously mixed within the particle. These results suggested that (i) $CaCO_3$ in Aksu is not subject to reaction with acids during transport and (ii) small amount of $CaSO_4 \cdot 2H_2O$ relative to $CaCO_3$ may be directly transported from the Taklimakan Desert.

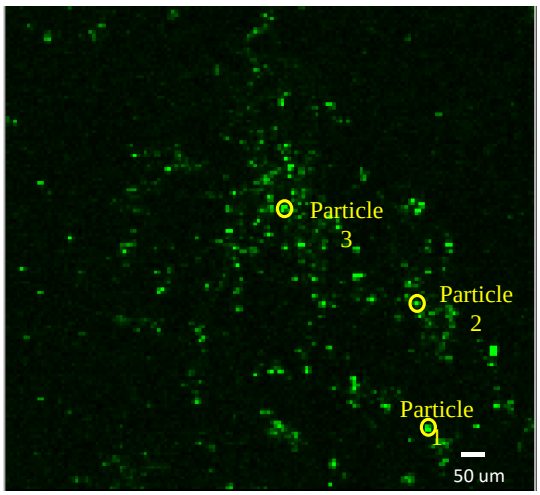

Fig. 3.2. XRF-mapping of aerosol sample collected in Aksu. The sample collected on PTFE filter was dispersed on carbon tape employed for μ-XRF mapping, where green spots indicate intensity of Ca K line. Ca K-edge XANES of three particles (Particles 1 to 3) were measured.

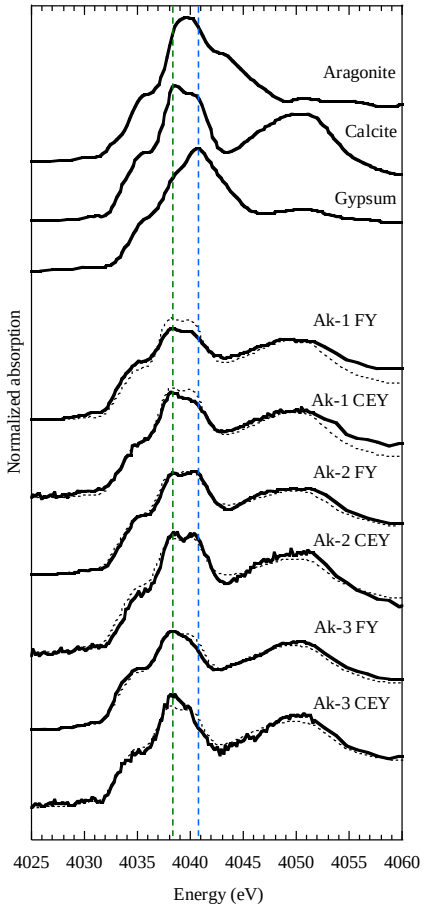

Fig. 3.3. Normalized Ca K-edge XANES spectra of aerosol samples collected in Aksu (Ak) and the fitting line by least-squares fitting (dashed line). The spectra of reference materials (calcite ($CaCO_3$), aragonite, and gypsum ($CaSO_4 \cdot 2H_2O$)) are also shown. Green dashed vertical line means peak top energy of $CaCO_3$, blue one means peak top energy of $CaSO_4 \cdot 2H_2O$.

Table 3.2. $CaCO_3$ (calcite) fraction (f_{cal}, %) in each particle analysed by both in the FY and CEY-mode, which were determined by fitting analysis. Another species was $CaSO_4 \cdot 2H_2O$, the $CaSO_4 \cdot 2H_2O$ fraction = $100 - f_{cal}$ (%).

Sampling site	Analysed particle No.	FY-mode (whole of particle)	CEY-mode (surface of particle)
Aksu	1	86%	81%
	2	73%	78%
	3	100%	100%
Qingdao	1	70%	43%
	2	88%	55%

We also applied the same methods to the individual particles collected in Qingdao during the dust event. The result of average $CaSO_4 \cdot 2H_2O$ fraction by XANES using mm-size X-ray beam for particles on the aerosol filter in FY- and CEY-modes (bulk analysis) were 37 mole% and 55 mole%, respectively, for the 3.3-4.7 μm diameter particles (Takahashi et al., 2009). This result suggested that $CaSO_4 \cdot 2H_2O$ can be formed selectively at the particle surfaces, but it is not clear whether the conversion of $CaCO_3$ to $CaSO_4 \cdot 2H_2O$ occurred at the surface the particles by the result, because it is possible to interpret that $CaSO_4 \cdot 2H_2O$ simply coated on any particles.

This ambiguity can be excluded using the depth-dependent μ-XAFS. The XRF mapping illustrated distribution of single particles containing Ca on the carbon tape for the same aerosol samples collected in Qingdao (Fig. 3.4). Figure 3.5 shows Ca K-edge μ-XANES spectra for one aerosol particle collected in Qingdao with reference spectra of $CaCO_3$, $CaSO_4 \cdot 2H_2O$, and anhydrite ($CaSO_4$). The result of μ-XANES in FY-mode showed that particles collected in Qingdao during a dust event consisted of $CaCO_3$ and $CaSO_4 \cdot 2H_2O$ (Fig. 3.5). When we compared FY- and CEY-XANES spectra for the particle, we can find differences in the shapes of the spectra: the FY-XANES was similar to that of $CaCO_3$, as seen from the shape around the peak-top. On the other hand, the shape around the peak top of CEY-XANES shifted to higher energy than that of FY-XANES and the energy of the peak top at 4040.5 eV was almost identical to that of $CaSO_4 \cdot 2H_2O$. The $CaCO_3$ fraction was f_{cal} = 70 vs. 43 in the FY- and CEY-modes, respectively, for Particle 1 in Fig. 3.5. Another particle examined showed that f_{cal} = 87 vs. 55, respectively. The fitting results are shown in Table 3.2.

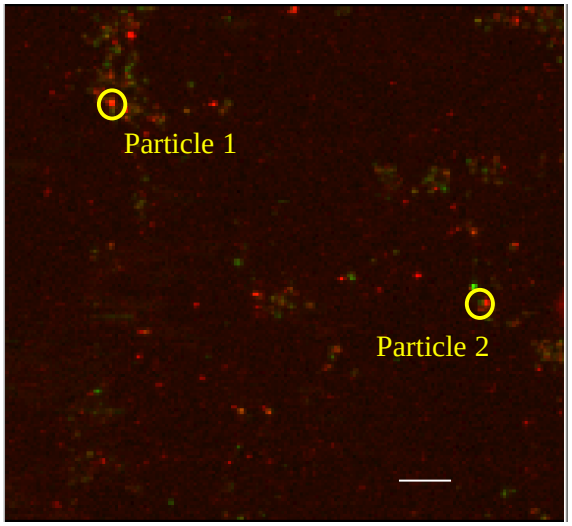

Fig. 3.4. XRF-mapping of aerosol sample collected in Qingdao. The sample collected on PTFE filter was dispersed on carbon tape employed for μ-XRF mapping, where red spots indicate intensity of Ca K line and green spots indicate intensity of Fe K line. Ca K-edge XANES of two particles (Particles 1 and 2) were measured.

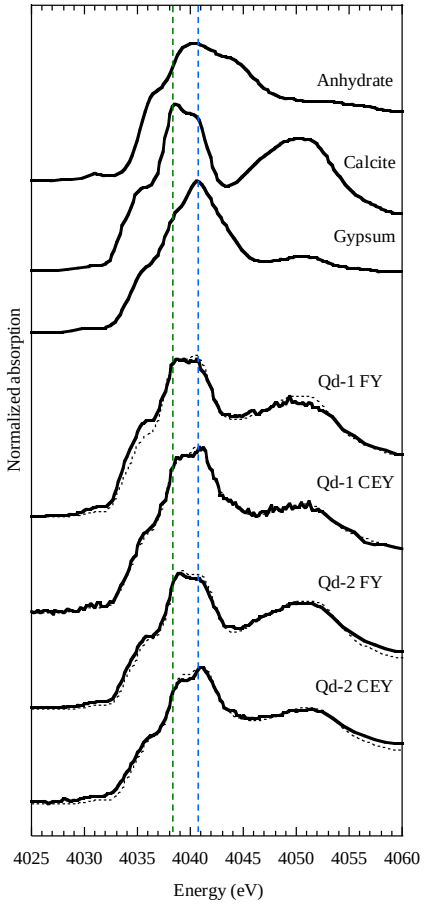

Fig. 3.5. Normalized Ca K-edge XANES spectra of aerosol samples collected in Qingdao (Qd) and the fitting line by least-squares fitting (dashed line). The spectra of reference materials (calcite ($CaCO_3$), aragonite, and gypsum ($CaSO_4 \cdot 2H_2O$)) are also shown. Green dashed vertical line means peak top energy of $CaCO_3$, blue one means peak top energy of $CaSO_4 \cdot 2H_2O$.

The results showed that the mole ratio of $CaSO_4$･$2H_2O$ was larger in the CEY-mode than that in the FY-mode for individual particle, showing clearly that $CaSO_4$·$2H_2O$ was mainly formed at the surface of the individual aerosol particles in Qingdao. In particular, coexistence of $CaCO_3$ and $CaSO_4$･$2H_2O$ at different ratios in the whole and at the surface of the particles in Qingdao suggested that $CaSO_4$･$2H_2O$ was formed at the surface of the $CaCO_3$ particle during long-range transport from Aksu to Qingdao. This information of the reaction occurring on each particle cannot be obtained using mm-size X-ray beam, because the FY- and CEY- information provides average Ca species in the whole and surface of various particles, respectively.

3.4 Conclusion

The depth-dependent Ca speciation using μ-XAFS both in FY- and CEY-modes was applied to individual aerosol particles collected at two sites (Aksu and Qingdao), which are near sources of mineral dust and urban area in East Asia, respectively. The results directly showed that $CaCO_3$ was subject to reaction in the atmosphere and transformation to $CaSO_4$·$2H_2O$ at the surface of individual particle in the atmosphere. This result was not clear in the reported study using bulk analysis. Therefore, it is expected that depth-dependent μ-XAFS will be a useful tool in future to understand chemical processes occurring at the surface of aerosols, or mineral dust, which is important to know the subsequent effects caused by aerosols in environment, such as cooling effect in climate change, which is related to hygroscopicity of aerosol particles.

Chapter 4.

Neutralization process of $CaCO_3$ in the atmosphere recorded in the aerosol particles transported and trapped in Greenland ice core sample related to secular change of SO_2 emission

本章については、5 年以内に雑誌等で

刊行予定のため、非公開。

Chapter 5.

Sulfate aerosols collected in Noto peninsula: estimation of their species, sources, reaction process, and roles for CCN

本章については、5 年以内に雑誌等で
刊行予定のため、非公開。

Chapter 6.

General discussion and conclusions

6.1 Summary of this thesis

The estimation of indirect radiative forcing reported in IPCC has large uncertainty (IPCC, 2013). The uncertainty was mainly caused by discrepancy of estimation results given by different simulations mainly due to unknown factors in the interactions between aerosols and clouds. In order to understand cloud droplet formation from CCN, physicochemical properties of aerosols acting as CCN should be clarified (Lohmann and Feichter, 2010). Estimating the concentration of sulfate aerosols in modeling studies has been mostly based on (i) the emission of the precursor gases (e.g., SO_2), (ii) the fraction of deposition amount of SO_2, and (iii) the chemical transformation rate of SO_2 to sulfate (Penner et al., 2011). The anthropogenic SO_2 emission was generally calculated from database of emission inventory by consumption of fossil fuel. Therefore, sulfate aerosols are uniformly treated as hygroscopic components, thereby difference of hygroscopicity among various sulfate species has not been taken into account.

This thesis aimed at clarification of size distribution and seasonal variation of sulfate species in aerosol in East Asia based on X-ray absorption near-edge absorption structure (XANES) spectroscopy with other multiple analyses. Based on the results, formation and reaction processes of sulfate aerosol in the atmosphere were discussed. In addition, effects of change of physicochemical properties of sulfate aerosol by the processes on its activity as cloud condensation nuclei (CNN) were also evaluated related to its influence on the indirect cooling effect as a radiative forcing of the climate change of the earth. The summary is as follows:

1. As a result of speciation of sulfate in aerosols collected in Higashi-Hiroshima using sulfur (S) K-edge XANES spectroscopy, major sulfate species were ammonium sulfate ($(NH_4)_2SO_4$), ammonium hydrogen sulfate (NH_4HSO_4), hydrated SO_4^{2-}, and gypsum ($CaSO_4 \cdot 2H_2O$). $CaSO_4 \cdot 2H_2O$ is suggested to be preferentially formed in particles and not converted to $(NH_4)_2SO_4$ once $CaSO_4 \cdot 2H_2O$ was formed due to its high stability. Additionally,

Calcium (Ca) K-edge XANES analysis for bulk aerosol samples indicated that $CaSO_4 \cdot 2H_2O$ was preferentially formed at particle surface, which suggested that $CaSO_4 \cdot 2H_2O$ was secondarily formed by surface reaction of the particles.

2. Ca species in aerosol particles collected near emission sources of mineral dust consisted of $CaSO_4 \cdot 2H_2O$ and calcite ($CaCO_3$), and the latter is a major mineral in Asian dust (Krueger et al., 2004; Nishikawa et al., 2000). Meanwhile, $CaSO_4 \cdot 2H_2O$ fraction to total Ca became large at surface of particles than that of whole of particles in urban area in eastern China. Consequently, it was concluded that $CaSO_4 \cdot 2H_2O$ was formed by surface reaction of $CaCO_3$ particles during its transportation in the atmosphere.
3. $CaCO_3$ fraction to total calcium in particles trapped in a Greenlandic ice core was larger in the layers corresponding to 1971, 1978, and 1987 than those to 1995 and 2004. In contrast, $CaSO_4 \cdot 2H_2O$ fraction to total calcium were larger in the latter layers (1995 and 2004) than those in the former layers (1971, 1978, and 1987). The increase trend of $CaSO_4 \cdot 2H_2O$ had a positive correlation with the growth of SO_2 annual emission in China. Consequently, it is suggested that (i) $CaSO_4 \cdot 2H_2O$ formed by the reaction possibly in the East Asia and (ii) $CaSO_4 \cdot 2H_2O$ in aerosol formed by the reaction remains unchanged through the long range transportation from China to Greenland.
4. As a result of analysis of aerosol samples collected at Noto peninsula for about one year, it is suggested that low hygroscopic $CaSO_4 \cdot 2H_2O$ formation in coarse particles decreased hygroscopic sulfate in fine particles and consequently decrease CCN amount in the atmosphere. In addition, emission sources of sulfate in aerosol was discussed using $[NO_3^-]/[nss{-}SO_4^{2-}]$ ratio, enrichment factor (EF) of trace elements, Pb/V ratio, and sulfur isotope ratio ($\delta^{34}S$). Consequently, discrimination diagram using $\delta^{34}S$ and Pb/V also with sulfate species enable us to discuss not only the sources but also formation and reaction

process of the particles in the atmosphere.

This thesis based on direct observation of aerosols pointed out the importance of sulfate speciation in aerosols, because $CaSO_4 \cdot 2H_2O$ with low hygroscopicity was major sulfate species (Chapters 2 and 5). The $CaSO_4 \cdot 2H_2O$ was formed by reaction of $CaCO_3$ in mineral particles with SO_2 and/or sulfate in the atmosphere (Chapter 3), which is suggested by laboratory studies (Ma et al., 2013; Tang et al., 2017b). The reaction of mineral particles and sulfate has not been sufficiently considered in the estimation of the radiative forcing. Additionally, the results in this thesis have indicated that (i) $CaSO_4 \cdot 2H_2O$ was preferentially formed among sulfate species depending on the availability of Ca^{2+} due to its high stability (Chapters 2 and 4), (ii) $CaSO_4 \cdot 2H_2O$ was formed during transportation of mineral particles from East Asia which is the main reaction site of mineral aerosols with sulfate emitted from fossil fuel combustion in China (Chapters 2, 4, and 5), and (iii) the formation of $CaSO_4 \cdot 2H_2O$ decreases amount of hygroscopic sulfate in fine particles (Chapter 5). The variation of number concentrations of hygroscopic aerosols such as fine sulfates (e.g., $(NH_4)_2SO_4$) will change the number concentration of CCN, and hence the indirect radiative forcing (Albrecht, 1989; Lohmann and Feichter, 2010; Twomey, 1959).

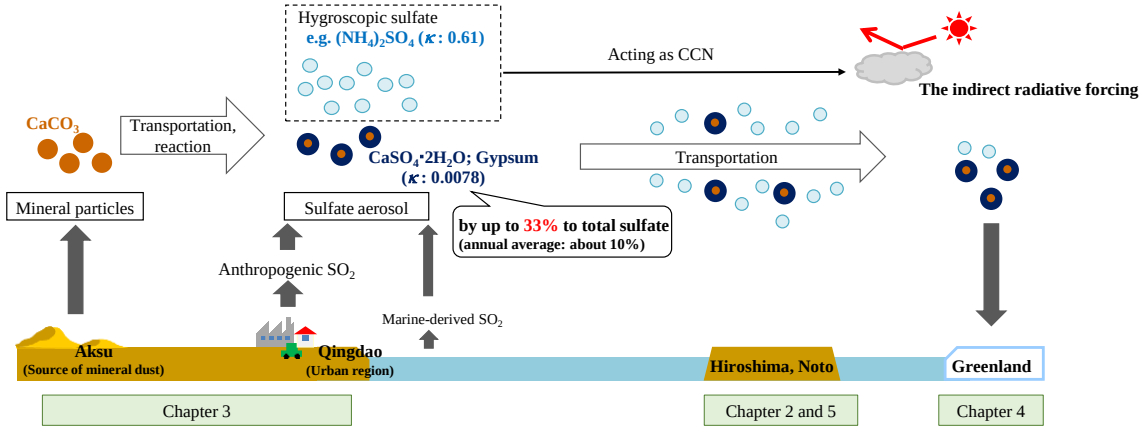

Fig. 6.1. Summary of this thesis. κ is hygroscopicity parameter. A larger κ value indicates higher hygroscopicity (Petters and Kreidenweis, 2007).

6.2 General discussion

以下、5 年以内に雑誌等で刊行予定のため、非公開。

Acknowledgements

I am deeply grateful to Prof. Yoshio Takahashi. Without his patient guidance, encouragement, and supports, this thesis would not have been possible. In addition, he gave me a lot of chances to try various experiments and attend conferences. I deeply respect him for his attitude toward research and meticulous mentorship. I have greatly benefited from Dr. Takaaki Itai. He gave me a lot of insightful comments and suggestions. He helped me so much when I measured sulfur isotope compositions. I would like to express my gratitude to laboratory members of “Team Aerosol”, Dr. Kohei Sakata (National Institute for Environmental Studies), Ms. Aya Miyahara, Mr. Yoshiaki Yamakawa, Ms. Minako Kurisu, and Mr. Takehiro Teranishi. They taught me sampling and analytical methods and discussions with them have been illuminating and interesting. Especially, a lot of advice and comments given by Dr. Sakata has been a great help in my research. In addition, I received generous support from Ms. Kurisu who is a same-age colleague. I would like to express my gratitude to all laboratory members: Dr. Masato Tanaka, Dr. Haibo Qin, Dr. Shitong Yang, Dr. Jing Sun, Dr. Hiroki Suga, Ms. Akiko Yamaguchi, Mr. Hikaru Miura, Mr, Hiroyuki Tsuboi, Mr. Shogo Kawashima, Ms. Sachika Natori, Ms. Keika Suzuki, Mr. Makoto Nagasawa, Ms. Nanako Hasegawa, Ms. Kazusa Tamura, Mr. Hiroki Ishimizu, and Ms. Shinobu Matsukura. I would like to show my greatest appreciation to Prof. Toshihiro Kogure, Dr. Yohey Suzuki, Prof. Takashi Murakami, Prof. Makoto Koike, Dr. Nobuhiro Moteki and other SES, BMS, and climate and material science seminar members.

My heartfelt appreciation goes to research collaborators. Dr. Yoshinori Iizuka (Inst. Low Temperature Science, Hokkaido Univ.) distributed me SE-Dome ice core samples and gives me constructive comments and warm encouragement. Dr. Sumito Matoba (Inst. Low Temperature Science, Hokkaido Univ.) and other members of research project of SE-core gives insightful comments and suggestions. Dr. Atsushi Matsuki gave me opportunities for aerosol sampling at

NOTO Grand−based Research Observatory (NOTOGRO) and kindly supports. Dr. Shohei Hattori kindly helped me in various respect both in SE-core and Noto projects. Dr. Teruhiko Kashiwabara and Dr. Katsuhiko Suzuki (JAMSTEC) gave me precious opportunities for measurements of sulfur isotope compositions by MC-ICP-MS. Dr. Shogo Higaki gave me opportunities for measurement of sulfate concentration by ICP-MS/MS. I used modeling data simulated by SPRINTERS (Figs. 2.11 and 5.20) and I thank Prof. Takemura who is developer of the transport model.

Finally, I my sincere gratitude to my family and friends. Without their support in every respect, I could not continue this research.

References

Adachi, K., Buseck, P.R., 2010. Hosted and free-floating metal-bearing atmospheric nanoparticles in Mexico city. Environmental Science and Technology 44, 2299–2304. https://doi.org/10.1021/es902505b

Adams, P.J., Seinfeld, J.H., Koch, D.M., 1999. Global concentrations of tropospheric sulfate, nitrate, and ammonium aerosol simulated in a general circulation model. Journal of Geophysical Research Atmospheres 104, 13791–13823. https://doi.org/10.1029/1999JD900083

Al-Hosney, H.A., Grassian, V.H., 2005. Water, sulfur dioxide and nitric acid adsorption on calcium carbonate: A transmission and ATR-FTIR study. Physical Chemistry Chemical Physics 7, 1266–1276. https://doi.org/10.1039/b417872f

Al-Hosney, H.A., Grassian, V.H., 2004. Carbonic acid: An important intermediate in the surface chemistry of calcium carbonate. Journal of the American Chemical Society 126, 8068–8069. https://doi.org/10.1021/ja0490774

Albalat, E., Telouk, P., Balter, V., Fujii, T., Bondanese, V.P., Plissonnier, M.L., Vlaeminck-Guillem, V., Baccheta, J., Thiam, N., Miossec, P., Zoulim, F., Puisieux, A., Albarède, F., 2016. Sulfur isotope analysis by MC-ICP-MS and application to small medical samples. Journal of Analytical Atomic Spectrometry 31, 1002–1011. https://doi.org/10.1039/c5ja00489f

Albrecht, B.A., 1989. Aerosols, Cloud Microphysics, and Fractional Cloudiness. Science 245, 1227–1230. https://doi.org/10.1126/science.245.4923.1227

Amrani, A., Deev, A., Sessions, A.L., Tang, Y., Adkins, J.F., Hill, R.J., Moldowan, J.M., Wei, Z., 2012. The sulfur-isotopic compositions of benzothiophenes and dibenzothiophenes as a proxy for thermochemical sulfate reduction. Geochimica et Cosmochimica Acta 84, 152–

164. https://doi.org/10.1016/j.gca.2012.01.023

Amrani, A., Said-Ahmad, W., Shaked, Y., Kiene, R.P., 2013. Sulfur isotope homogeneity of oceanic DMSP and DMS. Proceedings of the National Academy of Sciences of the United States of America 110, 18413–18418. https://doi.org/10.1073/pnas.1312956110

Andreae, M.O., Rosenfeld, D., 2008. Aerosol-cloud-precipitation interactions. Part 1. The nature and sources of cloud-active aerosols. Earth-Science Reviews 89, 13–41. https://doi.org/10.1016/j.earscirev.2008.03.001

Arimoto, R., Duce, R.A., Savoie, D.L., Prospero, J.M., Talbot, R., Cullen, J.D., Tomza, U., Lewis, N.F., Ray, B.J., 1996a. Relationships among aerosol constituents from Asia and the North Pacific during PEM-West a. Journal of Geophysical Research Atmospheres 101, 2011–2023. https://doi.org/10.1029/95JD01071

Arimoto, R., Duce, R.A., Savoie, D.L., Prospero, J.M., Talbot, R., Cullen, J.D., Tomza, U., Lewis, N.F., Ray, B.J., 1996b. Relationships among aerosol constituents from Asia and the North Pacific during PEM-West a. Journal of Geophysical Research Atmospheres 101, 2011–2023. https://doi.org/10.1029/95JD01071

Barnes, I., Hjorth, J., Mihalapoulos, N., 2006. Dimethyl sulfide and dimethyl sulfoxide and their oxidation in the atmosphere. Chemical Reviews 106, 940–975. https://doi.org/10.1021/cr020529+

Bauer, S.E., Koch, D., 2005. Impact of heterogeneous sulfate formation at mineral dust surfaces on aerosol loads and radiative forcing in the Goddard Institute for Space Studies general circulation model. Journal of Geophysical Research D: Atmospheres 110, 91–105. https://doi.org/10.1029/2005JD005870

Becagli, S., Sferlazzo, D.M., Pace, G., Di Sarra, A., Bommarito, C., Calzolai, G., Ghedini, C., Lucarelli, F., Meloni, D., Monteleone, F., Severi, M., Traversi, R., Udisti, R., 2012.

Evidence for heavy fuel oil combustion aerosols from chemical analyses at the island of Lampedusa: A possible large role of ships emissions in the Mediterranean. Atmospheric Chemistry and Physics 12, 3479–3492. https://doi.org/10.5194/acp-12-3479-2012

Bjørk, A.A., Kjær, K.H., Korsgaard, N.J., Khan, S.A., Kjeldsen, K.K., Andresen, C.S., Box, J.E., Larsen, N.K., Funder, S., 2012. An aerial view of 80 years of climate-related glacier fluctuations in southeast Greenland. Nature Geoscience 5, 427–432. https://doi.org/10.1038/ngeo1481

Bory, A.J.-M., Biscaye, P.E., Grousset, F.E., 2003. Two distinct seasonal Asian source regions for mineral dust deposited in Greenland (NorthGRIP). Geophysical Research Letters 30, 1167. https://doi.org/10.1029/2002GL016446

Bory, A.J.M., Abouchami, W., Galer, S.J.G., Svensson, A., Christensen, J.N., Biscaye, P.E., 2014. A Chinese imprint in insoluble pollutants recently deposited in central greenland as indicated by lead isotopes. Environmental Science and Technology 48, 1451–1457. https://doi.org/10.1021/es4035655

Bory, A.J.M., Biscaye, P.E., Svensson, A., Grousset, F.E., 2002. Seasonal variability in the origin of recent atmospheric mineral dust at NorthGRIP, Greenland. Earth and Planetary Science Letters 196, 123–134. https://doi.org/10.1016/S0012-821X(01)00609-4

Bouche, Olivier and Randall, D., 2013. Clouds and aerosols. Climate Change 2013 the Physical Science Basis: Working Group I Contribution to the Fifth Assessment Report of the Intergovernmental Panel on Climate Change 9781107057, 571–658. https://doi.org/10.1017/CBO9781107415324.016

Boucher, O., Lohmann, U., 1995. The sulfate-CCN-cloud albedo effect: A sensitivity study with two general circulation models. Tellus 47B, 281–300. https://doi.org/10.3402/tellusb.v47i3.16048

Calhoun, J.A., Bates, T.S., Charlson, R.J., 1991. Sulfur isotope measurements of submicrometer sulfate aerosol particles over the Pacific Ocean. Geophysical Research Letters 18, 1877–1880. https://doi.org/10.1029/91GL02304

Calvo, A.I., Vicente, A.M., Alves, C., Fraile, R., Castro, A., Pont, V., 2012. Research on aerosol sources and chemical composition: Past, current and emerging issues. Atmospheric Research 120–121, 1–28. https://doi.org/10.1016/j.atmosres.2012.09.021

Cao, J.J., Lee, S.C., Zhang, X.Y., Chow, J.C., An, Z.S., Ho, K.F., Watson, J.G., Fung, K., Wang, Y.Q., Shen, Z.X., 2005. Characterization of airborne carbonate over a site near Asian dust source regions during spring 2002 and its climatic and environmental significance. Journal of Geophysical Research D: Atmospheres 110, 1–8. https://doi.org/10.1029/2004JD005244

Chang, Q., Mishima, T., Yabuki, S., Takahashi, Y., Shimizu, H., 2000. Sr and Nd isotope ratios and REE abundances of moraines in the mountain areas surrounding the Taklimakan desert, NW China. Geochemical Journal 34, 407–427. https://doi.org/10.2343/geochemj.34.407

Charlson, R.J., Schwartz, S.E., Hales, J.M., Cess, R.D., Coakley JR., J.A., Hansen, J.E., Hofmann, D.J., 1992. Climate Forcing by Antlropogenic Aerosols. Science 255, 423–430. https://doi.org/10.1126/science.255.5043.423

Choi, J.C., Lee, M., Chun, Y., Kim, J., Oh, S., 2001. Chemical composition and source signature of spring aerosol in Seoul, Korea 106, 18,067-18,074.

Chun, Y., Kim, J., Cheon Choi, J., On Boo, K., Nam Oh, S., Lee, M., 2001. Characteristic number size distribution of aerosol during Asian dust period in Korea. Atmospheric Environment 35, 2715–2721. https://doi.org/10.1016/S1352-2310(00)00404-0

Coplen, Tyler B., Krouse, H.R., 1988. Sulphur isotope data consistency improved. Nature 392,

32. https://doi.org/10.1111/j.1748-7692.1988.tb00545.x

Craddock, P.R., Rouxel, O.J., Ball, L.A., Bach, W., 2008. Sulfur isotope measurement of sulfate and sulfide by high-resolution MC-ICP-MS. Chemical Geology 253, 102–113. https://doi.org/10.1016/j.chemgeo.2008.04.017

Crippa, M., Janssens-Maenhout, G., Dentener, F., Guizzardi, D., Sindelarova, K., Muntean, M., Van Dingenen, R., Granier, C., 2016. Forty years of improvements in European air quality: Regional policy-industry interactions with global impacts. Atmospheric Chemistry and Physics 16, 3825–3841. https://doi.org/10.5194/acp-16-3825-2016

Dentener, F.J., 1996. Role of mineral aerosol as a reactive surface in the global troposphere. Journal of Geophysical Research 101, 22,869-22,889,.

Dentener, F.J., Carmichael, G.R., Zhang, Y., Lelieveld, J., Crutzen, P.J., 1996. Role of mineral aerosol as a reactive surface in the global troposphere 101, 22,869-22,889,.

Ding, T., Valkiers, S., Kipphardt, H., De Bièvre, P., Taylor, P.D.P., Gonfiantini, R., Krouse, R., 2001. Calibrated sulfur isotope abundance ratios three IAEA sulfur isotope reference materials and V-CDT with a reassessment of the atomic weight of sulfur. Geochimica et Cosmochimica Acta 65, 2433–2437. https://doi.org/10.1016/S0016-7037(01)00611-1

Fischer, H., Wagenbach, D., Kipfstuhl, J., 1998. Sulfate and nitrate firn concentrations on the Greenland ice sheet 2. Temporal anthropogenic deposition changes. Journal of Geophysical Research Atmospheres 103, 21935–21942. https://doi.org/10.1029/98JD01886

Forster P, Ramaswamy V, Artaxo P, Berntsen T, Betts R, Fahey DW, Haywood J, Lean J, Lowe DC, Myhre G, Nganga J., Prinn R., Raga, G, Schultz M., Van Dorland, R., 2007. Changes in atmospheric constituents and in radiative forcing. Chapter 2. In: Solomon, S., D. Qin, M. Manning, Z. Chen, M. Marquis, K.B. Averyt, M.Tignor and H.L. Miller (eds.), Climate

Change 2007: The Physical Science Basis. Contribution of Working Group. https://doi.org/10.20892/j.issn.2095-3941.2017.0150

Fowler, D., Coyle, M., Skiba, U., Sutton, M., Cape, J.N., Reis, S., Sheppard, L., Jenkins, A., Grizetti, B., Galloway, J.N., Vitousek, P., Leach, A., Bouwman, L., Butterbach-Bahl, K., Dentener, F., Stevenson, D., Amann, M., Voss, M., 2013. The global nitrogen cycle in the 21th century. Philisophical Transactions of the Royal Society of London, B Biological Sciences 368, 20130165. https://doi.org/http://dx.doi.org/10.1098/rstb.2013.0164

Furukawa, R., Uemura, R., Fujita, K., Sjolte, J., Yoshimura, K., Matoba, S., Iizuka, Y., 2017. Seasonal-Scale Dating of a Shallow Ice Core From Greenland Using Oxygen Isotope Matching Between Data and Simulation. Journal of Geophysical Research: Atmospheres 122, 10,873-10,887. https://doi.org/10.1002/2017JD026716

Furukawa, T., Takahashi, Y., 2011. Oxalate metal complexes in aerosol particles: Implications for the hygroscopicity of oxalate-containing particles. Atmospheric Chemistry and Physics 11, 4289–4301. https://doi.org/10.5194/acp-11-4289-2011

Girardeau, T., Mimault, J., Jaouen, M., Tourillon, G., 1992. Sampling depth in conversion-electron detection used for x-ray absorption 46.

Goodman, A.L., Underwood, G.M., Grassian, V.H., 2000. A laboratory study of the heterogeneous reaction of nitric acid on calcium carbonate particles 105, 29,053-29,064.

Gu, W., Li, Y., Zhu, J., Jia, X., Lin, Q., Zhang, G., Ding, X., Song, W., Bi, X., Wang, X., Tang, M., 2017. Investigation of water adsorption and hygroscopicity of atmospherically relevant particles using a commercial vapor sorption analyzer. Atmospheric Measurement Techniques 10, 3821–3832. https://doi.org/10.5194/amt-10-3821-2017

Hameed, S., Dignon, J., 1988. Changes in the geographical distributions of global emissions of NOx and SOx from fossil-fuel combustion between 1966 and 1980. Atmospheric

Environment (1967) 22, 441–449. https://doi.org/10.1016/0004-6981(88)90190-4

Han, X., Guo, Q., Liu, C., Fu, P., Strauss, H., Yang, J., Hu, J., Wei, L., Ren, H., Peters, M., Wei, R., Tian, L., 2016. Using stable isotopes to trace sources and formation processes of sulfate aerosols from Beijing, China. Scientific Reports 6, 29958. https://doi.org/10.1038/srep29958

Haywood, J., Boucher, O., 2000. Estimates of the direct and indirect radiative forcing due to tropospheric aerosols: A review. Reviews of Geophysics 38, 513–543. https://doi.org/10.1029/1999RG000078

Honda, M., Shimizu, H., 1998. Geochemical, mineralogical and sedimentological studies on the Taklimakan Desert sands. Sedimentology 45, 1125–1143. https://doi.org/10.1046/j.1365-3091.1998.00202.x

Hong, Y., Zhang, H., Zhu, Y., 1993a. Sulfur isotopic characteristics of coal in China and sulfur isotopic fractionation during coal-burning process. Chinese Journal of Geochemistry 12, 51–59. https://doi.org/10.1007/BF02869045

Hong, Y., Zhang, H., Zhu, Y., 1993b. Sulfur isotopic characteristics of coal in China and sulfur isotopic fractionation during coal-burning process. Chinese journal of geochemistry 12, 51–59.

Huang, J., Mendoza, B., Daniel, J.S., Nielsen, C.J., Rotstayn, L., Wild, O., 2013. Anthropogenic and natural radiative forcing. Climate Change 2013 the Physical Science Basis: Working Group I Contribution to the Fifth Assessment Report of the Intergovernmental Panel on Climate Change 9781107057, 659–740. https://doi.org/10.1017/CBO9781107415324.018

Iizuka, Y., Matoba, S., Yamasaki, T., Oyabu, I., Kadota, M., Aoki, T., 2016. Glaciological and meteorological observations at the SE-Dome site, southeastern Greenland Ice Sheet. Bulletin of Glaciological Research 34, 1–10.

Iizuka, Y., Miyake, T., Hirabayashi, M., Suzuki, T., Matoba, S., Motoyama, H., Fujii, Y., Hondoh, T., 2009. Constituent elements of insoluble and non-volatile particles during the Last Glacial Maximum exhibited in the Dome Fuji (Antarctica) ice core. Journal of Glaciology 55, 552–562.

Iizuka, Y., Miyamoto, A., Hori, A., Matoba, S., Furukawa, R., Saito, T., Fujita, S., Hirabayashi, M., Yamaguchi, S., Fujita, K., Takeuchi, N., 2017. A Firn Densification Process in the High Accumulation Dome of Southeastern Greenland. Arctic, Antarctic, and Alpine Research 49, 13–27. https://doi.org/10.1657/AAAR0016-034

Iizuka, Y., Uemura, R., Fujita, K., Hattori, S., Seki, O., Miyamoto, C., Suzuki, T., Yoshida, N., Motoyama, H., Matoba, S., 2018. A 60 Year Record of Atmospheric Aerosol Depositions Preserved in a High-Accumulation Dome Ice Core, Southeast Greenland. Journal of Geophysical Research: Atmospheres 123, 574–589. https://doi.org/10.1002/2017JD026733

Iizuka, Y., Uemura, R., Motoyama, H., Suzuki, T., Miyake, T., Hirabayashi, M., Hondoh, T., 2012. Sulphate–climate coupling over the past 300,000 years in inland Antarctica. Nature 490, 81–84. https://doi.org/10.1038/nature11359

Inomata, Y., Ohizumi, T., Saito, T., Morohashi, M., Yamashita, N., Takahashi, M., Sase, H., Takahashi, K., Kaneyasu, N., Fujihara, M., Iwasaki, A., Nakagomi, K., Shiroma, T., Yamaguchi, T., 2019. Estimating transboundary transported anthropogenic sulfate deposition in Japan using the sulfur isotopic ratio. Science of The Total Environment 691, 779–788. https://doi.org/10.1016/j.scitotenv.2019.07.004

IPCC, 2013: Climate Change 2013: The Physical Science Basis. Contribution of Working Group I to the Fifth Assessment Report of the Intergovernmental Panel on Climate Change [Stocker, T.F., D. Qin, G.-K. Plattner, M. Tignor, S.K. Allen, J. Boschung, A. Nauels, Y.

Xia, V. Bex and P.M. Midgley (eds.)]. Cambridge University Press, Cambridge, United Kingdom and New York, NY, USA, 1535 pp

Jeong, G.Y., 2008. Bulk and single-particle mineralogy of Asian dust and a comparison with its source soils. Journal of Geophysical Research Atmospheres 113, 1–16. https://doi.org/10.1029/2007JD008606

Köhler, H., 1936. The nucleus in and the growth of hygroscopic droplets. Transactions of the Faraday Society 32, 1152–1161.

Kawamura, K., Kaplan, I.R., 1983. Organic Compounds In the Rainwater of Los Angelest. Environmental Science and Technology 17, 497–501. https://doi.org/10.1021/es00114a011

Kellogg, C.A., Griffin, D.W., 2006. Aerobiology and the global transport of desert dust. Trends in Ecology and Evolution 21, 638–644. https://doi.org/10.1016/j.tree.2006.07.004

Kim, B.M., Teffera, S., Zeldin, M.D., 2000. Characterization of PM25 and PM10 in the South Coast Air Basin of Southern California: Part 1-Spatial Variations. Journal of the Air and Waste Management Association 50, 2034–2044. https://doi.org/10.1080/10473289.2000.10464242

Kotani, Takashi, Yanagisawa, Fumitaka, Kanai, Yutaka, Miyaoka, Akiko, and Akita, N., 2012. Combination of Sulfur Isotope Ratio of Non-sea Salt Sulfate and Lead-210 Concentration in Aerosols as an Index of Long-range Transported Aerosols. Radioisotopes 61, 65–70.

Kreutz, K.J., Sholkovitz, E.R., 2000. Major element, rare earth element, and sulfur isotopic composition of a high-elevation firn core: Sources and transport of mineral dust in central Asia. Geochemistry, Geophysics, Geosystems 1, 1525–2027.

Krueger, B.J., Grassian, V.H., Cowin, J.P., Laskin, A., 2004. Heterogeneous chemistry of individual mineral dust particles from different dust source regions: The importance of

particle mineralogy. Atmospheric Environment 38, 6253–6261. https://doi.org/10.1016/j.atmosenv.2004.07.010

Kuramoto, T., Goto-Azuma, K., Hirabayashi, M., Miyake, T., Motoyama, H., Dahl-Jensen, D., Steffensen, J.P., 2011. Seasonal variations of snow chemistry at NEEM, Greenland. Annals of Glaciology 52, 193–200. https://doi.org/10.3189/172756411797252365

Kwamura, K., Sakaguchi, F., 1999. Molecular distributions of water soluble dicarboxylic acids in marine aerosols over the Pacific Ocean including tropics. Journal of Geophysical Research 104, 3501–3509.

Laurent, B., Marticorena, B., Bergametti, G., Léon, J.F., Mahowald, N.M., 2008. Modeling mineral dust emissions from the Sahara desert using new surface properties and soil database. Journal of Geophysical Research Atmospheres 113, 1–20. https://doi.org/10.1029/2007JD009484

Laurent, B., Marticorena, B., Bergametti, G., Mei, F., 2006. Modeling mineral dust emissions from Chinese and Mongolian deserts. Global and Planetary Change. https://doi.org/10.1016/j.gloplacha.2006.02.012

Lavanchy, V.M.H., Gäggeler, H.W., Schotterer, U., Schwikowski, M., Baltensperger, U., 1999. Historical record of carbonaceous particle concentrations from a European high-alpine glacier (Colle Gnifetti, Switzerland). Journal of Geophysical Research Atmospheres 104, 21227–21236. https://doi.org/10.1029/1999JD900408

Lee, E.H., Sohn, B.J., 2009. Examining the impact of wind and surface vegetation on the Asian dust occurrence over three classified source regions. Journal of Geophysical Research Atmospheres 114, 1–12. https://doi.org/10.1029/2008JDO10687

Legrand, M., Mayewski, P., 1997. Glaciochemistry of polar ice cores: A review. Reviews of Geophysics 35, 219–243. https://doi.org/10.1029/96RG03527

Li, W., Shao, L., Zhang, D., Ro, C.U., Hu, M., Bi, X., Geng, H., Matsuki, A., Niu, H., Chen, J., 2016. A review of single aerosol particle studies in the atmosphere of East Asia: Morphology, mixing state, source, and heterogeneous reactions. Journal of Cleaner Production 112, 1330–1349. https://doi.org/10.1016/j.jclepro.2015.04.050

Li, W.J., Shao, L.Y., 2009. Observation of nitrate coatings on atmospheric mineral dust particles. Atmospheric Chemistry and Physics 9, 1863–1871. https://doi.org/10.5194/acp-9-1863-2009

Linak, W.P., Wendt, J.O.L., 1994. Trace metal transformation mechanisms during coal combustion. Fuel Processing Technology 39, 173–198. https://doi.org/10.1016/0378-3820(94)90179-1

Logan, J.A., 1983. Heterogeneous and multiphase chemistry in the troposphere. Journal of Geophysical Research 88, 10785–10807. https://doi.org/10.1126/science.276.5315.1058

Lohmann, U., Feichter, J., 2010. Global indirect aerosol effects: a review. Atmospheric Chemistry and Physics Discussions 4, 7561–7614. https://doi.org/10.5194/acpd-4-7561-2004

Ma, Q., He, H., 2012. Synergistic effect in the humidifying process of atmospheric relevant calcium nitrate, calcite and oxalic acid mixtures. Atmospheric Environment 50, 97–102. https://doi.org/10.1016/j.atmosenv.2011.12.057

Ma, Q., He, H., Liu, Y., Liu, C., Grassian, V.H., 2013. Heterogeneous and multiphase formation pathways of gypsum in the atmosphere. Physical Chemistry Chemical Physics 15, 19196–19204. https://doi.org/10.1039/c3cp53424c

Ma, Q., Liu, C., Ma, J., Chu, B., He, H., 2019. A laboratory study on the hygroscopic behavior of H2C2O4-containing mixed particles. Atmospheric Environment 200, 34–39. https://doi.org/10.1016/j.atmosenv.2018.11.056

Ma, Q., Liu, Y., Liu, C., He, H., 2012a. Heterogeneous reaction of acetic acid on MgO, α-Al 2O 3, and CaCO 3 and the effect on the hygroscopic behaviour of these particles. Physical Chemistry Chemical Physics 14, 8403–8409. https://doi.org/10.1039/c2cp40510e

Ma, Q., Liu, Y., Liu, C., Ma, J., He, H., 2012b. A case study of Asian dust storm particles: Chemical composition, reactivity to SO 2 and hygroscopic properties. Journal of Environmental Sciences 24, 62–71. https://doi.org/10.1016/S1001-0742(11)60729-8

Manktelow, P.T., Carslaw, K.S., Mann, G.W., Spracklen, D. V., 2010. The impact of dust on sulfate aerosol, CN and CCN during an East Asian dust storm. Atmospheric Chemistry and Physics 10, 365–382. https://doi.org/10.5194/acp-10-365-2010

Marcus, M.A., MacDowell, A.A., Celestre, R., Manceau, A., Miller, T., Padmore, H.A., Sublett, R.E., 2004. Beamline 10.3.2 at ALS: A hard X-ray microprobe for environmental and materials sciences. Journal of Synchrotron Radiation 11, 239–247. https://doi.org/10.1107/S0909049504005837

Maruyama, T., Ohizumi, T., Taneoka, Y., Minami, N., Fukuzaki, N., Murai, H., Murano, K., Kusakabe, M., 2000. Sulfur isotope ratios of coals and oils used in China and Japan. Nippon Kagaku Kaishi / Chemical Society of Japan - Chemistry and Industrial Chemistry Journal. https://doi.org/10.1246/nikkashi.2000.45

Matsuki, A., Schwarzenboeck, A., Venzac, H., Laj, P., Crumeyrolle, S., Gomes, L., 2009. Effect of surface reaction on the cloud nucleating properties of mineral dust: AMMA aircraft campaign in summer 2006. Atmospheric Chemistry and Physics Discussions 9, 1797–1830. https://doi.org/10.5194/acpd-9-1797-2009

Mazzei, F., D'Alessandro, A., Lucarelli, F., Nava, S., Prati, P., Valli, G., Vecchi, R., 2008. Characterization of particulate matter sources in an urban environment. Science of the Total Environment 401, 81–89. https://doi.org/10.1016/j.scitotenv.2008.03.008

McFiggans, G., Artaxo, P., Baltensperger, U., Coe, H., Facchini, M.C., Feingold, G., Fuzzi, S., Gysel, M., Laaksonen, A., Lohmann, U., Mentel, T.F., Murphy, D.M., O'Dowd, C.D., Snider, J.R., Weingartner, E., 2006. The effect of physical and chemical aerosol properties on warm cloud droplet activation. Atmospheric Chemistry and Physics 6, 2593–2649. https://doi.org/10.5194/acpd-5-8507-2005

Mikami, M., Shi, G.Y., Uno, I., Yabuki, S., Iwasaka, Y., Yasui, M., Aoki, T., Tanaka, T.Y., Kurosaki, Y., Masuda, K., Uchiyama, A., Matsuki, A., Sakai, T., Takemi, T., Nakawo, M., Seino, N., Ishizuka, M., Satake, S., Fujita, K., Hara, Y., Kai, K., Kanayama, S., Hayashi, M., Du, M., Kanai, Y., Yamada, Y., Zhang, X.Y., Shen, Z., Zhou, H., Abe, O., Nagai, T., Tsutsumi, Y., Chiba, M., Suzuki, J., 2006. Aeolian dust experiment on climate impact: An overview of Japan-China joint project ADEC. Global and Planetary Change 52, 142–172. https://doi.org/10.1016/j.gloplacha.2006.03.001

Miyamoto, C., Marcus, M.A., Sakata, K., Kurisu, M., Takahashi, Y., 2016. Depth-dependent calcium speciation in individual aerosol particles by combination of fluorescence yield and conversion electron yield XAFS using X-ray microbeam. Chemistry Letters 45. https://doi.org/10.1246/cl.160392

Miyamoto, C., Sakata, K., Yamakawa, Y., and Takahashi, Y., 2020. Determination of calcium and sulfate species in aerosols associated with the conversion of its species through reaction processes in the atmosphere and its influence on cloud condensation nuclei activation, Atmospheric Environment, in press, https://doi.org/10.1016/j.atmosenv.2019.117193

Motoyama R., Yanagisawa F., Kotani T., Kawabata A., and U.A., 2000. Sulfur Isotope Ratio of Non Sea Salt Sulfate in Aerosol and Wet Deposition in Yamagata, Japan. Seppyo 63, 215–224.

Mukai, H., Tanaka, A., Fujii, T., Zeng, Y., Hong, Y., Tang, J., Guo, S., Xue, H., Sun, Z., Zhou, J., 2001. Regional characteristics of sulfur and lead isotope ratios in the atmosphere at several Chinese urban sites. Environmental science & technology 35, 1064–1071.

Nishikawa, M., Hao, Q., Morita, M., 2000. Preparation and evaluation of certified reference materials for asian mineral dust. Global Environ. R4esearch.

Ohara, T., Akimoto, H., Kurokawa, J., Horii, N., Yamaji, K., Yan, X., Hayasaka, T., 2007. Atmospheric Chemistry and Physics An Asian emission inventory of anthropogenic emission sources for the period 1980-2020. Atmos. Chem. Phys 7, 4419–4444.

Ohizumi, T., Fukuzaki, N., Kusakabe, M., 1997. Sulfur isotopic view on the sources of sulfur in atmospheric fallout along the coast of the Sea of Japan. Atmospheric Environment 31, 1339–1348.

Ohizumi, T., Take, N., Inomata, Y., Yagoh, H., Endo, T., 2016. Long-term variation of the source of sulfate deposition in a leeward area of Asian continent in view of sulfur isotopic composition. Atmospheric Environment 140, 42–51. https://doi.org/10.1016/j.atmosenv.2016.05.057

Okuda, T., Tenmoku, M., Kato, J., Mori, J., Sato, T., Yokochi, R., Tanaka, S., 2006. Long-term observation of trace metal concentration in aerosols at a remote island, Rishiri, Japan by using inductively coupled plasma mass spectrometry equipped with laser ablation. Water, Air, and Soil Pollution 174, 3–17. https://doi.org/10.1007/s11270-005-9000-2

Ooki, A., Uematsu, M., 2005. Chemical interactions between mineral dust particles and acid gases during Asian dust events. Journal of Geophysical Research: Atmospheres 110.

Oyabu, I., Matoba, S., Yamasaki, T., Kadota, M., Iizuka, Y., 2016. Seasonal variations in the major chemical species of snow at the South East Dome in Greenland. Polar Science 10, 36–42. https://doi.org/10.1016/j.polar.2016.01.003

Paris, G., Sessions, A.L., Subhas, A. V., Adkins, J.F., 2013. MC-ICP-MS measurement of δ34S and Δ33S in small amounts of dissolved sulfate. Chemical Geology 345, 50–61. https://doi.org/10.1016/j.chemgeo.2013.02.022

Penner, J.E., Authors, L., Andreae, M., Annegarn, H., Barrie, L., Feichter, J., Hegg, D., Jayaraman, A., Leaitch, R., Murphy, D., Nganga, J., Pitari, G., Authors, C., Ackerman, A., Adams, P., Austin, P., Boers, R., Boucher, O., Chin, M., Chuang, C., Collins, B., Cooke, W., Demott, P., Feng, Y., Fischer, H., Fung, I., Ghan, S., Ginoux, P., Gong, S.-L., Guenther, A., Herzog, M., Higurashi, A., Kaufman, Y., Kettle, A., Kiehl, J., Koch, D., Lammel, G., Land, C., Lohmann, U., Madronich, S., Mancini, E., Mishchenko, M., Nakajima, T., Quinn, P., Rasch, P., Roberts, D.L., Savoie, D., Schwartz, S., Seinfeld, J., Soden, B., Tanré, D., Taylor, K., Tegen, I., Tie, X., Vali, G., Dingenen, R. Van, Van Weele, M., Zhang, Y., 2011. Aerosols, their Direct and Indirect Effects. Climate Change 2001: The Physical Science Basis. Contribution of Working Group 1 to the Third Assesment Report of the Intergovernmental Panel on Climate Change 291–336. https://doi.org/10.1016/j.resuscitation.2012.08.009

Petters, M.D., Kreidenweis, S.M., 2008. A single parameter representation of hygroscopic growth and cloud condensation nucleus activity - Part 2: Including solubility. Atmospheric Chemistry and Physics 8, 6273–6279. https://doi.org/10.5194/acp-8-6273-2008

Petters, M.D., Kreidenweis, S.M., 2007. A single parameter representation of hygroscopic growth and cloud condensation nucleus activity. Atmospheric Chemistry and Physics 7, 1961–1971.

Pilinis, C., Seinfeld, J.H., Seigneur, C., 1987. Mathematical Modeling of the Dynamics of Multicomponent Atmospheric Aerosols. Atmospheric Environment 21, 943–953.

Qi, H.P., Coplen, T.B., 2003. Evaluation of the 34S/32S ratio of Soufre de Lacq elemental

sulfur isotopic reference material by continuous flow isotope-ratio mass spectrometry. Chemical Geology 199, 183–187. https://doi.org/10.1016/S0009-2541(03)00075-5

Qu, Y., An, J., He, Y., Zheng, J., 2016. An overview of emissions of SO2 and NOx and the long-range transport of oxidized sulfur and nitrogen pollutants in East Asia. Journal of Environmental Sciences (China) 44, 13–25. https://doi.org/10.1016/j.jes.2015.08.028

Ratafia-Brown, J.A., 1994. Overview of trace element partitioning in flames and furnaces of utility coal-fired boilers. Fuel Processing Technology 39, 139–157. https://doi.org/10.1016/0378-3820(94)90177-5

Rees C. E., Jenkins, W.J., Monster, J., 1978. The sulphur isotopic composition. Geochimxa et Cosmochimica Acta 42, 377–381.

Rossi, M.J., 2003. Heterogeneous Reactions on Salts. Chemical Reviews 103, 4823–4882. https://doi.org/10.1021/cr020507n

Rubasinghege, G., Grassian, V.H., 2013. Role(s) of adsorbed water in the surface chemistry of environmental interfaces. Chemical Communications 49, 3071–3094. https://doi.org/10.1039/c3cc38872g

Sakata, K., Sakaguchi, A., Tanimizu, M., Takaku, Y., Yokoyama, Y., Takahashi, Y., 2014. Identification of sources of lead in the atmosphere by chemical speciation using X-ray absorption near-edge structure (XANES) spectroscopy. Journal of Environmental Sciences (China) 26, 343–352. https://doi.org/10.1016/S1001-0742(13)60430-1

Sakata, M., Ishikawa, T., Mitsunobu, S., 2014. Contribution of Asian outflow to atmospheric concentrations of sulfate and trace elements in aerosols during winter in Japan. Geochemical Journal 48, 479–490. https://doi.org/10.2343/geochemj.2.0323

Sakata, M., Ishikawa, T., Mitsunobu, S., 2013. Effectiveness of sulfur and boron isotopes in aerosols as tracers of emissions from coal burning in Asian continent. Atmospheric

Environment 67, 296–303. https://doi.org/10.1016/j.atmosenv.2012.11.025

Sander, S.P., Friedl, R.R., Barker, J.R., Golden, D.M., Kurylo, M.J., Wine, P.H., Abbatt, J.P.D., Burkholder, J.B., Kolb, C.E., Moortgat, G.K., Huie, R.E., Orkin, V.L., 2011. Chemical Kinetics and Photochemical Data for Use in Atmospheric Studies, Evaluation Number 17. Jet Propulsion Laboratory 684.

Satheesh, S.K., Krishna Moorthy, K., 2005. Radiative effects of natural aerosols: A review. Atmospheric Environment 39, 2089–2110. https://doi.org/10.1016/j.atmosenv.2004.12.029

Schroeder, S.L.M., 1996. Towards a "universal curve" for total electron-yield XAS. Solid State Communications 98, 405–409. https://doi.org/10.1016/0038-1098(96)00035-X

Seinfeld, J.H. and Pandis, S.N., 2016. Atmospheric Chemistry and Physics: From Air Pollution to Climate Change. 3rd Edition, John Wiley & Sons

Seinfeld, J.H. and Pandis, S.N., 2006. Atmospheric Chemistry and Physics: From Air Pollution to Climate Change. 2nd Edition, John Wiley & Sons. https://doi.org/10.1080/00139157.1999.10544295

Smith, S.J., Van Aardenne, J., Klimont, Z., Andres, R.J., Volke, A., Delgado Arias, S., 2011. Anthropogenic sulfur dioxide emissions: 1850-2005. Atmospheric Chemistry and Physics 11, 1101–1116. https://doi.org/10.5194/acp-11-1101-2011

Song, Chul H. and Carmichael, G.R., 2001. A three-dimensional modeling investigation of the evolution processes of dust and sea-salt particles in east Asia. Journal of Geophysical Research 106, 18131–18154. https://doi.org/https://doi.org/10.1029/2000JD900352

Stein, A.F., Draxler, R.R., Rolph, G.D., Stunder, B.J.B., Cohen, M.D., Ngan, F., 2015. NOAA's HYSPLIT atmospheric transport and dispersion modeling system. Bulletin of the American Meteorological Society 96, 2059–2077.

Storelvmo, T., Leirvik, T., Lohmann, U., Phillips, P.C.B., Wild, M., 2016. Disentangling

greenhouse warming and aerosol cooling to reveal Earth's climate sensitivity. Nature Geoscience 9, 286–289. https://doi.org/10.1038/ngeo2670

Streets, D.G., Bond, T.C., Carmichael, G.R., Fernandes, S.D., Fu, Q., He, D., Klimont, Z., Nelson, S.M., Tsai, N.Y., Wang, M.Q., Woo, J.H., Yarber, K.F., 2003. An inventory of gaseous and primary aerosol emissions in Asia in the year 2000. Journal of Geophysical Research D: Atmospheres 108. https://doi.org/10.1029/2002jd003093

Sullivan, R.C., Moore, M.J.K., Petters, M.D., Kreidenweis, S.M., Roberts, G.C., Prather, K.A., 2009. Effect of chemical mixing state on the hygroscopicity and cloud nucleation properties of calcium mineral dust particles. Atmospheric Chemistry and Physics 9, 3303–3316. https://doi.org/10.5194/acp-9-3303-2009

Sun, J., Ariya, P.A., 2006. Atmospheric organic and bio-aerosols as cloud condensation nuclei (CCN): A review. Atmospheric Environment 40, 795–820. https://doi.org/10.1016/j.atmosenv.2005.05.052

Takahashi, Y., Miyoshi, T., Higashi, M., Kamioka, H., Kanai, Y., 2009. Neutralization of calcite in mineral aerosols by acidic sulfur species collected in China and Japan studied by Ca K-edge X-ray absorption near-edge structure. Environmental Science and Technology 43, 6535–6540. https://doi.org/10.1021/es9010256

Takahashi, Y., Miyoshi, T., Yabuki, S., Inada, Y., Shimizu, H., 2008. Observation of transformation of calcite to gypsum in mineral aerosols by Ca K-edge X-ray absorption near-edge structure (XANES). Atmospheric Environment 42, 6535–6541. https://doi.org/10.1016/j.atmosenv.2008.04.012

Takahashi, Y., Kanai, Y., Kamioka, H., Ohta, A., Maruyama, H., Song, Z., Shimizu, H., 2006. Speciation of sulfate in size-fractionated aerosol particles using sulfur K-edge X-ray absorption near-edge structure. Environmental science & technology 40, 5052–5057.

Takemura, T., Nozawa, T., Emori, S., Nakajima, T.Y., Nakajima, T., 2005. Simulation of climate response to aerosol direct and indirect effects with aerosol transport-radiation model. Journal of Geophysical Research D: Atmospheres 110, 1–16. https://doi.org/10.1029/2004JD005029

Takemura, T., Uno, I., Nakajima, T., Higurashi, A., Sano, I., 2002. Modeling study of long-range transport of Asian dust and anthropogenic aerosols from East Asia. Geophysical Research Letters 29, 11-1-11–4. https://doi.org/10.1029/2002gl016251

Takemura, T., Okamoto, H., Maruyama, Y., Numaguti, A., Higurashi, A., Nakajima, T., 2000. Global three-dimensional simulation of aerosol optical thickness. Journal of Geophysical Research 105.

Tang, M., Cziczo, D.J., Grassian, V.H., 2016. Interactions of Water with Mineral Dust Aerosol: Water Adsorption, Hygroscopicity, Cloud Condensation, and Ice Nucleation. Chemical Reviews 116, 4205–4259. https://doi.org/10.1021/acs.chemrev.5b00529

Tang, M., Huang, X., Lu, K., Ge, M., Li, Y., Cheng, P., Zhu, T., Ding, A., Zhang, Y., Gligorovski, S., Song, W., Ding, X., Bi, X., Wang, X., 2017a. Heterogeneous reactions of mineral dust aerosol: implications for tropospheric oxidation capacity. Atmospheric Chemistry and Physics Discussions 1–124. https://doi.org/10.5194/acp-2017-458

Tang, M., Huang, X., Lu, K., Ge, M., Li, Y., Cheng, P., Zhu, T., Ding, A., Zhang, Y., Gligorovski, S., Song, W., Ding, X., Bi, X., Wang, X., 2017b. Heterogeneous reactions of mineral dust aerosol: Implications for tropospheric oxidation capacity. Atmospheric Chemistry and Physics 17, 11727–11777. https://doi.org/10.5194/acp-17-11727-2017

Tang, M.J., Whitehead, J., Davidson, N.M., Pope, F.D., Alfarra, M.R., McFiggans, G., Kalberer, M., 2015. Cloud condensation nucleation activities of calcium carbonate and its atmospheric ageing products. Physical Chemistry Chemical Physics 17, 32194–32203.

https://doi.org/10.1039/c5cp03795f

Tang, Y., Carmichael, G.R., Kurata, G., Uno, I., Weber, R.J., Song, C.H., Guttikunda, S.K., Woo, J.H., Streets, D.G., Wei, C., Clarke, A.D., Huebert, B., Anderson, T.L., 2004. Impacts of dust on regional tropospheric chemistry during the ACE-Asia experiment: A model study with observations. Journal of Geophysical Research D: Atmospheres 109, 1–21. https://doi.org/10.1029/2003JD003806

Taylor, B. E., Ding, T., Halas, S., Breas, O., Robinson, B. W., 2000. Accurate Calibration of the V-CDT Sulfur Isotope Scale: Proposed δ ^{34}S Values for Calibration and Reference Materials and Methods of Correction for SO_2-Based Analyses. Report of Sulfur Isotope Working Group 8th Advisory Group Meeting on Future Trends in Stable Isotope Reference Materials and Laboratory Quality Assurance, IAEA, Vienna, Austria.

Taylor S.R, 1964. Abundance of chemical elements in the continental crust : a new table. Geochimica et Cosmochimica Acta 28, 1273–1285.

Tegen, I., Schepanski, K., 2009. The global distribution of mineral dust. IOP Conference Series: Earth and Environmental Science 7, 012001. https://doi.org/10.1088/1755-1307/7/1/012001

Twomey, S., 1959. The nuclei of natural cloud formation part II: The supersaturation in natural clouds and the variation of cloud droplet concentration. Geofisica Pura e Applicata 43, 243–249. https://doi.org/10.1007/BF01993560

Újvári, G., Stevens, T., Svensson, A., Klötzli, U.S., Manning, C., Németh, T., Kovács, J., Sweeney, M.R., Gocke, M., Wiesenberg, G.L.B., Markovic, S.B., Zech, M., 2015. Two possible source regions for central Greenland last glacial dust. Geophysical Research Letters 42, 10399–10408. https://doi.org/10.1002/2015GL066153

Usher, C.R., Michel, A.E., Grassian, V.H., 2003. Reactions on Mineral Dust. Chemical Reviews

103, 4883–4940. https://doi.org/10.1021/cr020657y

Van Den Broeke, M., Bamber, J., Ettema, J., Rignot, E., Schrama, E., Van Berg, W.J. De, Van Meijgaard, E., Velicogna, I., Wouters, B., 2009. Partitioning recent Greenland mass loss. Science 326, 984–986. https://doi.org/10.1126/science.1178176

Verhulst, D., Buekens, A., Spencer, P.J., Eriksson, G., 1996. Thermodynamic behavior of metal chlorides and sulfates under the conditions of incineration furnaces. Environmental Science and Technology 30, 50–56. https://doi.org/10.1021/es940780+

Wang, G., Huang, L., Gao, Shixiang, Gao, Songting, Wang, L., 2002. Characterization of water-soluble species of PM10 and PM2.5 aerosols in urban area in Nanjing, China. Atmospheric Environment. https://doi.org/10.1016/S1352-2310(01)00550-7

Wang, J., Hoffmann, A.A., Park, R.J., Jacob, D.J., Martin, S.T., 2008. Global distribution of solid and aqueous sulfafte aerosols: Effect of the hysteresis of particle phase transitions. Journal of Geophysical Research Atmospheres 113, 1–11. https://doi.org/10.1029/2007JD009367

Xu, J., Bergin, M.H., Yu, X., Liu, G., Zhao, J., Carrico, C.M., Baumann, K., 2002. Measurement of aerosol chemical, physical and radiative properties in the Yangtze delta region of China. Atmospheric Environment 36, 161–173. https://doi.org/10.1016/S1352-2310(01)00455-1

Xu, M., Yan, R., Zheng, C., Qiao, Y., Han, J., Sheng, C., 2004. Status of trace element emission in a coal combustion process: A review. Fuel Processing Technology. https://doi.org/10.1016/S0378-3820(03)00174-7

Xu, M., Yan, R., Zheng, C., Qiao, Y., Han, J., Sheng, C., 2003. Status of trace element emission in a coal combustion process: A review. Fuel Processing Technology 85, 215–237. https://doi.org/10.1016/S0378-3820(03)00174-7

Yao, X., Chan, C.K., Fang, M., Cadle, S., Chan, T., Mulawa, P., He, K., Ye, B., 2002. The water-soluble ionic composition of PM2.5 in Shanghai and Beijing, China. Atmospheric Environment 36, 4223–4234. https://doi.org/10.1016/s1352-2310(02)00342-4

Zender, C.S., Miller, R.L., Tegen, I., 2004. Quantifying mineral dust mass budgets : Terminology, constraints, and current estimates. Eos 85. https://doi.org/10.1029/2004EO480002